Universidade de Aveiro
2017
Departamento de Engenharia de Materiais e Cerâmica

Maksim Starykevich

Electrosynthesis of 1-D metallic nanoparticles from DES using porous anodic templates

Eletrosíntese de nanopartículas metálicas 1-D de DES usando modelos anódicos porosos

Universidade de Aveiro
2017

Departamento de Engenharia de Materiais e Cerâmica

Maksim Starykevich

Electrosynthesis of 1-D metallic nanoparticles from DES using porous anodic templates

Eletrosíntese de nanopartículas metálicas 1-D de DES usando modelos anódicos porosos

Tese apresentada à Universidade de Aveiro para cumprimento dos requisitos necessários à obtenção do grau de Doutor em Ciência e Engenharia de Materiais, realizada sob a orientação científica do Professor Doutor Mário G.S. Ferreira, Professor Catedrático, e do Doutor Andrei N. Salak, ambos do Departamento de Engenharia de Materiais e Cerâmica da Universidade de Aveiro.

The financial support of the European Commission and Portuguese Foundation for Science and Technology (FCT) in frame of PIRSES-GA-2011-295273 – NANEL and PTDC/CTM-NAN/113570/2009 projects respectively is gratefully acknowledged.

Dedicated to my family
for their boundless love and care.

o júri

presidente

Prof. Doutor Nuno Miguel Gonçalves Borges de Carvalho
Professor Catedrático, Universidade de Aveiro

Prof. Doutor Jorge Ribeiro Frade
Professor Catedrático, Universidade de Aveiro

Doutor Carlos Manuel de Melo Pereira
Professor Auxiliar Com Agregação, Universidade do Porto

Doutor Jorge Manuel Palma Correia
Investigador Auxiliar, Universidade de Lisboa - Faculdade de Ciências

Doutor Dzmitry Ivanou
Estagiário de Pós-Doutoramento, Universidade do Porto - Faculdade de Engenharia

Prof. Doutor Mário Guerreiro Silva Ferreira (orientador)
Professor Catedrático da Universidade de Aveiro

aknowledgements

I would like to express my gratitude to my supervisors Professor Mário Ferreira and Dr. Andrei Salak for their continuous help, advising and support during my PhD research. All your work allowed me to grow as a research scientist.

Special thanks are owed to Professor Mikhail Zheludkevich and Professor Mário Ferreira for inviting me to Portugal and giving me an opportunity to work in this group. I am also thankful for the excellent examples that they provided as successful scientists and mindful people.

I address many thanks to Aleksey Lisenkov and Vitalii Ivanov for encouraging me on my first steps in the science.

I am especially grateful to Dr. Dzmitry Ivanou, Dr. Yuliya Ivanova, for their time, interesting discussions and valuable ideas.

My sincere thanks go to my friends and colleagues Dr. João Tedim, Dr. Kiryl Yasakau, Dr. Alexandre Bastos, Dr. Silvar Kalip, Dr. Aleksey Yaremchenko, Dr. Aliaksandr Shaula, Dr. Isabel Sousa, Dr. Tiago Galvão, Dr. Cristina Neves, Dr. Frederico Maia, Dr. Maria Serdechnova, Dr. Sergei Mikhalev, Dr. Javier Macías, Dr. Andrei Kovalevsky, Alena Kuznetsova, Aleksey Lisenkov, Kiryl Zakharchuk, Olga Karavai, Stanley Ofoegbu, Jorge Carneiro, Ana Caetano, Tatiana Zheludkevich, Inês Rondão, Diogo Almeida. It has been an honor to work in such a productive environment, with such talented people.

I want to thank everyone in DEMaC, especially Célia Miranda, Ana Ribeiro, Artur Sarabando and Marta Ferro, who assisted a lot with different techniques on our department; many thanks to Alexandra Vale, Luísa Costa, Rita Vieira, José Ruas for their patients and helping me to overcome numerous bureaucratic barriers.

Finally, I wish to thank Anastasiya for giving me motivation, being carrying and loving person, especially on the final stage of the PhD thesis.

,

palavras-chave electrodeposição, camada barreira, solventes eutécticos profundos, modelos porosos anódicos, titânia anódica, alumina anódica.

resumo

O método de síntese de nanoparticulas 1-D assistido por um modelo tornou-se um tópico em voga na química após o desenvolvimento de filmes anódicos com poros bem ordenados. Contudo, a maioria dos trabalhos nesta área tem sido feita utilizando filmes porosos destacados devido à presença de uma barreira no fundo dos poros. No entanto, esta estratégia segue demasiados passos, o que aumenta o seu custo, torna mais difícil a execução e impõe várias limitações. Consequentemente, existe a necessidade de uma técnica que permita o enchimento (electrofilling) dos tubos sem remover a camada barreira – esta tese representa o nosso contributo para esse trabalho. Utilizámos uma técnica mais simples que permite a electrodeposição e "electrofilling" de nanoestruturas directamente nos modelos sobre o substrato metálico, utilizando solventes eutécticos profundos à base de cloreto de colina como electrólito. Relativamente à água, os solventes eutécticos profundos demonstram superior estabilidade térmica e uma janela electroquímica mais alargada, o que aumenta o número de materais secundários depositados.

Como materiais a investigar foram escolhidos titânia e alumina dada a sua capacidade para formar estruturas porosas altamente ordenadas, propriedades eletroquímicas distintas e uso generalizado em síntese assistida por padrão. O estudo aqui apresentado encontra-se dividido em duas etapas. Primeiramente, a influência da camada barreira foi investigada em sistemas modelo através da utilização de filmes barreira densos na superfície dos elétrodos. Para os filmes de alumina e titânia, identificaram-se vários parâmetros que afectam a electrodeposição, dos quais se destacam a influência da voltagem de anodização, a espessura da camada de barreira, a dupla camada eléctrica e o perfil de corrente. Durante esta etapa detectaram-se efeitos nefastos, como a formação de uma densa camada orgânica na superfície do eléctrodo, que foram ultrapassados aumentando a temperatura ou alternando o potencial aplicado.

A segunda etapa consistiu em passar de elétrodos planos (primeira etapa) para modelos porosos (segunda etapa). Foi realizado, com sucesso, o preenchimento dos poros de alumina e dos poros de titânia. Parâmetros como o perfil de corrente, temperatura de solução, entre outras, foram ajustadas para melhorar o fator de preenchimento e a homogeneidade do preenchimento. Foi desenvolvido um processo de preenchimento de moldes de alumina anódica em duas etapas, nucleação AC (1º passo) e preenchimento galvanostático (2º passo). Foram utilizadas três condições diferentes de modelos de titânia anódica porosa no "electrofilling". O primeiro é sem modificação e demonstrou que a electroredução do zinco ocorre de forma aleatória ao longo de todo o comprimento do poro, o que leva ao fecho do poro e a um enchimento não homogéneo. A segunda modificação, cristalização total por têmpera, permite a preparação de estruturas coaxiais devido à deposição uniforme de zinco nas paredes dos poros. A última modificação foi a cristalização selectiva do fundo do poro. Foi descoberto que uma anodização adicional em eletrólitos não agressivos leva à cristalização da parte barreira dos tubos (fundo) e, consequentemente, a maior condutividade na parte inferior do que nas paredes. Este efeito permite um enchimento ascendente dos modelos porosos de titânia. As estratégias aqui apresentadas alargam a gama de possibilidades para a aplicação de modelos porosos anódicos na electrodeposição de diferentes nanoestruturas.

keywords electrodeposition, barrier layer, deep eutectic solvent, porous template, anodic titania, anodic alumina.

abstract

The template assisted method of 1-D nanoparticles synthesis has become a hot topic in Chemistry after the development of high-ordered porous anodic films. Most studies in this field have focused on the use of detached porous films due to the presence of the barrier layer on the pore bottom. However, this strategy follows a great number of steps, which raises its cost while decreasing convenience of operation and imposing several limitations. Consequently, there is a need for a technique which allows electrofilling of tubes without removing the barrier layer – this thesis represents our contribution to that enterprise. We have devised a simpler technique which allows electrodeposition of nanostructures directly in the templates on metallic substrate, using choline chloride based deep eutectic solvents (DES) as electrolyte. Compared to water, DES have improved thermal stability and a wider electrochemical window, dramatically increasing the number of possible secondary materials deposited.

Titania and alumina were chosen as materials under study due to their known capacity to form highly-ordered porous structures, different electrochemical profiles and widespread use in template assisted synthesis. The present work is divided in two parts. First, the influence of the barrier layer has been investigated by using dense barrier films on the electrode surface as a model system. For both alumina and titania films, several parameters affecting the electrodeposition of zinc have been identified, notably the influence of the anodization voltage, barrier layer thickness, electrical double layer and current profile. During this stage, some negative effects have been detected, such as a dense organic layer formation on electrode surface, a hurdle which has been overcome by either increasing the temperature or applying the alternating potential.

The second stage consisted in transferring the method from the flat electrodes (the first stage) to the porous templates. The successful filling of both porous alumina and porous titania, has been achieved. Parameters such as current profile, solution temperature, among others, have been tuned to improve the fill factor and homogeneity of the filling. A two-step porous anodic alumina template filling with AC nucleation (1^{st} step) and galvanostatic filling (2^{nd} step) has been developed. Three different types of porous anodic titania templates have been used for electrofilling. The first one was used as-prepared, showing that zinc electroreduction occurs in random places along all pore length, resulting in pore sealing and non-homogeneous filling. The second modification, full crystallization by annealing, allows the preparation of coaxial structures due to uniform zinc deposition on the pore walls. The last modification is selective bottom crystallization. It has been found that additional anodization in unaggressive electrolytes leads to crystallization of the barrier (bottom) part of the tubes and, thus, to higher conductivity of the bottom part than that of the walls. This effect allows a bottom-up filling of the titania porous template.

The strategies presented here widen the range of possibilities for the application of porous anodic templates in the electrodeposition of different nanostructures.

Table of Contents

List of abbreviations

General

AFM	Atomic force microscopy
ATR-FTIR	Attenuated total reflection Fourier infrared spectroscopy
CV	Cyclic voltammetry
DES	Deep eutectic solvent
EDX/EDS	Energy dispersive X-ray analysis
EIS	Electrochemical impedance spectroscopy
EW	Electrochemical window
FAB MS	Fast atom bombard mass spectrometry
Fc/Fc+	Ferrocene/Ferrocinium
FTO	Fluorine doped Tin Oxide
GC	Glassy carbon
GDOES	Glow discharge optical emission spectroscopy
HBD	Hydrogen bond donors
ILs	Ionic liquids
OCP	Open circuit potential
PAA	Porous anodic alumina
PAT	Porous anodic titania
RTIL	Room temperature ionic liquids
SEM	Scanning electron microscopy
STEM	Scanning transmission electron microscopy
TEM	Transmission electron microscopy
XRD	X-ray diffraction

Ionic liquids / DES

$[(CF_3SO_2)_2N^-]$	Bis-(trifluoromethanesulphonyl)imide
$[BF_4]^-$	Tetrafluoroborate
$[PF_6]^-$	Hexafluorophosphate
BMIM	1-butyl-3-methylimidazolium
CF_3COO^-	Trifluoroacetat

$CF_3SO_3^-$	Trifluromethylsulphonate
ChCl	Choline chloride
EG	Ethylene glycol
EMIM	1-ethyl-3-methylimidazolium
Gl	Glycerol
Hal	Halogen
HMIM	1-hexyl-3-methylimidazolium
OMIM	1-octyl-3-methylimidazolium

List of figures

List of tables

Introduction

Stretch your Limits,
Lift your Spirits
and Aim for the Top

UIAA Mountain Ethics Declaration
Porto, 2009

The main objective of this work is the electrodeposition of 1-D nanoparticles in porous anodic templates. The main idea is to find a possible way of formation of nanorods by direct electrodeposition in porous non-detached oxide matrixes, avoiding expensive and time consuming steps such as substrate removal, pores opening and contact sputtering. The negative feature of the barrier layer on the pores bottoms is vanished by templates modification or by application of a specific current profile.

This PhD thesis reports a part of the work on the metal electrodeposition that has been performed during the last four years. For the template investigation, step-by-step analysis has been used. Different approaches were used in order to achieve the homogeneous pores electrofilling. Some of them either had a negative effect or resulted in no visible effect, while others were found to enhance the electrodeposition process.

The work is divided into seven chapters. The first one demonstrates the state of the art related to objects of the thesis and gives useful information concerning those subjects. The second chapter provides information about the performed experimental work and about the experimental techniques that were applied. Detailed description of the procedures, which were used in this work, is presented in the corresponding individual chapters.

The core results are presented in chapters III-VI. These chapters are constituted by the published papers starting from the oldest to the newest. Chapters III and IV report the investigation of the anodic alumina oxide. The chapter III describes the two-step technique of filling the anodic alumina pores with zinc. The importance of application of the pulse nucleation step and the galvanostatic step is shown in detail. Chapter IV contains experimental data on the influence of the alumina barrier layer on the electrochemical reduction processes. In this work, the impacts of several parameters such as film thickness, temperature of the solution, additional sinusoidal potential oscillation, have been demonstrated. An evidence of formation of a dense organic layer on the alumina/electrolyte interface which hindered the zinc reduction and a possible way to avoid the obstacles caused by this layer are given in the chapter.

Results presented in chapters V and VI correspond to studies carried out on anodic titania. In the same way, initially, the planar anodic film on the titanium interface has been investigated in terms of influence of both the oxide film thickness and the anodization voltage on the nucleation processes and kinetics of zinc reduction (chapter V). Then, based on the results presented in the chapter V, several possible template modifications were studied and successfully used for filling of the porous titania

templates. The modifications such as annealing and selective bottom crystallization are described and characterized in the chapter VI. The chapter also gives a description of the filling of the modified templates. The results reported in chapters III-VI have been published in SCI peer reviewed journals in the area of Electrochemistry.

The last chapter (chapter VII) summarizes the general conclusions of the work and shows possible future activities in the area of anodic films and ionic liquids.

Chapter I

State of the art

Thales, a Greek philosopher, discovered that if amber was rubbed with a woollen fabric it started to attract light items such as small pieces of wood, feathers and leaves. He was among the first to develop electricity in VI B.C. century. Nevertheless, two thousand years after that, knowledge about the electricity was hardly progressed at all. A new wave of studies in the field started in the beginning of XVII century. There was a considerable number of scientists who tried to explore the phenomenon. Particularly, Otto Von Guericke created the first electrical machine, Stephen Gray developed the conception of conductors and nonconductors, Pieter Van Musschenbroek discovered the principle of the Leyden jar (the first capacitor). Only in 1746, an American philosopher and statesman Benjamin Franklin suggested the single-fluid theory of electricity. In 1775, after the work of Luigi Galvani, Alessandro Volta announced the construction of the voltaic pile, the first electric battery, which transforms chemical energy to electrical energy. The main laws of electricity, such as Ampere law, that explained the nature of electric current, Ohm law, Faraday's law and many others, were developed during the next 50 years. The decomposition process of a compound by electricity was named "electrolysis" by Faraday in 1833. Furthermore, he discovered the laws of electrochemical decomposition: "the amount decomposed by an electrical current is proportional to the current flowing and to the time during which it flows; and when an electrolyte, or a series of electrolytes, is decomposed by an electric current, the components into which it is separated are always chemically equivalent". This moment can be considered the origin of Electrochemistry [1].

1. Valve metals

Application of anodic potential to a metallic electrode in water based electrolyte initiates the oxygen evolution. There is an additional process, namely the oxide layer formation on all metals, even before reaching the oxygen evolution potential [2]. These oxides can be divided into three groups. The first group is commonly formed on noble metals such as platinum, gold, iridium, ruthenium *etc*. and all of them are highly conductive oxides. The oxide layers with semiconductor properties (on nickel, tungsten, titanium, molybdenum *etc*.) belong to the second group. According to the same logic, the last group consists of the oxides with insulator properties, such as oxides of the valve metals: aluminium, tantalum, zirconium *etc*. The oxide layer formation is the main

reaction that takes place during anodic polarization of the third metals group (valve metals) [2].

There is a variety of factors that can influence formation of the oxide layer on the electrode interface (so-called passivation), for example, metal nature, composition of the electrolyte and electrochemical conditions. Alteration of these parameters (electrode material, solution composition, potential and current density, temperature of the solution *etc*.) will affect the electrochemical reaction on the anode.

Figure I. 1 shows the typical linear potential sweep curve from open circuit potential to anodic values. Initial potential growth leads to increasing of dissolution rate. However, after reaching the critical current, dissolution almost stops and further potential growth does not influence current significantly. The voltage with the highest current of dissolution is named a primary passivation potential, while the highest current is named the critical corrosion current. The current will start rising sharply at more positive potential, named breakdown potential. The second current increase occurs because of dielectric, chemical or structural film breakdown accompanied by intense electrolyte decomposition and dissolution of electrode material [2]. The stable region with a very low current density is a passive region. The barrier layer forms at this potential range. It is similar to the chemical barrier layers, such as those grown on iron in concentrated nitric solution or on aluminium in air, which block further reactions [2]. The biggest advantage of the valve metals is a high breakdown potential (wide passive region (Figure I. 1 dotted line)) which can be up to several hundred volts.

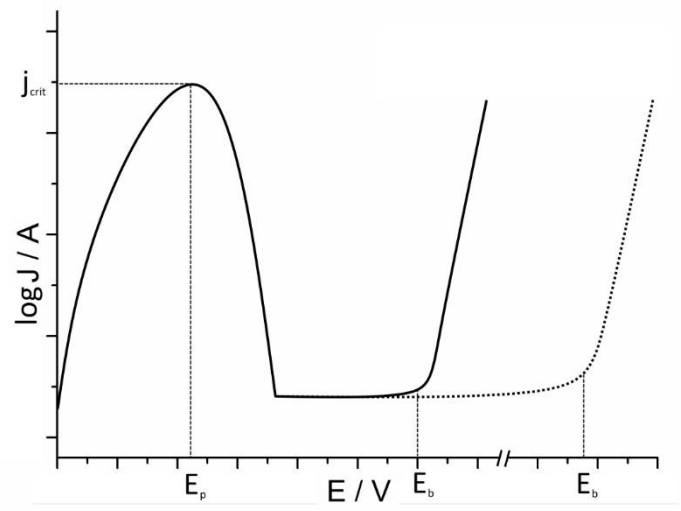

Figure I. 1 The typical current/potential dependence of anodic polarization with passivation behaviour.

It is possible to obtain various processes by changing voltage that subsequently leads to different types of surfaces on the electrode. All of these regimes are actively used for broad-ranging applications, for instance electropolishing [3, 4], metal passivation [5, 6], plasma electrolytic oxidation [7-9], porous anodic template formation [10-12].

1.1 Dense anodic films

As it was mentioned before, the valve metals have a wide passive region. At this potential range oxide thickness grows as the voltage increases. It leads to thick film formation if there are no aggressive ions capable to dissolve oxide [2].

The barrier anodic film forms via ions migration. As shown in Figure I. 2, metallic cation and oxygen anion migrate through the oxide layer in the opposite directions: from the metal surface to the oxide/electrolyte interface and from electrolyte to the metal, correspondingly. Cations combine with anions and form metal oxide [5]. The anodic reaction is the following:

$$M + zH_2O - 2ze^- \rightleftarrows MOz + 2zH^+ \quad (I.1)$$

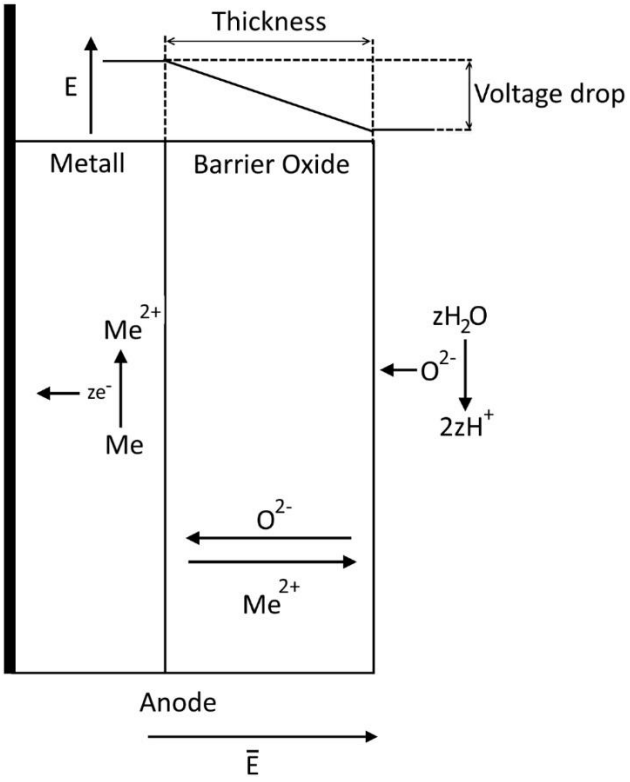

Figure I. 2 Schematic representation of the barrier anodic film formation on a metal surface.

Ideally, the barrier layer is a non-porous oxide film both electrons and ions conductive, although ions move only at high electric field strength [13]. The barrier layers are commonly characterized by low electronic, but high ionic conductivity. It means that ionic conductivity is predominant in this type of films and anodization will occur until the ionic current flow stops. The different factors, such as the electric field strength, nature of the metal and metal oxide, influence the ionic current. It is also clear that the resulting film thickness depends on the relation between the electric field and the ionic current density [13]. This relation is named an anodization ratio (oxide thickness nanometres per volt, nm V^{-1}). The oxide film thickness can be approximately calculated by multiplying the anodization ratio by the applied potential. Unfortunately, the anodization ratio strongly depends on the electrode material, the solution composition, temperature, applied current *etc*. The typical anodizing ratios for different valve metals are present in Table I. 1.

Table I. 1 Properties of several oxide/metal systems.

System	Anodization ratio (nm V^{-1})	Density (g cm^{-3})	Dielectric constant
Al/Al_2O_3	1.3-1.4 [5]	3.1	9 [21]
Ti/TiO_2	2-3 [14-18]	3.9	57 [17, 18]
Zr/ZrO_2	2.7-3.0 [19]	5.7	27 [22]
Ta/Ta_2O_5	1.6 [20]	8.5	21 [20]

1.1.1 Anodic alumina film

The history of the dense anodic film on aluminium has started more than 100 years ago. Over the course of decades aluminium and aluminium alloys attract a lot of attention due to the surface barrier layer. The layer protects the main metallic part from corrosion. It was found that the Al and Al-based alloys have a better corrosion resistance than that of iron and steels. Moreover, such property of the aluminium alloys as low density, makes it attractive for aircraft industry. After development of chemical- and electropolishing, aluminium surfaced are intensively used as reflectors. Additionally, a possibility to prepare anodic alumina films with different colours opens a wide prospect for its application in decoration. Since recently, anodic alumina films are intensively studied for creation metal-insulator-metal and metal-insulator-semiconductor devices, which can be used as sub-wavelength plasmonic waveguides [23, 24] and supercapacitors [25, 26].

Application of a positive potential to the aluminium electrode in a suitable, i.e. aggressive ions free, electrolyte such as ammonium pentaborate and ammonium citrate, leads to formation of compact and adherent film of the anodic alumina on the electrode interface according to the aforementioned general mechanism. After formation of the oxide monolayer, the oxidation should stop because of insulator properties of the alumina. Nevertheless, the barrier layer continue growing owing to ions migration in the high electric field. Obviously, continuous growth of the oxide requires continuous voltage increasing, otherwise the film becomes too thick and the anodic current flow stops [5]. The typical $I(t)$ curve for barrier layer formation at constant potential is presented in Figure I. 3.

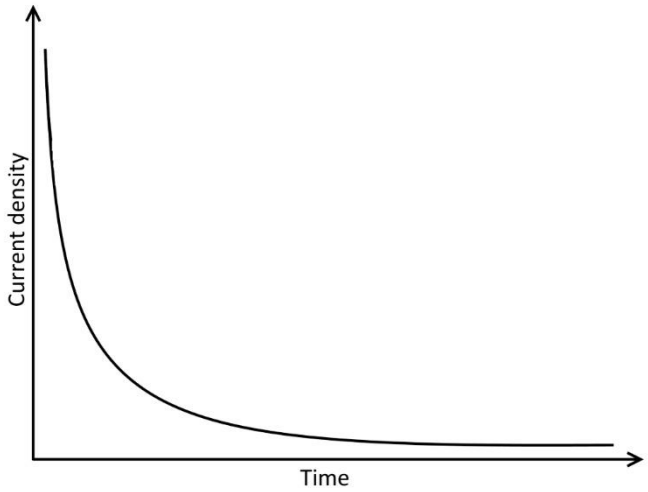

Figure I. 3 Typical current – time transient obtained at constant potential for barrier layer formation.

As it was specified in Table I. 1, the anodization ratio for alumina is about 1.4 nm V^{-1}, which matches to the high electric field, values higher than $7x10^6$ V cm^{-1} [27]. The thickness of the barrier layer can reach 0.7 μm at voltage of about 500 V [28]. Unfortunately, higher voltage is problematic to achieve because of electrical breakdown of a film.

The structure of the obtained film depends on temperature, applied voltage, solution composition *etc*. [13] The electron diffraction study has been done by Harrington and Nelson [29] for anodic alumina film formed at different electrolytes. The results showed that films are amorphous. The influence of temperature was investigated by several researchers. Firstly, it was reported by Taylor *et al*. [30] in 1945 that films remain amorphous independently on the electrolyte used up 100 V of anodization. Application of a higher voltage leads to formation of γ-Al_2O_3 phase detected by XRD. 15 years later, similar conclusions were made by Stirland and Bicknell [31]. They used the electron diffraction for the film examination. The authors found that at a voltage below 100 V the barrier film is absolutely amorphous. The films prepared at a voltage above 100 V remained mostly amorphous, but some γ-alumina phase was also detected.

Composition of the barrier layer depends on the electrolyte used because of the anions incorporation. In conformity with the ions nature, Thompson *et al*. [32, 33] divided all anions in three groups:

- mobile inwards (phosphate, sulfate);
- immobile (borate, silicate);

- mobile outwards (tungstate, molybdate);

The ions from the first group incorporate into the layer and migrate inside the film under electric field because of their negative charge. The immobile species are adsorbed on the electrode surface and afterwards they incorporate into the film as oxide (B_2O_3 and SiO_2). The species from the third group move from the inner part of the oxide to the alumina/electrolyte interface. This tendency can be explained by anions oxidation to cations during anodization with subsequent cations movement in the same direction with Al^{3+} under the influence of electric field [32]. Thompson *et al*. [32] obtained the incorporation level of the electrolyte species in the range of 0.6 – 5.5 at%. Moreover, the amount of incorporated ions also depends on the anodization voltage and the electrolyte temperature. It was shown by Mason [34] that at higher current density and lower solution temperature the anodic film was richer in extra species. The same behavior was found for barrier film on tantalum and niobium [35]. The preparation of a relatively pure anodic alumina layer is described by Skeldon *et al*. [36]. The authors used potassium hydroxide solution as electrolyte. Since the only OH^- anions were present, the obtained film was free of additional elements.

Although in some cases, the water incorporation during the film formation can be detected, but nonporous films are generally observed to be anhydrous. The amount of incorporated water is determined by the formation conditions. Furthermore, no water is incorporated in a free form, commonly it is hydroxide or hydrated oxide [13].

1.1.2 Anodic titania film

Titanium standard potential value is almost equal to that of aluminium: -1.63 V and -1.66 V for Ti/Ti^{2+} and Al/Al^{3+}, correspondingly. Thereby, Ti is a very active metal, although shows typical properties of the valve metals. Titanium does not corrode in air only due to thin oxide film on the interface which forms immediately after a contact with oxygen. The titanium dioxide films have distinguished properties, namely catalytic and photocatalytic [37, 38], self-cleaning and wetting [39]. The TiO_2 films find use in solar cells [40] and optical devices [41].

Generally, anodic titania and alumina are resembling materials, for example, the mechanism of the titania formation is comparable to that of alumina and other barrier films. At the same time, alumina is an insulator as, while titania is a n-type semiconductor with a comparatively high electronic conductivity. Therefore, there are two reactions that

simultaneously. The first, titanium oxidation, occurs with ionic current under high electric field and is responsible for the film growth:

$$Ti + 2H_2O \rightleftarrows TiO_2 + 4H^+ + 4e^- \quad (I.2)$$

The second one is the oxygen oxidation on the barrier/electrolyte interface (electronic current) and does not contribute to the film growth [42].

The number of possible electrolytes applicable for the titania film formation is much bigger than those available for alumina preparation because of titania insensitivity to different aggressive ions. Hwang and Hwang [43] have studied kinetics of the titanium anodization in a 0.5M sulfuric acid. The authors applied atomic absorption spectroscopy for calculation of the titanium concentration in the solution after anodization and concluded that the dissolution rate is exiguous. There are series of publications reporting on successful preparation of thin titania layers in sulfuric acid with different concentrations [18, 44, 45], phosphoric acid [44, 46], sodium hydroxide [45] *etc*. During the film formation the electrolyte anions migrate inside the titania film in the same manner as described above for the case of aluminium anodization. Moreover, the nature and concentration of the solution affect not only the final composition of the titania layer, but also the oxide growth behaviours. Sul *et al*. [47] investigated properties of anodic oxide layer as function of current density, the electrolyte compositions and concentrations, and temperature. All of these parameters have a significant influence on anodic formation factor, current efficiency, anodic forming voltage and oxide forming rate. Moreover, the formation rate was found to have a strong impact on surface properties of the layer. Blackwood *et al*. [48] found that a higher formation rate results in a higher defect concentration. The dielectric constant is also affected by the growth rate.

The regime of film preparation influences the crystallinity of the film. There are three main characteristics determining the film crystallinity, namely temperature, current and voltage. The crystalline state of an anodic oxide film on titanium was found to be dependent on the formation potential and the electrolyte temperature (Shibata and Zhu [49]). Film crystallization occurs at potentials that are more positive than 7.0 V or at temperatures above 333 K. Ohtsuka *et al*. also confirmed that at some critical voltage, amorphous titania transforms to crystalline anatase phase [50]. Furthermore, the solution concentration is critical for the titania crystal structure. Diamanti and Pedeferri [51] investigated the influence of oxidation parameters on the anodic titanium dioxide layer. The authors have demonstrated that at higher potential titania became more crystalline as

it was also shown in Shibata and Ohtsuka works. Moreover, a film growth at lower current density and/or at lower concentration of the electrolyte results in a smaller fraction of anatase in the oxide.

1.2 Porous anodic templates

In the electrolytes that contain aggressive ions, porous oxide film and not only dense barrier layers form (Figure I. 4). The ions considered as aggressive are different for different metals. For instance, porous alumina film can be easily prepared in oxalic, sulphuric, phosphoric and tartaric acids containing solutions. However, most of the valve metals demand the presence of the fluoride anions in the electrolyte. Oxidation of titanium, zirconium, hafnium, tungsten, thallium, vanadium and even iron in the appropriate electrolytes is accompanied with formation of porous oxide layers. Moreover, optimization of the anodization conditions such as electrolyte composition, voltage, temperature, results in formation of ordered pores, which are arranged perpendicularly to the substrate (Figure I. 4).

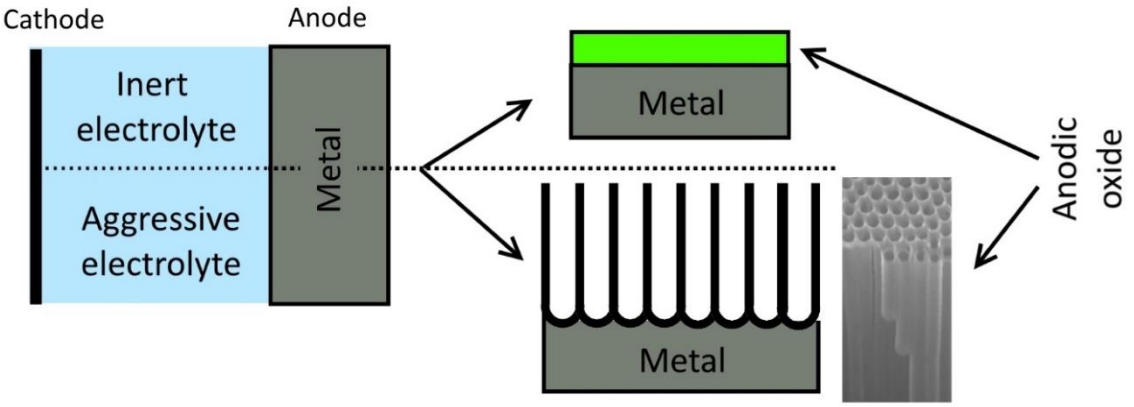

Figure I. 4 Valve metals electrooxidation, depending on solution composition, occurs with formation of dense barrier or porous anodic film.

The porous anodic templates on transition metals have ubiquitous applications due to the electronic, chemical and optical properties. For example, ZrO_2, WO_3, Al_2O_3, Ta_2O_5, TiO_2 *etc*. have promising properties, which allow them to be used in many application such as solar energy conversion [52, 53], energy [54] and data [55] storage, as well as in optical [55, 56], photocatalytic [57-60], biomedical [59], and electrochromic devices [61, 62]. Moreover, titania shows perfect biocompatibility. This characteristic promotes the use of titania in medical technologies, such as in orthopedics and dentistry.

1.2.1 Porous anodic alumina

Porous anodic alumina has been known since 1953 [63], but it was given a due consideration only in 1995, after development of highly ordered hexagonal pore structures by Masuda *et al*. [64]. This material is under active investigation during last decades as template or host system for formation of nanostructures such as nanorods, nanowires, nanodots, nanotubes *etc*.

The porous anodic alumina (PAA) is mainly synthesized in acid base electrolyte [55] with pH lower than 5. Low pH is one of the most crucial factors necessary for dissolution of the alumina and formation of a porous structure. Different acids and mixtures of acids can be used. Some possible electrolytes as well as the anodization conditions are presented in Table I. 2 (based on Chu's *et al*. work [65]).

Table I. 2 Examples of electrolytes and anodization conditions for PAA preparation.

Electrolyte	Concentration	Voltage (V)	Temperature (K)	Interpore distance (nm)
Oxalic	0.5 wt%	100	276	220
	0.25 wt%	160	274	440
Phosphoric	2.5 vol%	195	273	420
	1 vol%	235	273	480
Sulfuric	10 vol%	70	273	130
Tartaric	2 wt%	235	278	600
Malic	4 wt%	220	283	550
	2 wt%	450	283	950
Citric	4 wt%	270	293	650
	2 wt%	370	293	980
Glycolic	10 wt%	50	283	150
	1 wt%	150	283	320

Results of the Chu's *et al*. work clearly showed ample opportunities of the PAA use as a template due to wide ranges of interpore distance, pore diameter and pore density [55] (from 10^8 to 10^{12} pores cm^{-2}). Three most common conditions used for PAA preparation are the following: sulfuric acid at 25 V [66], oxalic acid at 40 V [64] and phosphoric acid at 195 V [67, 68].

Furthermore, the pore diameter can be tuned by immersion of the template in acid electrolytes without application of any potential. It leads to dissolution of the alumina and consequently to pores widening. The typical SEM images of the anodic alumina oxide after pore widening are shown in Figure I. 5.

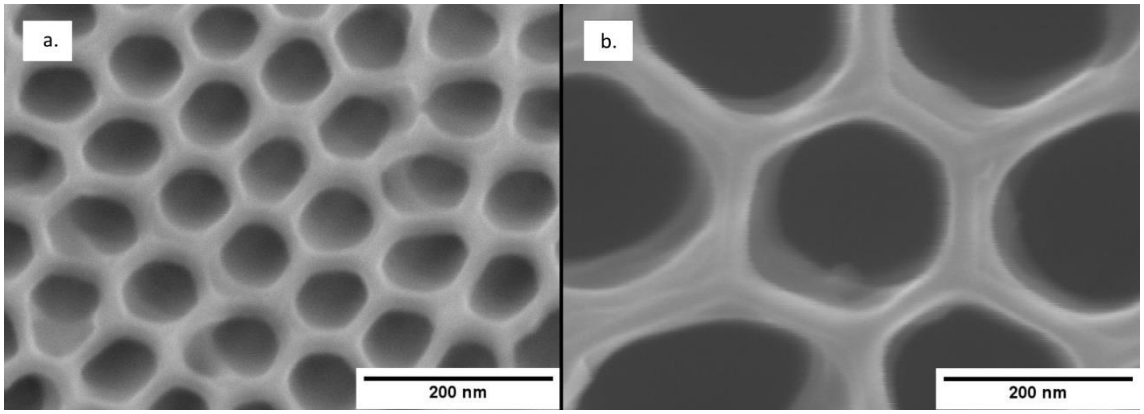

Figure I. 5 Typical porous alumina templates prepared in a 3M oxalic acid at 40 V (a) and in a 8 wt% phosphoric acid at 152 V (b) after pore widening in the same anodization electrolytes at 40ºC for 2.5 and 0.5 h correspondingly.

The growth mechanism of the self-organized alumina nanopores is still largely unknown. Electrochemical reactions are the same for both porous and dense anodic films formation, but chemical dissolution takes place only during porous film preparation. The cathode reaction is a hydrogen evolution:

$$2H^+ + 2e^- \rightleftarrows H_2 \quad (I.3)$$

$$2H_2O + 2e^- \rightleftarrows H_2 + 2OH^- \quad (I.4)$$

Reactions on the anode should be divided in two groups:

- electrochemical oxidation (at the metal/oxide interface):

$$Al^0 - 3e^- \rightleftarrows Al^{3+} \quad (I.5)$$

$$2Al^0 + 6OH^- \rightleftarrows Al_2O_3 + 3H_2O + 6e^- \quad (I.6)$$

- chemical and field-enhanced chemical dissolution of the oxide layer in aggressive electrolyte (at the oxide/electrolyte interface):

$$Al_2O_3 + 6H^+ \rightleftarrows 2Al^{3+} + 3H_2O \quad (I.7)$$

However, simple chemical dissolution will not result in high-ordered film formation. Up to date, the most acknowledged mechanisms of ordering are based on mechanical stress and field assisted dissolution [69-72]. The pore growth can be separated in four successive steps:

- formation of the compact oxide;
- random chemical etching;
- pores nucleation;
- pores growth in steady-state conditions;

All the steps reflect to the current time transient which is schematically represented on Figure I. 6 and described by Parkhutik [73].

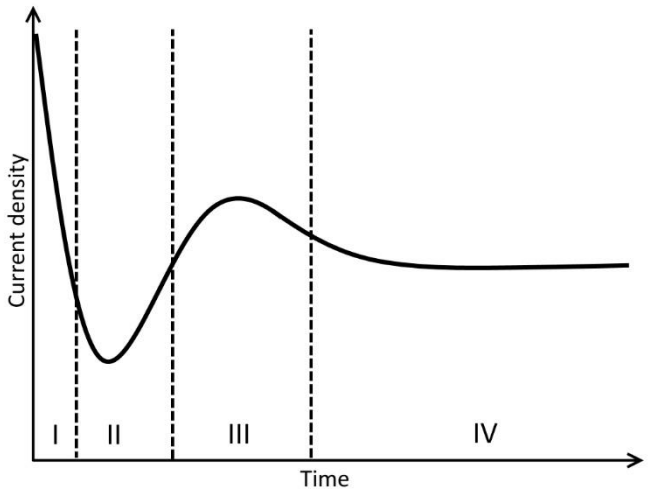

Figure I. 6 Typical current time transient obtained during aluminium anodization in acid electrolyte (adapted from Parkhutik [73]).

At the beginning of anodization (zone I), the aluminium surface is being covered by dense alumina. Since this bulk alumina film is insulator, it provides fast decreasing of the current density. In zone I, the current time transient has the same shape as that of a transient when anodizing in a neutral electrolyte. The barrier layer is uniform in large scale and the electric field is constant at the whole sample surface at that moment as shown in Figure I. 7 a [74]. The next stage is possible only in aggressive electrolyte and characterized by increase of the current density (Figure I. 6, zone II). During this stage, some pits occur on the oxide surface due to random chemical etching, stress after the oxide formation, impurities *etc*. In these places, alumina layer is thinner than in the rest of the film and it results in lower resistance of the film and consequently in higher local

current. Moreover, the electric field is stronger in vicinity of the irregularities of the surface. As a result, chemical dissolution, superimposed by field-enhanced dissolution, is faster in these pits than in the bulk oxide (Figure I. 7 b). However, not all the surface concavities will transform into pores, since some of them will close with time and the pore formation will stop. This process corresponds to the small current drop in the zone III (Figure I. 6).

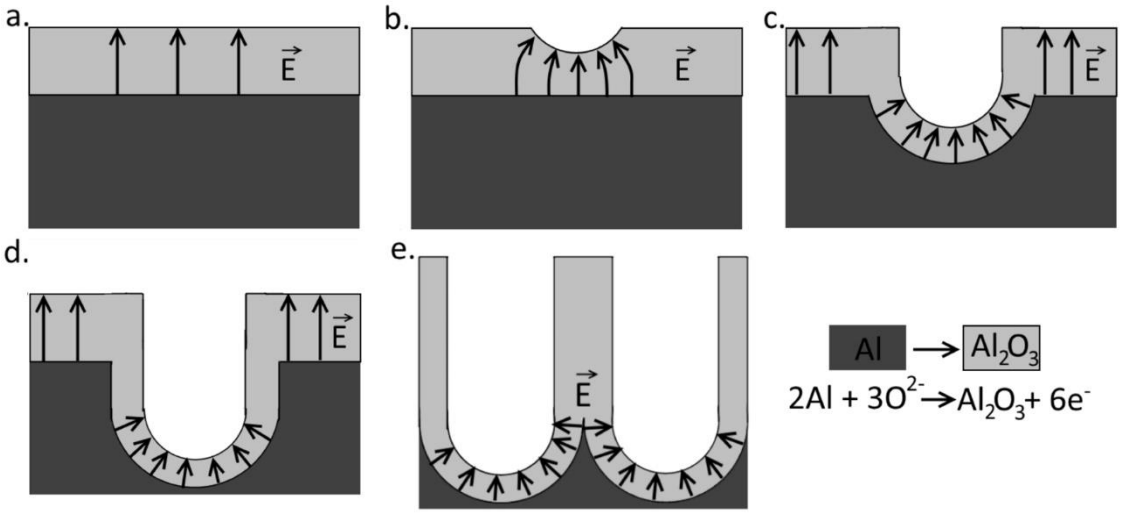

Figure I. 7 Schematic representation of the alumina pore formation by anodization: (a) formation of the planar layer with a uniform thickness; (b) onset of surface irregularities that change the field distribution in the layer; (c) initiation of the pore growing; (d) pore growing at steady-state conditions; (e) pores self-ordering (adapted from Su *et al.* [74]).

After the first three stages, the surface is stable and pores grow in a steady-state condition. The zone IV corresponds to the stable growth and is characterized by constant current density (Figure I. 6). Physically, at this stage, oxidation of the aluminium and dissolution of the alumina occur simultaneously, but dissolution of the pore wall is slower than that of the bottom barrier, where a stronger electrical field enhances the process (Figure I. 7 c, d). This difference in the rates of dissolution leads to pore formation. Duration of the pore growth depends on several factors such as type and concentration of the electrolyte, voltage, temperature and stirring. At the point, when the rate of chemical dissolution of the alumina will be the same as the oxidation rate, the thickness of the porous layer is kept constant. This point corresponds to maximal thickness of the template

(it is possible to have thickness higher than 50 µm). All the above described stages were observed directly and confirmed by Thompson *et al*. with the use of TEM [71].

Practically, the pores density is high and it could strongly affect the neighbour pores (Figure I. 7 e). According to mechanical stress model [68-70, 74], volume of the anodic alumina is twice bigger than volume of aluminium which was used for anodization. Consequently, the mechanical stresses appear in the oxide/metal interface owing to volume enlargement. Repulsive forces between the boundary pores determine self-organization in hexagonal structure.

In principle, ordered anodic alumina template can be manufactured using a single step anodization, but it is hardly achievable because of the random pore initiation. In 1995, Masuda and Fukuda introduced the two-step anodization approach [64] schematically represented in Figure I. 8.

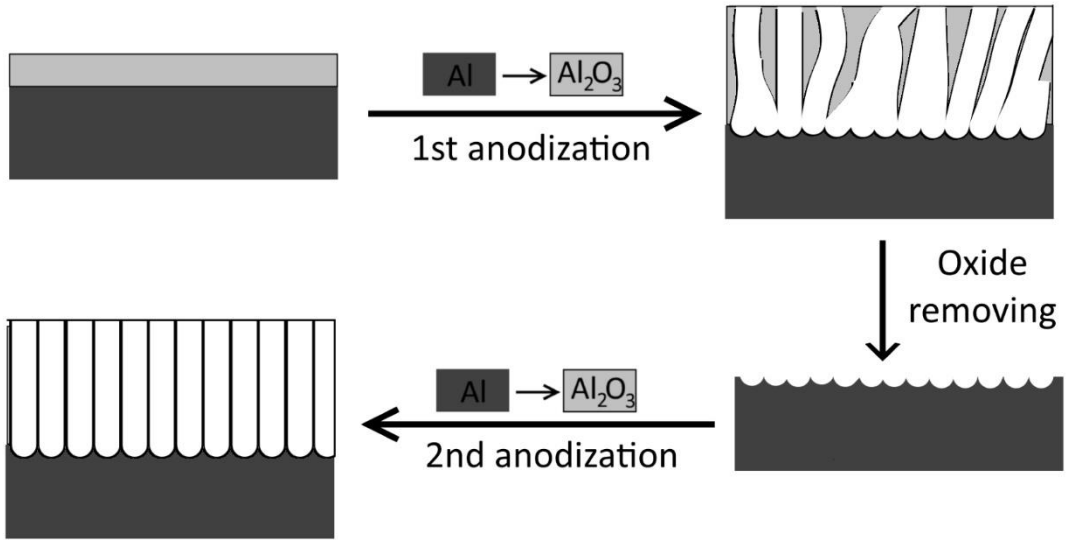

Figure I. 8 Schematic representation of the two-step anodization.

The first anodization is normally performed continuously during several hours. This step consists on formation of highly ordered pores structure at the metal/oxide interface and the aluminium surface texturing with a long-range order of dimples. Nevertheless, the upper part of the obtained porous oxide layer is irregular. After the first anodization, the electrode is immersed in a solution which dissolves the anodic alumina without any reaction with aluminium substrate. Commonly, solution of chromium (VI) oxide in phosphoric acid is used for this aim [75, 76]. The alumina dissolution leads to removal of the irregular porous layer and revealing of the periodically arranged dimples on the aluminium surface. The second step is normally carried out at the same conditions

as the first one. These ordered dimples form the initiation sites for growth of new pores. It excludes any random distribution of pores at the pore nucleation step and the new structure has long range order over the whole length of the pores [76-78].

Alternatively, pre-textured aluminium surface with controllable interpore distance can be manufactured by several techniques, such as mechanical imprinting [79-81], focused-ion-beam lithography [82-84], holographic lithography[85]. The key benefit of all these techniques is a single step process, which saves time and makes parameters of the template fully controllable. Unfortunately, the equipment for the aluminium surface pre-texturing is sophisticated and expensive.

There are several important points to be mentioned regarding the pore ordering. One can see, irregularities in pores structure are mainly concentrated in vicinities of the aluminium grain boundaries. Therefore, aluminium is annealed at near melting point temperature (500-600^{o}C) for several hours in order to increase the grain size and decrease the grains boundary thereby decreasing the amount of irregularities. Moreover, the purity of aluminium plays an important role because impurities lead to deviation in volume expansion of the oxide and, as a result, the disordering of the pores occurs. Furthermore, as it was shown before (on example of dimples), the surface roughness affects the pore ordering. Consequently, the surface smoothening is preferred and typically performed by means of electropolishing in mixture of the perchloric acid and ethanol [86, 87].

1.2.2 Porous anodic titania

Preparation of porous anodic titania has firstly reported by Zwilling *et al*. in 1999 [88]. Using a chromic acid electrolytes with hydrofluoric acid, a porous film of about 0.5 μm thick was obtained. The Zwilling *et al*. work shows the importance of the fluoride ions presence in the electrolyte for manufacturing of the porous layer. In the following years, several electrolytes for PAT preparation were used, such as the water based ones with sulphate [89], phosphate [90, 91], acetate [92] ions or in organic electrolytes [93] which were based on glycerol [94], ionic liquids [95], dimethyl sulfoxide [96]. In all the mentioned cases, the electrolytes contained also fluoride ions. Based on those studies, several dependences were found. Macak *et al*. [89] showed that at neutral pH, the maximal film thickness is about 2.5 μm while it is ≈1 μm [91] when preparing in acid electrolyte. Anodization in organic based electrolyte such as ethylene glycol [97, 98] results in formation of high-ordered and long (more than 250 μm [98]) tubes with smooth

walls, in contrast to the situation with water based electrolyte, where sidewall ripples were found. Furthermore, the two-step technique was used for preparation of high-ordered titania tubes in the same manner as described above for the case of porous anodic alumina [99].

The self-ordering and pore formation mechanism of both the porous anodic titania and the porous anodic alumina are similar. Initially, the dense barrier layer is formed on the electrode interface, then the pores nucleate randomly on the pits and defects followed by steady-state pore growth. The similarity of the current time transient and the steps during PAT preparation with aluminium oxidation (Figure I. 6) was proved in several works [100, 101]. Moreover, SEM studies confirmed that the main steps of PAT preparation and PAA preparation are the same.

Despite the obvious resemblance of the anodization of aluminium and titanium, there are some critical distinctions. The reaction on cathode is the same:

$$2H^+ + 2e^- \rightleftarrows H_2 \quad (I.8)$$

$$2H_2O + 2e^- \rightleftarrows H_2 + 2OH^- \quad (I.9)$$

Anodic oxidation of titanium occurs by a general mechanism for all valve metals:

$$Ti + 2H_2O \rightleftarrows TiO_2 + 4H^+ + 4e^- \quad (I.10)$$

However, the pore formation is impossible without dissolution of the oxide, that is why fluoride ions are added to solution. Titanium ions form soluble complexes with F^- and then these species go to the electrolyte. There are two possible ways of the complexation:

- chemical dissolution of the titanium dioxide;

$$TiO_2 + 6F^- + 4H^+ \rightleftarrows [TiF_6]^{2-} + 2H_2O \quad (I.11)$$

- direct complexation of the Ti^{4+} cations on the electrode/electrolyte interface

$$Ti^{4+} + 6F^- \rightleftarrows [TiF_6]^{2-} \quad (I.12)$$

The pores formation occurs as a result of competition between anodic oxide formation and oxide dissolution [53] in which the fluoride ions concentration plays an important role. The compact layer only forms at the very low concentration of F^- (lower

than 0.05% (wt.)). When concentration of fluoride ions is higher than 1% (wt.), the electropolishing happens due to solubility of the $[TiF_6]^{2-}$ species. Therefore, formation of the porous titania layer is only possible at the moderate concentration of the fluorides [102, 103].

One more distinction between titania and alumina films is the microstructure structure. Ordered anodic titania structure is often called tubes and not pores. However, the tubes near the bottom are compact and have hexagonal organization which is very similar to the pores arrangement in anodic alumina. One can see, that the tubes formation from the pores during anodization [99, 102] cannot be explained by a standard mechanism. The important step for understanding the difference between PAA and PAT was the development of multi-layer structure of a titania pore [104-107]. Schematic representation of the pore configuration is shown in Figure I. 9. Albu *et al*. [105] have found three main layers in a pore:

- outer shell of the tube (OST) mainly formed by TiO_2 with a small amount of F^-.
- inner shell of the tube (IST) formed by titanium oxide and hydroxide and containing the electrolyte components.
- fluoride-rich layer (FLR) formed by TiO_2 with a considerable amount of F^-.

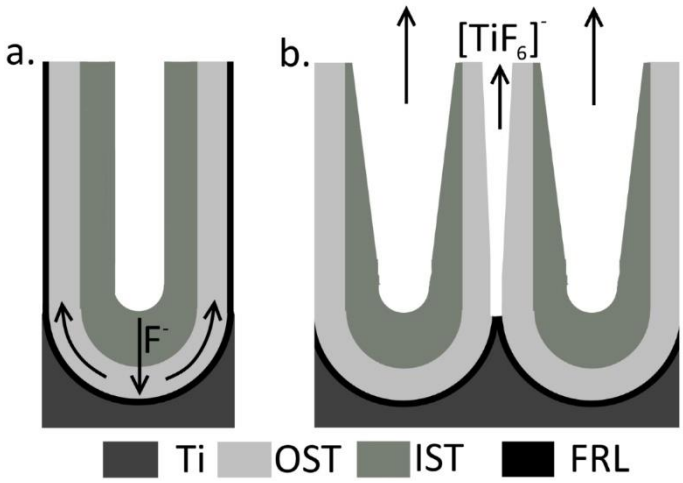

Figure I. 9 Schematic representation of a titanium pore structure with outer (OST) and inner (IST) oxide shell and a fluoride-rich layer (FRL); a) ideal condition without layer dissolution and b) real condition (adapted from Albu *et al*. [105]).

The IST layer is crumbly in comparison to the dense OST one and the IST layer is dissolved in electrolyte much easier and faster. Dissolution of the inner shell is

responsible for formation of a common V-shape of the tube [99, 104-107]. On the other hand, the OST layer has almost constant thickness along the whole pore length [105]. There is a number of works where the fluoride-rich layer was described as a very thin film on the border between titanium substrate and outer shell. The presence of this region is in agreement with the anodization mechanism. In high electric field, the negative ions, such as O^{2-}, OH^{-}, F^{-}, move through the oxide until the metal interface where they react with the substrate. Fluoride ion is very small and its migration occurs much faster than oxygen or hydroxide ions, which results in formation of a fluoride-rich layer on the metal/oxide interface. The thin layer (FRL) moves from the bottom to the tube walls according to the flow concept introduced by Hebert *et al*. [108]. The model shows that the viscous titania drifts up the pore walls induced by the forces which are originated by compressive stress and ionic movement. This titania flowing leads to growth of the tubes (Figure I. 9 a). It should be also mentioned that, in a real condition, all electrolytes contain water and it is mandatory for the titanium oxidation. The water dissolves the IST layer together with FLR and exactly because of the solubility of FLR the tube structure forms (Figure I. 9 b). Furthermore, Berger *et al*. [107] studied the influence of water in ethylene glycol electrolyte on the growth of the TiO_2 tubes. It was confirmed that at low water quantity, the dissolution of the fluoride-rich region is limited and tubes have cylindrical shape. In contrast, tapered tubes form when quantity of water is too high.

As-formed titania tubes are commonly amorphous [109]; a nanocrystaline anatase phase was detected in the tubes after anodization at relatively high voltage [94]. Crystalline state strongly affects properties of the titania layer, such as conductivity [109], photoresponse *etc*. For this reason, a considerable work was performed to investigate crystallization of titania films. Anatase and rutile are two main phases which can be obtained by annealing under oxidation condition (air or oxygen atmosphere) [89, 105, 110]. Crystallization of amorphous titania into anatase begins at relatively low temperature (250^{o}C) [94, 109, 111]. Increase of temperature up to 450^{o}C results in higher concentration of anatase phase. Moreover, annealing at 250^{o}C for a longer time (up to 20 h) also leads to a significant increase of the anatase fraction [109]. At temperature above 450^{o}C, the rutile phase is also detected in the layer [109] and at 900^{o}C, titania is completely converted to rutile [102].

Apart from crystalline state and crystal structure, annealing can affect composition of oxide film. Thus, reduction of the Ti^{4+} species to Ti^{3+}, which occurs when annealing in inert atmosphere (e.g. in Ar), impacts the conductivity of film. Additionally, it is well-

known that as-prepared nanotubes contain different species from electrolyte, such as hydroxide, fluoride, phosphate, carbon *etc*. These species can be also removed by annealing [105, 110].

Application of the TiO_2 nanostructures is commonly based on some unique behaviours of titania such as electronic, ionic and biocompatible. Moreover, the large surface area is an important factor as well [102]. For example, biocompatibility of the titanium and titanium based alloys allows wide application of these materials as implants. The implant surface is independent from the shape and it can be covered by anodic film with different tube sizes. It helps to use the best condition for the cell adhesion [112]. Moreover, the fast hydroxyapatite formation on the pores surface attracts a lot of attention in bone implants [59]. Semiconducting properties of titania nanosructures films found applications in photocatalytic [113, 114] and solar cells devices [115, 116].

1.2.3 Preparation of 1-D nanoparticles through template assisted electrodeposition

Templates assisted electrodeposition is well-priced and one of the most convenient technique for 1-D nanoparticles preparation. There is a variety of systems used for this aim, for instance Si/SiO_2 [117-119], polymer matrix [120, 121]. Nevertheless, most of the studies in the area were focused on the porous anodic templates due to simplicity of both preparation and parameters control. Unfortunately, their application templates for electrosynthesis requires additional modifications.

A disadvantage of application of porous anodic templates arises from the presence of a barrier layer at the bottom of pores. Commonly, the oxide film, formed as a result of anodization or immediate oxidation of valve metals, acts as a high resistive medium impairing the flow of current. One typical and frequently used template with this kind of problem is anodic aluminium oxide.

Nowadays, several approaches are actively used to solve the problem. The first, and probably the most common one, is the use of detached porous film. A multi-stage process of removal of both substrate and the barrier layer followed by contact deposition is typically applied [122]. In the first stage, a comparatively thick PAA layer is grown on the aluminium foil (Figure I. 10 a). Then, metallic aluminium (substrate) is removed by chemical etching in solution of $HgCl_2$ [123], $CuCl_2$ + HCl [124] or $SnCl_4$ [125] (Figure I. 10 b). Nonetheless, after the substrate is removed, the pores are still closed in one side.

Pores opening is commonly carried out in a diluted acidic or basic solution (Figure I. 10 c). The last step is metallization of the one side of the membrane. It can be performed by evaporation [123-125], filtration [126] or some other techniques (Figure I. 10 d). The result of these procedures is the highly-ordered matrix with insulating walls and conducting bottom. The free-standing membranes were successfully used for preparation of different metallic [125, 127], semiconductor [128, 129], multilayer [130] 1-D nanoparticles and nanowires via electrodeposition.

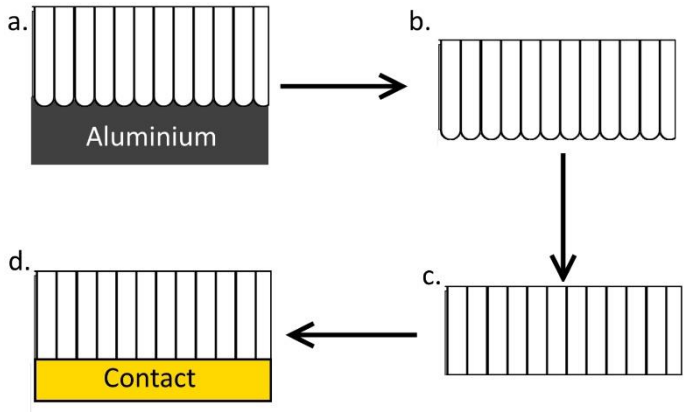

Figure I. 10 Schematic representation of the free-standing PAA template preparation. a) preparation of the PAA template; b) dissolution of the substrate; c) pores opening; d) contact evaporation.

Another technique is a deposition in the non-detached PAA film after barrier cracking or thinning. The barrier modification is performed by decreasing of the voltage at the end of anodization or/and chemical etching [131, 132]. The thickness of the barrier layer is proportional to the applied voltage. Hence, a decrease of the potential at the end of anodization leads to a decrease of the barrier layer thickness. Thus, electrodeposition occurs much easier in the modified template. However, there are no techniques that can remove absolutely the alumina layer due to immediate formation of the oxide layer on aluminium at ambient conditions. Hence, it is necessary to use AC regime and comparatively high voltage (10-20 V) for deposition [133].

In spite of the fact that titania barrier layer is conductive, far less works on electrodeposition in PAT template are available today. Because of the biggest weakness of the PAT, namely conductive walls, electrodeposition occurs in the whole pore surface and the pores are sealed on the top [134, 135]. In general, the approaches for electrodeposition inside the titania nanotubes are similar to the previously showed for

alumina: AC (pulse) electrodeposition [136, 137], electrodeposition in detached template [138] and bottom modification. Bottom modification of PAT is different from that applicable for PAA and based on improving the barrier conductivity without changing the walls. One of the most considerable and interesting work in the area was performed by Macak *et al* [139]. The authors increased conductivity of the bottom part of the tubes via proton intercalation ($Ti^{4+} + e^- + H^+ = Ti^{3+}H^+$). In this way, successful bottom-up filling of the PAT with copper from a water-based solution was achieved.

2. Ionic liquids and DES

Electroplating was used for the first time in XIX century to deposit thin gold coatings on various jewellery and decorative products. Nowadays, electrodeposition gains widespread use in all areas of industry, for example, electronics [140], corrosion protection[141], metal production. Electrodeposition is considered as a cheap and appropriate method for preparation of coatings with diverse thicknesses, compositions for variety of applications [142]. Unfortunately, electrodeposition from the most classical and generally available solvent, water, often requires the use of toxic components in solution. In addition, it can be followed by undesirable extra processes (hydrogen reduction provokes the loss of efficiency and, what is more important, it could lead to hydrogen embrittlement). Varied media for deposition, such as organic solvents, eutectic mixture and ionic liquids, have been investigated as methods to avoid these secondary processes [2].

The main driving force to study electrochemistry of non-aqueous solutions is the electrodeposition of certain metals such as titanium, aluminium and tungsten. These metals are well-known as materials with excellent corrosion resistance because of the thin oxide layer formed in the ambient conditions. It was observed that the layer is very stable and prevents corrosion. On the other hand, the same factor (oxide layer formation) makes the electrodeposition of these metals from aqueous media impossible. Organic solvents and melting salts are not suitable for common applications because of high volatility, toxicity, flammable and high power consumption.

Ionic liquid is a good compromise between organic solvents and melting salts. A typical definition of an ionic liquid is “low-melting salts (melting-point typically <100^{o}C) obtained by the combination of large organic cations with a variety of anions” [143]. Usually, ionic materials have a high lattice energy and their melting temperature is high.

In general, one part of the ionic liquids is a big organic ion where the charge is delocalized. It allows to decrease the lattice energy and to have liquid ionic materials at room temperature [144]. Typical ions, which form ionic liquids, are presented in Table I. 3.

Table I. 3 Typical ions of ionic liquids.

Cations		Anions	
Name	Structure	Name	Structure
Ammonium	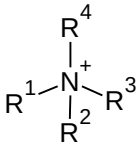	Tetrafluoroborate	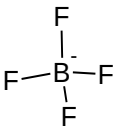
Imidazolium	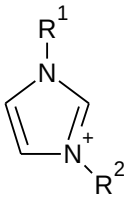	Hexafluorophosphate	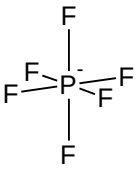
Phosphonium	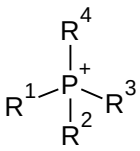	Halogens	F-, Cl-, Br-, I-
Piperidinium	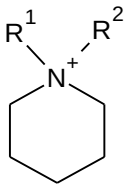	Thiocianate	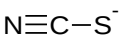
Pyridinium	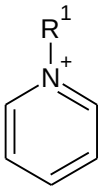	Dicyanamide	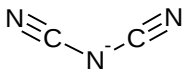
Pyrrolidinium	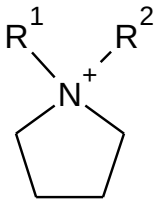	Trifluoroacetate	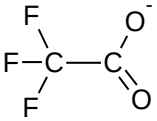
Sulfonium	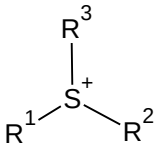	Methylsulfonate	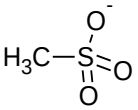

2.1 Ionic liquids

Conventional ionic liquids can be divided into two big groups [144, 145]. Electrodeposition of metals from ionic liquids was firstly studied in $AlCl_3$-based ionic liquids, which form the first group (first generation). This electrolyte contains two components: the Lewis acid (most commonly $AlCl_3$ or $AlBr_3$) and a 1,3-dialkylimidazolium, alkylpyridinium or quaternary ammonium compound. The most common method for synthesis of this type of ionic liquids is a solid state reaction by mixing the components under active stirring. The preparation should be performed under inert atmosphere by using Schlenk techniques or glove box.

Mixing of a quaternary halide salt where the cation is typically an amine, phosphine or sulfide (Cat^+Hal^-) with a Lewis acid ($MeHal_x$) leads to formation of the ($Cat^+MeHal^-_{x+1}$) salt. The most frequently used quaternary salt is 1-ethyl-3-methylimidazolium chloride ([EMIM]Cl) and the Lewis acid is $AlCl_3$. Unfortunately, composition of the final electrolyte is rather uncertain because it has a strong dependence on the ratio organic salt : Lewis acid and on temperature [145]. Reactions that occur during the ILs synthesis are the following:

$$[EMIM]^+Cl^- + AlCl_3 \rightleftarrows [EMIM]^+[AlCl_4]^- \quad (I.13)$$

$$[EMIM]^+[AlCl_4]^- + AlCl_3 \rightleftarrows [EMIM]^+[Al_2Cl_7]^- \quad (I.14)$$

$$[EMIM]^+[Al_2Cl_7]^- + AlCl_3 \rightleftarrows [EMIM]^+[Al_3Cl_{10}]^- \quad (I.15)$$

The ionic liquids can be also divided into three groups according to their acidity by analogy with water. Autosolvolysis of water can be described as:

$$2H_2O \rightleftarrows H_3O^+ + OH^- \quad (I.16)$$

In the same manner autosolvolysis reaction of $[AlCl_4]^-$ species can be written as:

$$2[AlCl_4]^- \rightleftarrows [Al_2Cl_7]^- + Cl^- \quad (I.17)$$

The Lewis acidity/basicity can be easily changed by means of variation of the ratio between [EMIM]Cl and $AlCl_3$, because Cl^- is a typical Lewis base and $[Al_2Cl_7]^-$ is a Lewis acid (in water, these are OH^- and H^+, respectively). For the foregoing reasons, the three groups of the ionic liquids are:

1) Acidic (with an excess of $[Al_2Cl_7]^-$ (i.e., [EMIM]Cl:$AlCl_3$ < 0.5 (molar ratio)).
2) Basic (with an excess of Cl^- (i.e., [EMIM]Cl:$AlCl_3$ > 0.5 (molar ratio)).
3) Neutral (with a molar ratio [EMIM]Cl:$AlCl_3$ = 0.5).

It is well known that electrodeposition of metals from a water solution often is carried out at low or high pH and it has a great influence on the deposition process. The analogous situation with ILs and Lewis acidity was found.

A representative of the second generation or discrete ions ionic liquids was firstly reported by Wilkes and Zaworotko in 1992 [146]. It consisted of 1-ethyl-3-methylimidazolium cation and tetrafluoroborate anion. In contrast to the first generation electrolyte, the second one has isolated ions. Nowadays, the discrete ions ILs attract a great attention due to a wider electrochemical window [147] that allows electrodeposition of reactive metals. Moreover, ILs based on tetrafluoroborate and hexafluorophosphate are water insensitive despite the fact that slow hydrolyse with HF evolution [148] occurs. The systems with similar physical properties but absolutely water insensitive were prepared with tri-fluromethanesulphonate ($CF_3SO_3^-$) and bis-(trifluoromethanesulphonyl)imide [$(CF_3SO_2)_2N^-$] [149]. There are available several reviews about these ILs [144, 145].

2.2 Deep eutectic based ionic liquids

The ideal mixture of two components, without any interaction between them, has linear dependence of the melting temperature on composition. In fact, mixture of two different compounds has lower melting temperature than it should be in ideal mixture [150]. This negative deviation appears if components of the system have strong physical interaction between each other. Schematically it is shown in Figure I. 11.

A mixture of two components is entirely solid regardless of the molar ratio at a temperature, which is lower than the eutectic isotherm line, and is entirely liquid upper the liquidus line (Figure I. 11). A transition zone between liquidus and solidus lines has a liquid phase and a solid component (it depends on molar ratio). Eutectic point is a composition of the mixture with the lowest melting temperature [150].

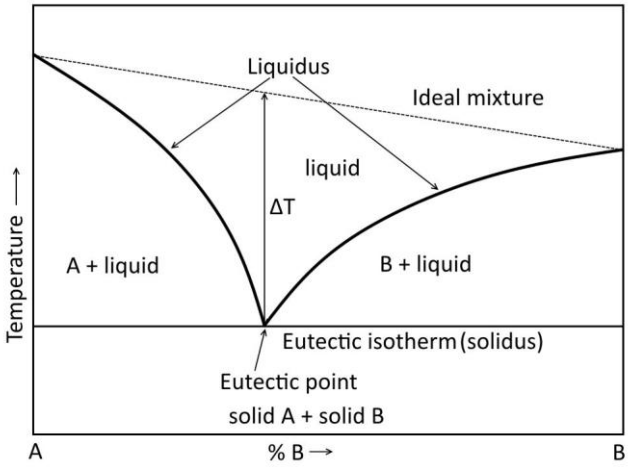

Figure I. 11 Schematic representation of a two component phase diagram (adapted from Atkins *et al.* [150]).

Some eutectic mixtures are used for electrowinning of metals such as aluminium. However, their melting temperatures are comparatively high, which raises the costs of the metal manufacturing. Only development of chloroaluminate ionic liquids allowed decrease of the melting point down to room temperature. This system is of the interest due to industrial importance of the aluminium. Several decades after the ionic liquids introduction, Abbott *et al*. and Sun *et al*. showed that quarter ammonium halides also formed eutectics with zinc halides [151-153]. The general formula of such a system can be written as $(R_1R_2R_3R_4N^+)X^-$ Y, where ammonium (sulfonium, phosphonium) cation ($R_1R_2R_3R_4N^+$) and halide anion (X^-) formed the first component of the eutectic. The second component (Y) is a Lewis or Bronstad acid complexing agent, which complexes the anion and delocalizes its charge. Charge delocalization leads to decrease of interaction between cation and anion and thereby to a decrease of the melting point.

Depending on the complexing agent nature the deep eutectic solvents (DES) can be divided into four groups [154]:

- Eutectic Type 1: $Y=MCl_x$ M= Zn, Sn, Fe, Al, Ga, In
- Eutectic Type 2: $Y=MCl_x\ yH_2O$ = Cr. Co, Cu, Ni, Fe
- Eutectic Type 3: Y=RZ, $Z=CONH_2$, COOH, OH.
- Eutectic Type 4: MCl_x + RZ, M=Zn, Sn, Fe and $Z=CONH_2$, OH

2.2.1 Type I eutectics

A deep eutectic solvent from the first group is formed from quaternary ammonium salts and anhydrous metal halides. The type I eutectics are analogous to the chloroaluminate ionic liquids. The DESs can be formed from the metal halides which have relatively low melting points such as $ZnCl_2$ [151, 155], $SnCl_2$ [151, 155], $FeCl_3$ [156], $GaCl_3$ [157], $InCl_3$ [158]. The composition of the system strongly depends on molar ratio of the components likewise for the chloraluminate ILs [151, 159]. It was shown that although Cl^- and $ZnCl_3^-$ ions dominate in Lewis basic liquids, there are several chlorozincate clusters ($ZnCl_3^-$, $Zn_2Cl_5^-$, $Zn_3Cl_7^-$) in Lewis acidic liquids. A similar behaviour was demonstrated for the chlorostannate systems [151, 159].

2.2.2 Type II eutectics

The hydration water decreases the lattice energy and it leads to reducing of the melting point of the salts. It extends number of metals which can form DES such as $CaCl_2 \cdot 6H_2O$, $LaCl_3 \cdot 6H_2O$, $CoCl_2 \cdot 6H_2O$, $LiNO_3 \cdot 4H_2O$, $Zn(NO_3)_2 \cdot 4H_2O$ [160], $MgCl_2 \cdot 6H_2O$[161]. The type II eutectics are not strictly ionic liquids because of presence of hydration water, but in spite of that, their physical properties are comparable with those of the conventional ILs and water is rather ligand than solvent [162]. The water molecules are strongly coordinated to the ions and it is very difficult to reduce them that provides wider electrochemical windows than those in water based electrolytes. Unfortunately, this type of DES is rarely studied and nowadays the influence of water molecules is not fully understandood. The DES containing chromium is the most investigated system [162-164]. Abbott *et al*. have studied this system and the lowest melting point was found for 2:1 $CrCl_3$ $6H_2O$/ChCl ratio. Composition of this eutectic mixture was investigated using UV-vis spectrometry and it was shown that the DES contains mainly the $Cr(H_2O)_3Cl_3$ species with small amount of $[CrCl_4 \cdot 2H_2O]^-$. The presence choline cations and $CrCl_4^-$ in the eutectic was found by electrospray mass spectroscopy. Authors made a conclusion that $ChCl^+$ and Cl^- are the main charge carrying species [162]. The cyclic voltammogram of the 2:1 $CrCl_3$ $6H_2O$/ChCl system shows no water reduction current which means that the water molecules are highly coordinated and the electrolyte is not just a concentrated solution [165].

2.2.3 Type III eutectics

DES of the third type are based on formation of complexes between halogen anions and hydrogen bond donors (HBD) [166]. Formation of deep eutectic solvents was found for a range of amides, alcohols and carboxylic acids (Figure I. 12 [154]). These liquids are easy to prepare, relatively cheap, water- and air-stable and mainly biodegradable [144, 154]. DES of this type have been used in the current work.

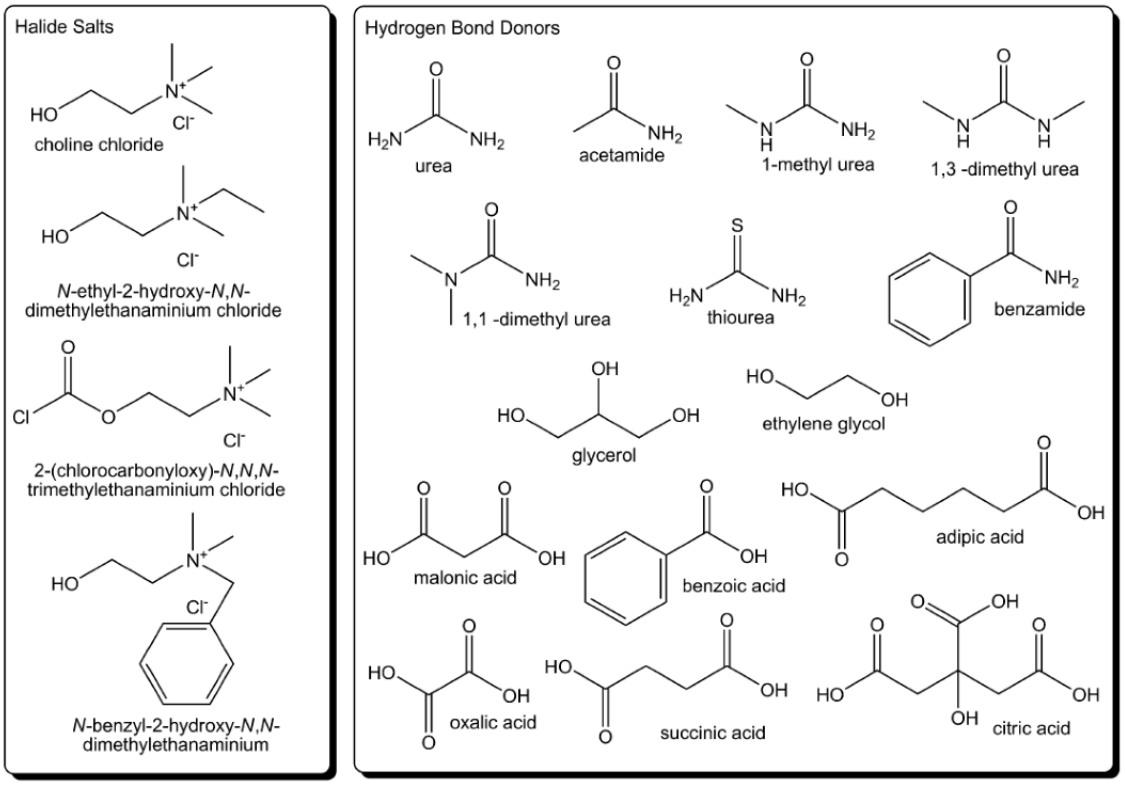

Figure I. 12 Structures of some halide salts and hydrogen bond donors used in the formation of deep eutectic solvents (taken from Smith *et al*. [154]).

Composition of a deep eutectic solvent depends on the quantity of functional groups of the hydrogen bond donors; for instance, molar ratio between urea, oxalic acid, citric acid and quaternary ammonium salt (choline chloride) are 2:1, 1:1 and 1:2, correspondingly. Complexation (charge delocalization) of the halide anions occurs through hydrogen bond formation with HBDs. An additional proof of the presence of hydrogen bonding in the system was obtained using Heteronuclear Overhauser effect spectroscopy for choline fluoride/urea system and using FAB MS for choline chloride

(ChCl)/urea system. The signals which correspond to two urea molecules and Cl^- (M^- =155) and to one urea and chloride (M^-=95) were observed by FAB MS [167].

The III type eutectics have large temperature difference between real melting point and theoretical melting point of ideal mixture, for example the practical melting point of 1ChCl/2urea is lower for 180^{o}C than the theoretical one [167]. Moreover, the large number of available hydrogen bond donors makes this class of ionic liquids attractive for industrial application because it can be easily adopted for specific usage with a capability to dissolve a wide range of metal salts and oxide.

The DES based on the choline chloride and glycols are non-toxic and accessible to the industry [154]. For instance ChCl is a vitamin and it is produced on a large scale as animal feed supplement. The ChCl based solvents were used in the experimental work on the thesis because these ionic liquids have the highest conductivity, the lowest viscosity and comparatively large potential windows. These parameters are extremely important for electrodeposition processes.

2.2.4 Type IV eutectics

The mixture of metal halide with hydrogen bond donors in some situation is eutectic with a near room temperature melting point. The possibility of such an eutectic has been shown by Abbott *et al*. for zinc, tin (II) and iron (III) chlorides in a mixture with ethylene glycol, urea or acetamide [168]. It was proposed by the authors to classify these systems as type IV eutectics. The zinc chloride forms eutectics with urea, acetamide, ethylene glycol and hexandiol in the ratios (eutectic donor/$ZnCl_2$) 3.5, 4, 4 and 3, correspondingly. Ionic species identification was performed by FAB MS [168] and it was shown that together with common zinc complexes $[ZnCl_3]^-$, $[Zn_2Cl_5]^-$ and $[Zn_3Cl_7]^-$, there are also positive species such as $[ZnCl(urea)]^+$, $[ZnCl(urea)_2]^+$, $[ZnCl(urea)_3]^+$ in the IV type of eutectics.

2.3 Physico-chemical properties

There is a number of properties that makes ionic liquids attractive for electrochemistry. These properties allow deposition of different compounds which is impossible with other solutions.

Ionic liquids are particularly noteworthy from the electrochemical point of view, owing to their wide potential window. Typical electrochemical window for an ionic liquid

is about 4 V, although the IL with a 7 V window was also reported (electrochemical window of water is less than 2 V). This specific electrochemical parameter allows electrodeposition of different active materials such as aluminum, magnesium, lithium, sodium, silicon.

The electrochemical window is not the only significant factor. The roles of such properties as electrical and thermal conductivity, melting point and temperature of decomposition, viscosity and diffusion coefficient, solubility of metal salts, density are also undeniable in electrochemical processes.

The main physico-chemical properties of ILs are covered in series of books, papers and databases [143-145, 154, 169-171]. Moreover, properties of some ionic liquids are presented in Table I. 4.

Table I. 4 Main physico-chemical properties of different ionic liquids.

	Ionic liquid	Density g/cm^3	Viscosity cP	Melting Point ^oC	Conductivity $mS\ cm^{-1}$
1st generation	[EMIM][$AlCl_4$]	1,38 [169]	18 [169]	7 [169]	22,7 [173]
	[BMIM][$AlCl_4$]	1.25 [172]	34.0 [172]	-	-
2nd Generation	[n-Alkyl-] 3-methylimidazolium hexafluorophosphate				
	1-Ethyl-	1,56 [144]	solid	62 [178]	4.91 [180]
	1-Butyl-	1.36 [174]	395 [176]	-8 [174]	1.4 [174]
	1-Hexyl-	1.3 [175]	707 [177]	-61 [179]	3.86 [181]
	1-Octyl-	1.24 [175]	1052 [177]	-82 [179]	2.57 [181]
	1-Ethyl -3-methylimidazolium [X^-]				
	Methyl sulfate	1.29 [182]	99.7 [182]	-	6.02 [184]
	Butyl sulfate	1.18 [182]	242.3 [182]	-	-
	Hexyl sulfate	1.13 [182]	428.3 [182]	-	-
	Octyl sulfate	1.1 [182]	856.0 [182]	-	-
	[CF_3SO_3]	1.38 [149]	45 [149]	-9 [149]	8.6 [149]
	[CF_3COO]	1.29 [149]	32 [183]	-14 [149]	9.6 [149]
DES	I, II and IV type				
	$ChCl/2ZnCl_2$	-	85000 [151]	25 [151]	0.036 [151]
	$ChCl/2CrCl_3\ 6H_2O$	-	4500 [162]	13 [162]	0.7 [162]
	$3.5Urea/ZnCl_2$	1.63 [168]	11340 [168]	9 [168]	-
	III type				
	ChCl/2Urea	1.18 [185]	1100 [167]	12 [167]	1.5 [167]
	ChCl/2EG	1.11 [185]	23 [185]	-	7.2 [185]
	ChCl/Oxalic acid	-	160 [166]	34 [166]	3 [166]

2.3.1 Density

In general, ionic liquids have higher density than that of water. One can see from Table I. 4 that the density values are in the range from 1.1 to 1.6 g/cm^3.

Although a dependence between structure of ions and density of the corresponding ionic liquids has not been found yet, several tendencies described in literature [143, 144, 169, 171] should be mentioned here. First of all, a noteworthy detail is that an increase of the length of alkyl radicals both in cations and in anions leads to density decreasing [186]. A good example of this is imidazolium based ionic liquids. Changing of the carbon number in the row 1-Ethyl-; 1-Butyl-; 1-Hexyl-; 1-Octyl-3-methylimidazolium hexafluorophosphate results in a decrease in density as 1.56; 1.37; 1.31; 1.23 g/cm^3, correspondingly. Similar trend with growing of alkyl radicals can be observed in anions. For example, 1-Ethyl-3-methylimidazolium cation ([EMIM]) with different alkyl-sulphate anions methyl; butyl; hexyl; octyl sulphate have the density values 1.29; 1.18; 1.13 and 1.1 g/cm^3, correspondingly [182]. Moreover, it is important to mention that substitution of light radical for a heavier one, without big difference of sizes, leads to an increase in density. For instance, [EMIM][CH_3SO_3] and [EMIM][CF_3SO_3] have 1.25 and 1.38 g/cm^3, correspondingly. However, for such heavy radicals the inverse dependence can be found: in spite of carbon chain growing, [EMIM][CF_3COO] and [EMIM][C_3F_7COO] have the densities of 1.29 and 1.45 g/cm^3.

2.3.2 Viscosity

Viscosity of ionic liquids is higher than that of the molecular solvents. Values of the viscosity of most of the ILs presented in Table I. 4 are in the range of 10-1000 cP (0.01-1 Pa s). This is higher than the water viscosity by one to four orders of magnitude (water – 0.89 cP). The ionic liquids viscosity is determined by the Van Der Waal's forces and by abilities of the ions to form hydrogen bonds [169]. Size and structure of the ions have a strong influence on viscosity as they do on density. Growth of the alkyl radicals' length leads to reinforcement of the Van Der Waals interaction and increases viscosity. It was found that hydrogen bonding has a similar trend. Ionic liquids with BF_4^- and PF_6^- have a higher viscosity values due to the hydrogen bonds formation. The electrostatic interaction also plays an important role here [169].

Viscosity is a crucial parameter for electrochemistry because it has a strong impact on conductivity [171, 187] and kinetics. High viscosity of ILs mainly impairs diffusion

of metal species to the working electrode which means restrictions to the mass transport. Although it was reported that increasing of temperature results in decreasing of viscosity of ILs [188-192], but usage of them at high temperature partially contradicts the idea of room temperature ionic liquids. It was found that small amounts of different impurities, such as water, in ionic liquids lead to strong changes in physico-chemical properties including viscosity [193, 194]. Nowadays, dilutants are often added to ionic liquids and DES to decrease viscosity, remove diffusion limitations and increase conductivity [195-199]. These substances and their amounts are different for each specific case depending on the ionic liquid composition and materials planned to be deposited. Commonly they are different alcohols, hydrocarbons, ethers *etc*. In some cases, a small amount of water can be also used as dilutant.

2.3.3 Temperature range

Melting point and decomposition temperature are two main thermal characteristics of ionic liquids as electrolytes. First of all, it is important to know the melting temperature. Commonly, inorganic salts melt at temperature of the order of thousand degrees because of a strong electrostatic interaction between ions.

The term “room temperature ionic liquids” clearly indicates that these materials are in liquid state at room temperature. It is possible due to usage of organic molecules where charge is distributed over a big volume which significantly decreases interaction between ions. It is evident that structure of ions and composition of ionic liquid have a strong impact on the temperature parameters [169]. Unfortunately, as with viscosity and density, precise correlation between structure and melting or decomposition points has not been found yet. At the same time, the main tendencies can be revealed for certain number of parameters. Melting temperature of ionic liquids, by analogy with inorganic salts, decreases with increasing of the ions size. It happens because in molecule with bigger ions, distance between their centres increases and surface charge decreases, which results in lower electrostatic interactions [169]. Apart from the size effect, structure of the ILs species has a considerable effect on properties which makes an estimation of the thermal properties much more difficult. For example, ionic liquids with aromatic cation have lower melting points than that with aliphatic one because of the charge delocalization. Concerning side-chain size, initial increasing of carbon number leads to a

lower melting point, but with large radicals the orientation effect and solidification of the system can be observed.

Influence of the anion structure on the melting temperature is similar to the above-described one for the cation structure. Presence of bigger anions and the anions with higher charge delocalization implies lower electrostatic interaction and, thereby, a lower melting point.

The maximal temperature, at which the use of an ionic liquid without decomposition or other chemical changes can be implemented, is also an important parameter for certain applications. ILs with the decomposition temperature of about 400-450^{o}C were reported [178, 200]. However, it was mentioned that a degradation of the ILs starts below the above-mentioned range. That is why the usage of the electrolyte at temperatures which are close to the decomposition range for a long time is not recommended. Data on decomposition temperature of some ionic liquids is shown in Figure I. 13 [144].

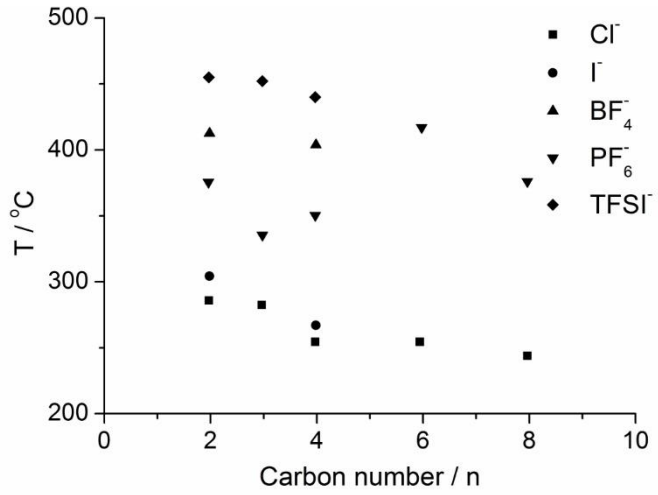

Figure I. 13 Relation between thermal decomposition temperature of 1-alkyl-3-methylimidazolium-type ILs with alkyl chain length (adapted from Endres and Abbott [144]).

2.3.4 Conductivity

Conductivity of ionic liquids is lower than that of the concentrated water solution (about 10 mS cm^{-1}), because the large size of ions and its aggregations lead to limited mobility of charge carriers. At the same time, ILs show good ionic conductivity, which is

makes them similar to the best non-aqueous electrolytes. Conductivity of a RTIL has a strong correlation with viscosity. These two parameters are combined in Walden's rule [201]:

$$\Lambda\varphi = \text{constant} \quad \text{(I.18)}$$

where Λ is molar conductivity of the ionic liquid, and φ is a viscosity

It is obvious from Walden's rule that ionic liquids with higher viscosity have lower conductivity. Moreover, as it was mentioned before, with temperature increasing the viscosity decreases and consequently conductivity increases [202]. Some ionic liquids might have conductivity of about 10 S cm^{-1} at 200^{o}C.

High resistivity of ILs as electrolyte is a negative factor and due to high Ohmic loss, their applications in industry are limited.

2.3.5 Electrochemical windows

Electrochemical window is a potential range for any electrolyte where no electrochemical processes i.e., oxidation or reduction of the electrolyte occur [203]. Therefore, electrochemical window (Ew) is a measure of electrochemical stability of the electrolyte. It is well known that this range is very narrow for water based electrolytes, namely about 1.2 V, which imposes constraints on their electrochemical behaviour. Although the electrochemical window of ILs is typically around 4-5 V [144], but the ionic liquid with 7 V [204] does also exist. Table I. 5 presents the electrochemical properties of some ionic liquids together with the measurement conditions.

Table I. 5 Main electrochemical properties of ionic liquids.

Ionic liquid [REF]	Ered (V)	Eox (V)	EW (V)	Working electrode	Reference electrode
Classical ionic liquids					
EMIM[$AlCl_4$] [205]	-2.1	2.35	4.45	GC	Al/A1C1$_3$:2DMPrIC
EMIM[$AlCl_4$] [205]	-2.1	2.3	4.4	W	Al/A1C1$_3$:2DMPrIC
EMIM[$AlCl_4$] [205]	-1.85	1.95	3.8	Pt	Al/A1C1$_3$:2DMPrIC
[EMIM][BF_4]$^-$ [204]	-2.6	2.6	5.2	GC	$Ag/AgNO_3$
[EMIM][BF_4]$^-$ [206]	-2	2	4	Pt	Ag/AgCl
[EMIM][BF_4]$^-$ [207]	-2.2	1.6	3.8	GC	Fc/Fc^+
[EMIM][$(CF_3SO_2)_2N^-$] [207]	-2.4	2.2	4.6	GC	Fc/Fc^+
1-butylpyridinium [BF_4]$^-$ [206]	-1	2.4	3.4	Pt	Ag/AgCl
Tetrabutylammonium [$(C_2F_5)_3PF_3$]$^-$ [204]	-3.3	3.7	7	GC	$Ag/AgNO_3$
Deep Eutectic Solvents					
ChCl/2$CrCl_3 \cdot 6H_2O$ [162]	0	1.5	1.5	Pt	Cr wire
ChCl/Urea [208]	-1.2	1.25	2.45	Pt	Ag wire
3.5Urea/1$ZnCl_2$ [168]	-0.75	1.25	2	Pt	Pt wire

Unfortunately, the ranges of electrochemical stability reported in literature for the same ionic liquids are different. Even small amount of impurities dramatically changes properties of ILs. For example, a negligible amount of water result in a decrease of the electrochemical window due to the hydrogen reduction [203]. Moreover, it is important to know the material of the working electrode; because, depending on the electrochemical properties of the materials, current appears at different potentials. It can be demonstrated for the case of either platinum or tungsten electrodes (Table I. 5). Platinum is a good catalyst and the electrochemical window for the platinum working electrode is smaller than that for tungsten one.

In general, ionic liquids with quaternary ammonium cations show a wide electrochemical window owing to a relatively low potential of the reduction. For instance, the reduction potential of the imidazolium based electrolytes is higher than that of the

quaternary ammonium based one (Table I. 5). It can be explained by the existence of the active proton in the imidazolium ion structure. At the same time, pyridinium can be reduced with less difficulties in comparison with the imidazolium [206]. Furthermore, structure and nature of anions influence significantly the electrochemical stability of ILs. Tetrafluoroborate and bis(trifluoromethylsulfonyl)imide are the ions with the highest oxidation potentials.

The electrochemical studies are often carried out in three electrode cells. There is a reference electrode together with the working and the counter electrodes in such cells. Electrochemistry of ionic liquids is relatively new area and a standard reference electrode to work in ILs has not been defined yet [209] as, for example, silver chloride, calomel and others for the water based electrolytes. Reference electrodes used in ILs today can be divided in three groups [210]. The first is a quasi-reference electrode, the simplest electrode in terms of design. It contains metallic wire (platinum, silver, aluminium, zinc *etc*.) which is immersed in the electrolyte and separated from the reaction area by a membrane. The second type of reference electrodes is similar to the common electrodes for aqueous electrolytes: for instance, a silver wire covered by silver chloride and immersed in solution of a silver compound in organic solvent. The third type of reference electrodes is an electrode with Red/Ox couple. Most frequently, researchers use a ferrocene (II/III) couple, which is recommended by IUPAC, or an I^-/I_3^- couple. Unfortunately, it is impossible to use the same redox couple in all types of ionic liquids because these compounds can affect electrochemistry of the system. Detailed pre-experimental investigations should be performed to determine the potential for use in each specific ILs [210]. A wide number of available electrodes leads to different values of oxidation and reduction potential of ionic liquids presented in literature.

Wide electrochemical window is an electrochemical property of high importance, but for successful plating it is also critical to pay attention to all factors, depending on the desirable aims.

2.4 Electrochemical application of ionic liquids and deep eutectic solvents

One of the major applications of the ionic liquids is electrodeposition [211]. Nowadays, most of the metals can reduced from different ILs (Figure I. 14). All marked elements can be deposited as pure metals or as alloys [144, 154, 165, 171, 209, 212, 213].

1																	18
1 H 1.008	2											13	14	15	16	17	2 He 4.0026
3 Li 6.94	4 Be 9.0122											5 B 10.81	6 C 12.011	7 N 14.007	8 O 15.999	9 F 18.998	10 Ne 20.180
11 Na 22.990	12 Mg 24.305	3	4	5	6	7	8	9	10	11	12	13 Al 26.982	14 Si 28.085	15 P 30.974	16 S 32.06	17 Cl 35.45	18 Ar 39.948
19 K 39.098	20 Ca 40.078	21 Sc 44.956	22 Ti 47.867	23 V 50.942	24 Cr 51.996	25 Mn 54.938	26 Fe 55.845	27 Co 58.933	28 Ni 58.693	29 Cu 63.546	30 Zn 65.38	31 Ga 69.723	32 Ge 72.630	33 As 74.922	34 Se 78.97	35 Br 79.904	36 Kr 83.798
37 Rb 85.468	38 Sr 87.62	39 Y 88.906	40 Zr 91.224	41 Nb 92.906	42 Mo 95.95	43 Tc (98)	44 Ru 101.07	45 Rh 102.91	46 Pd 106.42	47 Ag 107.87	48 Cd 112.41	49 In 114.82	50 Sn 118.71	51 Sb 121.76	52 Te 127.60	53 I 126.90	54 Xe 131.29
55 Cs 132.91	56 Ba 137.33	57-71 *	72 Hf 178.49	73 Ta 180.95	74 W 183.84	75 Re 186.21	76 Os 190.23	77 Ir 192.22	78 Pt 195.08	79 Au 196.97	80 Hg 200.59	81 Tl 204.38	82 Pb 207.2	83 Bi 208.98	84 Po (209)	85 At (210)	86 Rn (222)
87 Fr (223)	88 Ra (226)	89-103 #	104 Rf (265)	105 Db (268)	106 Sg (271)	107 Bh (270)	108 Hs (277)	109 Mt (276)	110 Ds (281)	111 Rg (280)	112 Cn (285)	113 Nh (286)	114 Fl (289)	115 Mc (289)	116 Lv (293)	117 Ts (294)	118 Og (294)

Figure I. 14 Periodic table with highlighted elements which were deposited from ILs.

2.4.1 Electrodeposition from ionic liquids

Historically, the $AlCl_3$-based ILs were the first type of ionic liquids applied for electrodeposition of metals. These ionic liquids have several drawbacks such as the electrochemical window limitation through reduction of aluminium, as well as water- and air sensitivity. The last two disadvantages can be avoided by using close atmosphere, whereas the first one (electrochemical window) strongly limits the number of deposited materials. It means that a lot of diverse metals were deposited not at pure state but as alloys with aluminium. Nevertheless, a great number of metals was deposited from this type of ionic liquids.

First of all, attention should be paid to aluminium, because the majority of works in chloroaluminate ILs is done on electrodeposition of this metal. The aluminium electrodeposition is of interest for industry owing to high corrosion stability provided by oxide layer formed on the metal interface. Aluminium was successfully deposited from ionic liquids containing different cations such as EMIM [214, 215], BMIM [216], butylpyridinium [217], benzyltrimethylammonium [218]. Different cations offer different physical properties of ILs such as viscosity, electrochemical window, water sensitivity *etc*., as it was described in the previous part. Moreover, electrodeposition of aluminium was performed on different substrates including glassy carbon, steel, gold, platinum. These first experiments show a wide range of possible ionic liquids applications.

The electrodeposition of lithium from EMIMCl/$AlCl_3$ with addition of lithium chloride was demonstrated for the first time in 1985 [219]. 10 years later, sodium was

firstly reduced from the same ionic liquid by Gray *et al* [220]. Some less reactive elements such as silver, copper [221], indium [222], cobalt [223], zinc [224], gallium [225], antimony [226], tellurium [227], gold [228] were also successfully deposited afterwards. Furthermore, the experiments with deposition of alloys, rather than pure metals, were also successfully implemented (magnesium alloy [229], titanium alloy [230]).

The chloroaluminate based ILs were substituted in 1990s by the discrete ions ILs [146]. The use of tetrafluoroborate, hexafluorophosphate, bis(trifluoromethylsulfonyl)imide anions improves both chemical and electrochemical stabilities. The increase of the electrochemical stability extends the number of metals available for deposition. The second generation of ILs allows to deposit not only comparatively noble metals e.g., cadmium [231], gold [232], copper [233], selenium [158, 234] but also materials that can be reduced neither from water based solution nor from chloroaluminate systems (magnesium [235], titanium (thin film) [236], silicon [237, 238], caesium [239]).

Apart from the pure metals the electrodeposition of alloys and other compounds was also widely studied in available ionic liquids. Several technically important alloys and semiconductors such as Zn/Sn [240], GaAs [241], InSb [242], ZnTe [243] were deposited.

2.4.2 Electrodeposition from deep eutectic solvent

The third type of deep eutectics based on choline chloride is not toxic and has a low cost and, therefore, it has been intensively studied after the introduction made by Abbott *et al*. in 2004 [166]. These DES are flexible and adaptable for necessary conditions due to the large number of available HBD. The applications of DES are limited by electrochemical window (normally about 3 V), that does not allow the electrodeposition of electronegative metals such as titanium, aluminium and alkali metals from these eutectics. Nevertheless, at the industry scale, DES are deemed to be promising substitutes of the water electrolytes for deposition of metals (zinc [208, 244-246], copper [247], nickel [248], tin [208]) and alloys, for instance Zn/Sn [208], Zn/Ni [249]. Increase of the current efficiency and improvement of the surface reproducibility are the most significant effects of choline based electrolytes application.

Zinc is one of the most important metals in plating industry due to the corrosion resistance and a low price. Electrodeposition of this metal has been widely studied. Initial

studies of zinc electrodeposition from choline chloride ethylene glycol (1:2) DES were carried out by Whitehead *et al.* [246]. They showed that electroreduction of zinc on glassy carbon rod occurs much faster when the potential is increased from more negative (-0.8V) to -0.4 - -0.2V vs Zn/Zn^{2+} quasi-reference electrode. It can be explained by formation of so-called Z species (intermediate compounds) which are reduced at higher potential. Then, Vieira together with Whitehead and Gollas studied this phenomenon particularly and confirmed the formation of Z species in the diffusion layer [250].

Abbott *et al.* have studied the influence of double layer on the zinc nucleation [185]. They used two types of ILs based on choline chloride with different HBD (either urea or ethylene glycol). It is shown that the deposit has different structures explained by blocking of certain crystal faces in glycol-contained electrolyte. Bakkar and Neubert [245] electrodeposited zinc on magnesium from choline based DES with four different HBDs: urea, ethylene glycol, glycerol and malonic acid. Such zinc coating was used in order to protect Mg from corrosion. The ChCl/urea eutectic is considered to be the most suitable liquid for successful electroplating. As it was recently shown by Vieira *et al*. [251], the working electrode materials also have a strong impact on nucleation and deposition processes. These authors used glassy carbon, stainless steel, gold, platinum copper and zinc as substrates to study the hydrogen overpotential and possible Z species formation. Formation of a compact blocking layer on the electrode interface, which inhibits the electrodeposition of zinc, has been noted.

Nowadays, improvement of the coating quality, brightening, efficiency increment during electroplating are achieved via addition of some specific compounds. Nonetheless, additives for electrodeposition from DES are barely studied. The first full investigation of the influence of three polar additives (acetonitrile, ethylene diamine, and ammonium hydroxide) on the nucleation of zinc and the morphology of the coating was published by Abbott *et al.* in 2011 [199]. Ammonia and ethylene diamine additives result in effective brightening of the coating. Ibrahim [198] *et al.* also studied the influence of acetonitrile and ethylene diamine on electrodeposition of zinc. They mentioned that additives promote reduction at less negative potential, although the current efficiency decreases.

Application of DES for metals plating is new and promising area.

2.5 Electrode/electrolyte interface

The ionic liquids behaviour differ greatly from that of the common water based electrolytes and the properties of the electrode/electrolyte interface are not an exception. The main difference occurs because ILs contain only charged species in contrast to molecular liquid. As a result, additional interionic forces such as Coulomb, Van der Waals and hydrogen bonding arise. All these interactions promote formation of nanostructures in both bulk deposit and at the electrolyte/electrified interface [252, 253]. Formation of multilayered structure was confirmed by several independent techniques, namely high energy X-ray reflectivity, atomic force microscopy, nuclear magnetic resonance, electrochemical impedance spectroscopy. The strong ILs adsorbance onto solid interface and formation of multilayer superstructure was reported [253-257]. Moreover, it was also demonstrated that applied potential has a strong impact on the ions arrangement: the surface structure is more obvious both at more positive and more negative potentials. The generally accepted model of the electrode/ILs interface is presented in Figure I. 15 [209]. The single layer of ions mostly neutralizes the electrode charge and this layer is also compensated by other oppositely charged ion layers.

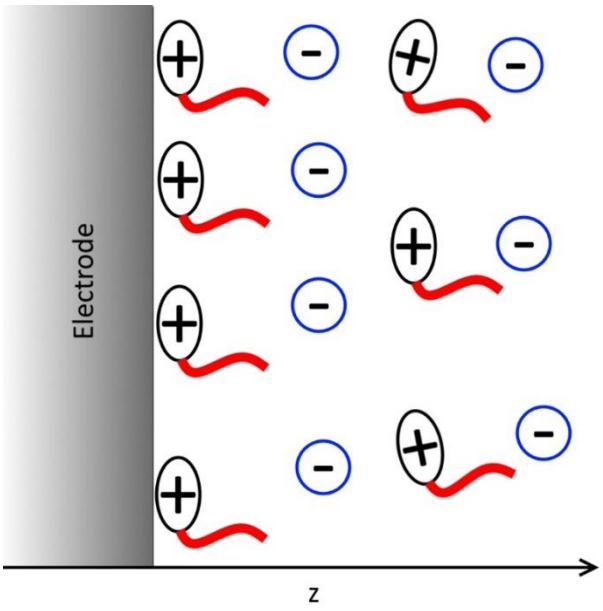

Figure I. 15 Schematic diagrams of the electrode-electrolyte interface in ionic liquid. (Adapted from Abbott *et al*. [209])

Besides experimental studies, the molecular dynamics calculations and Monte Carlo simulations [258-261] were also performed for theoretical descriptions of the electrolyte/electrode systems. The calculated data were found to be in a good agreement with the experimental results.

DES and classical ILs show similar behaviour on the electrode surface. Several studies of interfaces in the deep eutectic solvents based on choline chloride were reported [262, 263]. The electrochemical impedance spectroscopy and cyclic voltammetry were used in these works for the interface investigation. The capacitance values at different potentials were measured for the ChCl:2Glycerol eutectic on glassy carbon, platinum and gold electrodes [262]. It was shown that measured capacity depends on the electrode material. For instance, replacing glassy carbon electrode by platinum one leads to an increase of the capacity value for all potentials, although the shape of the curves remains similar. Moreover, increasing temperature results in an increase of the differential capacity. The results of the study [262] correlate with the reported data for conventional ionic liquids. Another study on the structure of double layer were performed on mercury electrode in choline based DESs with different hydrogen bond donors (urea, 1,2 and 1,3 propanediol, ethylene glycol) [263]. Authors concluded that at negative potential, the double layer structure on mercury electrode is similar to one observed in aqueous electrolyte solution. They assumed presence of a hydrogen bond donors layer between the electrode and cations at negative potential. The observed growth of the capacitance at positive potential was attributed to adsorption of free chloride ions.

The double layer structure in both ionic liquids and eutectic solvents is not well understood for both ionic liquids and eutectic solvents despite of the numerous studies and calculations performed. Therefore, new studies should be undertaken in order to improve the understanding of role of the ionic species and their behaviour on the electrified interface.

Thesis objectives

The main goal of this PhD work is electrosynthesys of 1-D zinc nanorods from choline chloride based ionic liquid by using the template assisted techniques. A novelty of this research is a use of the not-detached template, which allows reducing the price and the time for the nanomaterials preparation. During the work, two most common porous anodic templates (porous anodic titania and porous anodic alumina) were carefully studied with particular attention to barrier layer influence. The electrochemical processes that occur during nanowires fabrication have a noticeable influence of the barrier layer thickness. This specific influence was studied step-by-step from a flat dense oxide layer to the porous templates. The studies revealed several ways of deposition and modification of the porous templates for the successful nanoparticles preparation.

Zinc has been used as a model material with a possible further conversion to semiconductive materials such as zinc oxide, zinc sulfide, zinc selenide or substitution by other materials. The use of the ionic liquids as electrolyte also gives vast array of possible secondary materials and excludes several negative effects of the water based electrolytes namely a narrow electrochemical window, hydrogen evolution, toxic components. We also observed the specific adsorption of the electrolyte components on the electrode surface which hinders the reduction of the zinc species. An appropriate way to solve the problem was also developed.

Regarding the main objectives, it is possible to highlight the followings:

1) synthesis of the dense and porous anodic films on the valve metals (aluminium and titanium);

2) physico-chemical characterization of the templates;

3) correlation of the applied voltage, film thickness, film structure with the observed kinetics of zinc reduction on the dense barrier layer;

4) investigation of the electrical double layer on the oxide/electrolyte interface and its influence on deposition process;

5) adaptation of the results obtained on the dense anodic films to the porous templates;

6) modification of porous anodic template for the synthesis of nanoparticles;

7) electrodeposition of zinc inside the porous templates and characterization of the obtained materials.

References

[1] N.E.M. Association, *A chronological history of electrical development from 600 B.C*, National Electrical Manufacturers Association, 1946.
[2] E. Gileadi, *Electrode kinetics for chemists, chemical engineers, and materials scientists*, VCH, New York, 1993.
[3] A.P. Abbott, G. Capper, K.J. McKenzie, A. Glidle, K.S. Ryder, Electropolishing of stainless steels in a choline chloride based ionic liquid: an electrochemical study with surface characterisation using SEM and atomic force microscopy, *Physical Chemistry Chemical Physics*, 8 (2006) 4214-4221.
[4] P. Neufeld, D.M. Southall, The electropolishing of aluminum, *Electrodeposition and Surface Treatment*, 3 (1975) 159-168.
[5] M.G. Fontana, R.W. Staehle, *Advances in Corrosion Science and Technology*, Plenum Press, 1970.
[6] B. Kuznetsov, M. Serdechnova, J. Tedim, M. Starykevich, S. Kallip, M.P. Oliveira, T. Hack, S. Nixon, M.G.S. Ferreira, M.L. Zheludkevich, Sealing of tartaric sulfuric (TSA) anodized AA2024 with nanostructured LDH layers, *RSC Advances*, 6 (2016) 13942-13952.
[7] D.K. Ivanou, M. Starykevich, A.D. Lisenkov, M.L. Zheludkevich, H.B. Xue, S.V. Lamaka, M.G.S. Ferreira, Plasma anodized ZE41 magnesium alloy sealed with hybrid epoxy-silane coating, *Corrosion Science*, 73 (2013) 300-308.
[8] D.K. Ivanou, K.A. Yasakau, S. Kallip, A.D. Lisenkov, M. Starykevich, S.V. Lamaka, M.G.S. Ferreira, M.L. Zheludkevich, Active corrosion protection coating for a ZE41 magnesium alloy created by combining PEO and sol-gel techniques, *RSC Advances*, 6 (2016) 12553-12560.
[9] M. Serdechnova, M. Mohedano, B. Kuznetsov, C.L. Mendis, M. Starykevich, S. Karpushenkov, J. Tedim, M.G.S. Ferreira, C. Blawert, M.L. Zheludkevich, PEO Coatings with Active Protection Based on In-Situ Formed LDH-Nanocontainers, *Journal of The Electrochemical Society*, 164 (2017) C36-C45.
[10] R.C. Furneaux, W.R. Rigby, A.P. Davidson, The formation of controlled-porosity membranes from anodically oxidized aluminium, *Nature*, 337 (1989) 147-149.
[11] S. Berger, F. Jakubka, P. Schmuki, Formation of hexagonally ordered nanoporous anodic zirconia, *Electrochemistry Communications*, 10 (2008) 1916-1919.
[12] E.P. Haripriya, K.V. Oomman, P. Maggie, K.M. Gopal, A.G. Craig, Synthesis and photoelectrochemical properties of nanoporous iron (III) oxide by potentiostatic anodization, *Nanotechnology*, 17 (2006) 4285.
[13] J.W. Diggle, T.C. Downie, C.W. Goulding, Anodic oxide films on aluminum, *Chemical Reviews*, 69 (1969) 365-405.
[14] T. Ohtsuka, M. Masuda, N. Sato, Ellipsometric Study of Anodic Oxide Films on Titanium in Hydrochloric Acid, Sulfuric Acid, and Phosphate Solution, *Journal of The Electrochemical Society*, 132 (1985) 787-792.
[15] J.L. Delplancke, R. Winand, Galvanostatic anodization of titanium—I. Structures and compositions of the anodic films, *Electrochimica Acta*, 33 (1988) 1539-1549.
[16] M. Kozlowski, W.H. Smyrl, L. Atanasoska, R. Atanasoski, Local film thickness and photoresponse of thin anodic TiO_2 films on polycrystalline titanium, *Electrochimica Acta*, 34 (1989) 1763-1768.
[17] M. Schneider, S. Schroth, J. Schilm, A. Michaelis, Micro-EIS of anodic thin oxide films on titanium for capacitor applications, *Electrochimica Acta*, 54 (2009) 2663-2671.
[18] S.K. Poznyak, A.D. Lisenkov, M.G.S. Ferreira, A.I. Kulak, M.L. Zheludkevich, Impedance behaviour of anodic TiO_2 films prepared by galvanostatic anodisation and powerful pulsed discharge in electrolyte, *Electrochimica Acta*, 76 (2012) 453-461.
[19] R.D. Misch, Dissolution of the oxide film on zirconium, *Acta Metallurgica*, 5 (1957) 179-180.
[20] J. Klerer, Determination of the Density and Dielectric Constant of Thin Ta_2O_5 Films, *Journal of The Electrochemical Society*, 112 (1965) 896-899.
[21] C.K. Dyer, R.S. Alwitt, Ellipsometric measurements of the barrier layer in composite aluminum oxide films, *Electrochimica Acta*, 23 (1978) 347-354.
[22] L. Young, Kinetics of formation of anodic oxide films on zirconium, *Transactions of the Faraday Society*, 55 (1959) 632-642.
[23] D.F.P. Pile, Two-dimensionally localized modes of a nanoscale gap plasmon waveguide, *Appl. Phys. Lett.*, 87 (2005) 261114.
[24] R.F. Oulton, V.J. Sorger, D.A. Genov, D.F.P. Pile, X. Zhang, A hybrid plasmonic waveguide for subwavelength confinement and long-range propagation, *Nat Photon*, 2 (2008) 496-500.

[25] E. Hourdakis, A.G. Nassiopoulou, High performance MIM capacitor using anodic alumina dielectric, *Microelectronic Engineering*, 90 (2012) 12-14.
[26] E. Hourdakis, A.G. Nassiopoulou, High-Density MIM Capacitors With Porous Anodic Alumina Dielectric, *Electron Devices, IEEE Transactions on*, 57 (2010) 2679-2683.
[27] K.A. Yasakau, A.N. Salak, M.L. Zheludkevich, M.G.S. Ferreira, Volta Potential of Oxidized Aluminum Studied by Scanning Kelvin Probe Force Microscopy, *The Journal of Physical Chemistry C*, 114 (2010) 8474-8484.
[28] A. Charlesby, Ionic Current and Film Growth of Thin Oxide Layers on Aluminium, *Proceedings of the Physical Society. Section B*, 66 (1953) 317.
[29] R. Harrington, H. Nelson, An electron diffraction study of anodic films, *Trans. Am. Inst. Min. Metall. Pet. Eng.*, 137 (1940).
[30] C.S. Taylor, C.M. Tucker, J.D. Edwards, Anodic Coatings with Crystalline Structure on Aluminum, *Transactions of The Electrochemical Society*, 88 (1945) 325-333.
[31] D.J. Stirland, R.W. Bicknell, Studies of the Structure of Anodic Oxide Films on Aluminum, I, *Journal of The Electrochemical Society*, 106 (1959) 481-485.
[32] G.E. Thompson, Y. Xu, P. Skeldon, K. Shimizu, S.H. Han, G.C. Wood, Anodic oxidation of aluminium, *Philosophical Magazine Part B*, 55 (1987) 651-667.
[33] Y. Xu, G.E. Thompson, G.C. Wood, B. Bethune, Anion incorporation and migration during barrier film formation on aluminium, *Corrosion Science*, 27 (1987) 83-102.
[34] R.B. Mason, Factors Affecting the Formation of Anodic Oxide Coatings in Sulfuric Acid Electrolytes, *Journal of The Electrochemical Society*, 102 (1955) 671-675.
[35] J.J. Randall, W.J. Bernard, R.R. Wilkinson, A radiotracer study of the composition and properties of anodic oxide films on tantalum and niobium, *Electrochimica Acta*, 10 (1965) 183-201.
[36] P. Skeldon, G.E. Thompson, G.C. Wood, Formation of relatively pure alumina films by anodic polarization, *Thin Solid Films*, 148 (1987) 333-341.
[37] M.V. Diamanti, M. Ormellese, E. Marin, A. Lanzutti, A. Mele, M.P. Pedeferri, Anodic titanium oxide as immobilized photocatalyst in UV or visible light devices, *Journal of Hazardous Materials*, 186 (2011) 2103-2109.
[38] M. Valden, X. Lai, D.W. Goodman, Onset of catalytic activity of gold clusters on titania with the appearance of nonmetallic properties, *Science*, 281 (1998) 1647-1650.
[39] R. Wang, K. Hashimoto, A. Fujishima, M. Chikuni, E. Kojima, A. Kitamura, M. Shimohigoshi, T. Watanabe, Light-induced amphiphilic surfaces, *Nature*, 388 (1997) 431-432.
[40] M. Gratzel, Photoelectrochemical cells, *Nature*, 414 (2001) 338-344.
[41] A.K. Sharma, Anodizing titanium for space applications, *Thin Solid Films*, 208 (1992) 48-54.
[42] A. Mazzarolo, M. Curioni, A. Vicenzo, P. Skeldon, G.E. Thompson, Anodic growth of titanium oxide: Electrochemical behaviour and morphological evolution, *Electrochimica Acta*, 75 (2012) 288-295.
[43] B.J. Hwang, J.R. Hwang, Kinetic model of anodic oxidation of titanium in sulphuric acid, *Journal of Applied Electrochemistry*, 23 (1993) 1056-1062.
[44] S.A. Fadl-allah, Q. Mohsen, Characterization of native and anodic oxide films formed on commercial pure titanium using electrochemical properties and morphology techniques, *Applied Surface Science*, 256 (2010) 5849-5855.
[45] A. Müller, G.S. Popkirov, R.N. Schindler, The Anodic Growth and the Stability of Thin Passive Films on Titanium Electrodes, *Berichte der Bunsengesellschaft für physikalische Chemie*, 96 (1992) 1432-1437.
[46] E. Krasicka-Cydzik, *Studies on transition of titanium from active into passive state in phosphoric acid solutions*, in: Passivation of Metals and Semiconductors, and Properties of Thin Oxide Layers, Elsevier Science, Amsterdam, 2006, pp. 193-198.
[47] Y.-T. Sul, C.B. Johansson, Y. Jeong, T. Albrektsson, The electrochemical oxide growth behaviour on titanium in acid and alkaline electrolytes, *Medical Engineering & Physics*, 23 (2001) 329-346.
[48] D.J. Blackwood, L.M. Peter, The influence of growth rate on the properties of anodic oxide films on titanium, *Electrochimica Acta*, 34 (1989) 1505-1511.
[49] T. Shibata, Y.C. Zhu, The effect of film formation conditions on the structure and composition of anodic oxide films on titanium, *Corrosion Science*, 37 (1995) 253-270.
[50] T. Ohtsuka, J. Guo, N. Sato, Raman Spectra of the Anodic Oxide Film on Titanium in Acidic Sulfate and Neutral Phosphate Solutions, *Journal of The Electrochemical Society*, 133 (1986) 2473-2476.
[51] M.V. Diamanti, M.P. Pedeferri, Effect of anodic oxidation parameters on the titanium oxides formation, *Corrosion Science*, 49 (2007) 939-948.
[52] P. Roy, D. Kim, K. Lee, E. Spiecker, P. Schmuki, TiO_2 nanotubes and their application in dye-sensitized solar cells, *Nanoscale*, 2 (2010) 45-59.

[53] J.M. Macak, H. Tsuchiya, A. Ghicov, K. Yasuda, R. Hahn, S. Bauer, P. Schmuki, TiO_2 nanotubes: Self-organized electrochemical formation, properties and applications, *Current Opinion in Solid State and Materials Science*, 11 (2007) 3-18.
[54] Z.-W. Fu, F. Huang, Y.-Q. Chu, Y. Zhang, Q.-Z. Qin Characterization of Amorphous Ta_2O_5 Film as a Novel Anode Material, *Journal of The Electrochemical Society*, 150 (2003) A776-A782.
[55] G.E.J. Poinern, N. Ali, D. Fawcett, Progress in Nano-Engineered Anodic Aluminum Oxide Membrane Development, *Materials*, 4 (2011) 487.
[56] F. Trivinho-Strixino, H.A. Guerreiro, C.S. Gomes, E.C. Pereira, F.E.G. Guimarães, Active waveguide effects from porous anodic alumina: An optical sensor proposition, *Applied Physics Letters*, 97 (2010) 011902.
[57] Y.-Y. Song, P. Roy, I. Paramasivam, P. Schmuki, Voltage-Induced Payload Release and Wettability Control on TiO_2 and TiO_2 Nanotubes, *Angewandte Chemie International Edition*, 49 (2010) 351-354.
[58] H. Maltanava, S. Poznyak, M. Starykevich, M. Ivanovskaya, Electrocatalytic activity of Au nanoparticles onto TiO_2 nanotubular layers in oxygen electroreduction reaction: size and support effects, *Electrochimica Acta*, 222 (2016) 1013-1020.
[59] S.A. Ulasevich, S.K. Poznyak, A.I. Kulak, A.D. Lisenkov, M. Starykevich, E.V. Skorb, Photocatalytic Deposition of Hydroxyapatite onto a Titanium Dioxide Nanotubular Layer with Fine Tuning of Layer Nanoarchitecture, *Langmuir*, 32 (2016) 4016-4021.
[60] W. Lee, D. Kim, K. Lee, P. Roy, P. Schmuki, Direct anodic growth of thick WO_3 mesosponge layers and characterization of their photoelectrochemical response, *Electrochimica Acta*, 56 (2010) 828-833.
[61] A. Ghicov, H. Tsuchiya, R. Hahn, J.M. Macak, A.G. Muñoz, P. Schmuki, TiO_2 nanotubes: H^+insertion and strong electrochromic effects, *Electrochemistry Communications*, 8 (2006) 528-532.
[62] S. Berger, A. Ghicov, Y.C. Nah, P. Schmuki, Transparent TiO_2 Nanotube Electrodes via Thin Layer Anodization: Fabrication and Use in Electrochromic Devices, *Langmuir*, 25 (2009) 4841-4844.
[63] F. Keller, M. Hunter, D. Robinson, Structural features of oxide coatings on aluminum, *Journal of the Electrochemical Society*, 100 (1953) 411-419.
[64] H. Masuda, K. Fukuda, Ordered Metal Nanohole Arrays Made by a Two-Step Replication of Honeycomb Structures of Anodic Alumina, *Science*, 268 (1995) 1466-1468.
[65] S.Z. Chu, K. Wada, S. Inoue, M. Isogai, Y. Katsuta, A. Yasumori, Large-Scale Fabrication of Ordered Nanoporous Alumina Films with Arbitrary Pore Intervals by Critical-Potential Anodization, *Journal of The Electrochemical Society*, 153 (2006) B384-B391.
[66] H. Masuda, F. Hasegwa, S. Ono, Self- Ordering of Cell Arrangement of Anodic Porous Alumina Formed in Sulfuric Acid Solution, *Journal of The Electrochemical Society*, 144 (1997) L127-L130.
[67] M. Hideki, Y. Kouichi, O. Atsushi, Self-Ordering of Cell Configuration of Anodic Porous Alumina with Large-Size Pores in Phosphoric Acid Solution, *Japanese Journal of Applied Physics*, 37 (1998) L1340.
[68] A.P. Li, F. Müller, A. Birner, K. Nielsch, U. Gösele, Hexagonal pore arrays with a 50–420 nm interpore distance formed by self-organization in anodic alumina, *Journal of Applied Physics*, 84 (1998) 6023-6026.
[69] O. Jessensky, F. Müller, U. Gösele, Self-organized formation of hexagonal pore arrays in anodic alumina, *Applied Physics Letters*, 72 (1998) 1173-1175.
[70] K. Nielsch, J. Choi, K. Schwirn, R.B. Wehrspohn, U. Gösele, Self-ordering Regimes of Porous Alumina: The 10 Porosity Rule, *Nano Letters*, 2 (2002) 677-680.
[71] G.E. Thompson, R.C. Furneaux, G.C. Wood, J.A. Richardson, J.S. Goode, Nucleation and growth of porous anodic films on aluminium, *Nature*, 272 (1978) 433-435.
[72] Z. Su, G. Hahner, W. Zhou, Investigation of the pore formation in anodic aluminium oxide, *Journal of Materials Chemistry*, 18 (2008) 5787-5795.
[73] V.P. Parkhutik, The initial stages of aluminium porous anodization studied by Auger electron spectroscopy, *Corrosion Science*, 26 (1986) 295-310.
[74] Z. Su, W. Zhou, Formation Mechanism of Porous Anodic Aluminium and Titanium Oxides, *Advanced Materials*, 20 (2008) 3663-3667.
[75] M. Starykevich, A.D. Lisenkov, A.N. Salak, M.G.S. Ferreira, M.L. Zheludkevich, Electrodeposition of Zinc Nanorods from Ionic Liquid into Porous Anodic Alumina, *ChemElectroChem*, 1 (2014) 1484-1487.
[76] M. Hideki, S. Masahiro, Fabrication of Gold Nanodot Array Using Anodic Porous Alumina as an Evaporation Mask, *Japanese Journal of Applied Physics*, 35 (1996) L126.
[77] X. Wang, G.-R. Han, Fabrication and characterization of anodic aluminum oxide template, *Microelectronic Engineering*, 66 (2003) 166-170.
[78] M. Ghorbani, F. Nasirpouri, A. Iraji zad, A. Saedi, On the growth sequence of highly ordered nanoporous anodic aluminium oxide, *Materials & Design*, 27 (2006) 983-988.
[79] H. Masuda, H. Yamada, M. Satoh, H. Asoh, M. Nakao, T. Tamamura, Highly ordered nanochannel-array architecture in anodic alumina, *Applied Physics Letters*, 71 (1997) 2770-2772.

[80] H. Asoh, K. Nishio, M. Nakao, T. Tamamura, H. Masuda, Conditions for Fabrication of Ideally Ordered Anodic Porous Alumina Using Pretextured Al, *Journal of The Electrochemical Society*, 148 (2001) B152-B156.
[81] H. Masuda, H. Asoh, M. Watanabe, K. Nishio, M. Nakao, T. Tamamura, Square and Triangular Nanohole Array Architectures in Anodic Alumina, *Advanced Materials*, 13 (2001) 189-192.
[82] N.W. Liu, A. Datta, C.Y. Liu, C.Y. Peng, H.H. Wang, Y.L. Wang, Fabrication of Anodic-Alumina Films with Custom-Designed Arrays of Nanochannels, *Advanced Materials*, 17 (2005) 222-225.
[83] C.Y. Peng, C.Y. Liu, N.W. Liu, H.H. Wang, A. Datta, Y.L. Wang, Ideally ordered 10 nm channel arrays grown by anodization of focused-ion-beam patterned aluminum, *Journal of Vacuum Science & Technology B: Microelectronics and Nanometer Structures Processing, Measurement, and Phenomena*, 23 (2005) 559-562.
[84] N.-W. Liu, C.-Y. Liu, H.-H. Wang, C.-F. Hsu, M.-Y. Lai, T.-H. Chuang, Y.-L. Wang, Focused-Ion-Beam-Based Selective Closing and Opening of Anodic Alumina Nanochannels for the Growth of Nanowire Arrays Comprising Multiple Elements, *Advanced Materials*, 20 (2008) 2547-2551.
[85] Z. Sun, H.K. Kim, Growth of ordered, single-domain, alumina nanopore arrays with holographically patterned aluminum films, *Applied Physics Letters*, 81 (2002) 3458-3460.
[86] D. Ma, S. Li, C. Liang, Electropolishing of high-purity aluminium in perchloric acid and ethanol solutions, *Corrosion Science*, 51 (2009) 713-718.
[87] A. Rauf, M. Mehmood, M. Asim Rasheed, M. Aslam, The effects of electropolishing on the nanochannel ordering of the porous anodic alumina prepared in oxalic acid, *Journal of Solid State Electrochemistry*, 13 (2009) 321-332.
[88] V. Zwilling, E. Darque-Ceretti, A. Boutry-Forveille, D. David, M.Y. Perrin, M. Aucouturier, Structure and physicochemistry of anodic oxide films on titanium and TA6V alloy, *Surface and Interface Analysis*, 27 (1999) 629-637.
[89] J.M. Macak, K. Sirotna, P. Schmuki, Self-organized porous titanium oxide prepared in Na_2SO_4/NaF electrolytes, *Electrochimica Acta*, 50 (2005) 3679-3684.
[90] S. Bauer, S. Kleber, P. Schmuki, TiO_2 nanotubes: Tailoring the geometry in H_3PO_4/HF electrolytes, *Electrochemistry Communications*, 8 (2006) 1321-1325.
[91] A. Ghicov, H. Tsuchiya, J.M. Macak, P. Schmuki, Titanium oxide nanotubes prepared in phosphate electrolytes, *Electrochemistry Communications*, 7 (2005) 505-509.
[92] H. Tsuchiya, J.M. Macak, L. Taveira, E. Balaur, A. Ghicov, K. Sirotna, P. Schmuki, Self-organized TiO2 nanotubes prepared in ammonium fluoride containing acetic acid electrolytes, *Electrochemistry Communications*, 7 (2005) 576-580.
[93] J.M. Macak, P. Schmuki, Anodic growth of self-organized anodic TiO_2 nanotubes in viscous electrolytes, *Electrochimica Acta*, 52 (2006) 1258-1264.
[94] J.M. Macak, H. Hildebrand, U. Marten-Jahns, P. Schmuki, Mechanistic aspects and growth of large diameter self-organized TiO_2 nanotubes, *Journal of Electroanalytical Chemistry*, 621 (2008) 254-266.
[95] I. Paramasivam, J.M. Macak, T. Selvam, P. Schmuki, Electrochemical synthesis of self-organized TiO2 nanotubular structures using an ionic liquid (BMIM-BF4), *Electrochimica Acta*, 54 (2008) 643-648.
[96] S.P. Albu, P. Schmuki, TiO_2 nanotubes grown in different organic electrolytes: Two-size self-organization, single vs. double-walled tubes, and giant diameters, *physica status solidi (RRL) – Rapid Research Letters*, 4 (2010) 215-217.
[97] J.M. Macak, H. Tsuchiya, L. Taveira, S. Aldabergerova, P. Schmuki, Smooth Anodic TiO_2 Nanotubes, *Angewandte Chemie International Edition*, 44 (2005) 7463-7465.
[98] S.P. Albu, A. Ghicov, J.M. Macak, P. Schmuki, 250 µm long anodic TiO_2 nanotubes with hexagonal self-ordering, *physica status solidi (RRL) – Rapid Research Letters*, 1 (2007) R65-R67.
[99] J.M. Macak, S.P. Albu, P. Schmuki, Towards ideal hexagonal self-ordering of TiO_2 nanotubes, *physica status solidi (RRL) – Rapid Research Letters*, 1 (2007) 181-183.
[100] S. Berger, J. Kunze, P. Schmuki, D. LeClere, A.T. Valota, P. Skeldon, G.E. Thompson, A lithographic approach to determine volume expansion factors during anodization: Using the example of initiation and growth of TiO_2-nanotubes, *Electrochimica Acta*, 54 (2009) 5942-5948.
[101] L.V. Taveira, J.M. Macák, H. Tsuchiya, L.F.P. Dick, P. Schmuki, Initiation and Growth of Self-Organized TiO2 Nanotubes Anodically Formed in NH_4F / $(NH_4)_2SO_4$ Electrolytes, *Journal of The Electrochemical Society*, 152 (2005) B405-B410.
[102] P. Roy, S. Berger, P. Schmuki, TiO_2 Nanotubes: Synthesis and Applications, *Angewandte Chemie International Edition*, 50 (2011) 2904-2939.
[103] R. Beranek, H. Hildebrand, P. Schmuki, Self-Organized Porous Titanium Oxide Prepared in H_2SO_4 / HF Electrolytes, *Electrochemical and Solid-State Letters*, 6 (2003) B12-B14.

[104] A. Valota, D.J. LeClere, P. Skeldon, M. Curioni, T. Hashimoto, S. Berger, J. Kunze, P. Schmuki, G.E. Thompson, Influence of water content on nanotubular anodic titania formed in fluoride/glycerol electrolytes, *Electrochimica Acta,* 54 (2009) 4321-4327.
[105] S.P. Albu, A. Ghicov, S. Aldabergenova, P. Drechsel, D. LeClere, G.E. Thompson, J.M. Macak, P. Schmuki, Formation of Double-Walled TiO_2 Nanotubes and Robust Anatase Membranes, *Advanced Materials,* 20 (2008) 4135-4139.
[106] H. Habazaki, K. Fushimi, K. Shimizu, P. Skeldon, G.E. Thompson, Fast migration of fluoride ions in growing anodic titanium oxide, *Electrochemistry Communications,* 9 (2007) 1222-1227.
[107] S. Berger, J. Kunze, P. Schmuki, A.T. Valota, D.J. LeClere, P. Skeldon, G.E. Thompson, Influence of Water Content on the Growth of Anodic TiO_2 Nanotubes in Fluoride-Containing Ethylene Glycol Electrolytes, *Journal of The Electrochemical Society,* 157 (2010) C18-C23.
[108] K.R. Hebert, J.E. Houser, A Model for Coupled Electrical Migration and Stress-Driven Transport in Anodic Oxide Films, *Journal of The Electrochemical Society,* 156 (2009) C275-C281.
[109] A. Tighineanu, T. Ruff, S. Albu, R. Hahn, P. Schmuki, Conductivity of TiO_2 nanotubes: Influence of annealing time and temperature, *Chemical Physics Letters,* 494 (2010) 260-263.
[110] J.M. Macak, S. Aldabergerova, A. Ghicov, P. Schmuki, Smooth anodic TiO_2 nanotubes: annealing and structure, *physica status solidi (a),* 203 (2006) R67-R69.
[111] A. Ghicov, S.P. Albu, R. Hahn, D. Kim, T. Stergiopoulos, J. Kunze, C.-A. Schiller, P. Falaras, P. Schmuki, TiO_2 Nanotubes in Dye-Sensitized Solar Cells: Critical Factors for the Conversion Efficiency, *Chemistry – An Asian Journal,* 4 (2009) 520-525.
[112] J. Park, S. Bauer, K. von der Mark, P. Schmuki, Nanosize and Vitality: TiO_2 Nanotube Diameter Directs Cell Fate, *Nano Letters,* 7 (2007) 1686-1691.
[113] Y. Xie, Photoelectrochemical application of nanotubular titania photoanode, *Electrochimica Acta,* 51 (2006) 3399-3406.
[114] K. Shankar, J.I. Basham, N.K. Allam, O.K. Varghese, G.K. Mor, X. Feng, M. Paulose, J.A. Seabold, K.-S. Choi, C.A. Grimes, Recent Advances in the Use of TiO_2 Nanotube and Nanowire Arrays for Oxidative Photoelectrochemistry, *The Journal of Physical Chemistry C,* 113 (2009) 6327-6359.
[115] K. Shankar, J. Bandara, M. Paulose, H. Wietasch, O.K. Varghese, G.K. Mor, T.J. LaTempa, M. Thelakkat, C.A. Grimes, Highly Efficient Solar Cells using TiO_2 Nanotube Arrays Sensitized with a Donor-Antenna Dye, *Nano Letters,* 8 (2008) 1654-1659.
[116] K. Zhu, N.R. Neale, A. Miedaner, A.J. Frank, Enhanced Charge-Collection Efficiencies and Light Scattering in Dye-Sensitized Solar Cells Using Oriented TiO_2 Nanotubes Arrays, *Nano Letters,* 7 (2007) 69-74.
[117] D.K. Ivanou, E.A. Streltsov, A.K. Fedotov, A.V. Mazanik, D. Fink, A. Petrov, Electrochemical deposition of PbSe and CdTe nanoparticles onto p-Si(100) wafers and into nanopores in SiO_2/Si(100) structure, *Thin Solid Films,* 490 (2005) 154-160.
[118] Y.A. Ivanova, D.K. Ivanou, A.K. Fedotov, E.A. Streltsov, S.E. Demyanov, A.V. Petrov, E.Y. Kaniukov, D. Fink, Electrochemical deposition of Ni and Cu onto monocrystalline n-Si(100) wafers and into nanopores in Si/SiO_2 template, *Journal of Materials Science,* 42 (2007) 9163-9169.
[119] Y.A. Ivanova, D.K. Ivanou, E.A. Streltsov, A.K. Fedotov, Electrochemical deposition of Te and electroless deposition of Se nanoparticles in etched tracks of Au^+ ions in SiO_2 layer on n-Si(1 0 0) wafers, *Materials Science and Engineering: B,* 147 (2008) 271-275.
[120] Z. Liu, S.Z.E. Abedin, M.S. Ghazvini, F. Endres, Electrochemical synthesis of vertically aligned zinc nanowires using track-etched polycarbonate membranes as templates, *Physical Chemistry Chemical Physics,* 15 (2013) 11362-11367.
[121] Z. Liu, A.M. Elbasiony, S. Zein El Abedin, F. Endres, Electrodeposition of Zinc–Copper and Zinc–Tin Films and Free-Standing Nanowire Arrays from Ionic Liquids, *ChemElectroChem,* 2 (2015) 389-395.
[122] C.P. Chan, H. Lam, K.K. Leung, C. Surya, Growth Of Copper Zinc Tin Sulfide Nano-Rods By Eelectrodeposition Using Anodized Aluminium As The Growth Mask, *Journal of Nonlinear Optical Physics & Materials,* 18 (2009) 599-603.
[123] E.K. Schmitt, M. Nurnabi, R.J. Bushby, C. Steinem, Electrically insulating pore-suspending membranes on highly ordered porous alumina obtained from vesicle spreading, *Soft Matter,* 4 (2008) 250-253.
[124] T.T. Xu, R.D. Piner, R.S. Ruoff, An Improved Method To Strip Aluminum from Porous Anodic Alumina Films, *Langmuir,* 19 (2003) 1443-1445.
[125] L. Li, Y. Zhang, G. Li, L. Zhang, A route to fabricate single crystalline bismuth nanowire arrays with different diameters, *Chemical Physics Letters,* 378 (2003) 244-249.
[126] S.-H. Yoo, L. Liu, S. Park, Nanoparticle films as a conducting layer for anodic aluminum oxide template-assisted nanorod synthesis, *Journal of Colloid and Interface Science,* 339 (2009) 183-186.

[127] I.Z. Rahman, A. Boboc, K.M. Razeeb, M.A. Rahman, Analysis of magnetic interaction in Ni nanowire array grown using electrodeposition process, *Journal of Magnetism and Magnetic Materials*, 290–291, Part 1 (2005) 246-249.
[128] X.Y. Zhang, Y. Cai, J.Y. Miao, K.Y. Ng, Y.F. Chan, X.X. Zhang, N. Wang, Formation and phase transformation of selenium nanowire arrays in anodic porous alumina templates, *Journal of Crystal Growth*, 276 (2005) 674-679.
[129] C. Jin, X. Xiang, C. Jia, W. Liu, W. Cai, L. Yao, X. Li, Electrochemical Fabrication of Large-Area, Ordered Bi2Te3 Nanowire Arrays, *The Journal of Physical Chemistry B*, 108 (2004) 1844-1847.
[130] Y.-K. Su, D.-H. Qin, H.-L. Zhang, H. Li, H.-L. Li, Microstructure and magnetic properties of bamboo-like CoPt/Pt multilayered nanowire arrays, *Chemical Physics Letters*, 388 (2004) 406-410.
[131] J.M. Montero-Moreno, M. Belenguer, M. Sarret, C.M. Müller, Production of alumina templates suitable for electrodeposition of nanostructures using stepped techniques, *Electrochimica Acta*, 54 (2009) 2529-2535.
[132] A. Santos, L. Vojkuvka, J. Pallarés, J. Ferré-Borrull, L.F. Marsal, In situ electrochemical dissolution of the oxide barrier layer of porous anodic alumina fabricated by hard anodization, *Journal of Electroanalytical Chemistry*, 632 (2009) 139-142.
[133] K. Nielsch, F. Müller, A.P. Li, U. Gösele, Uniform Nickel Deposition into Ordered Alumina Pores by Pulsed Electrodeposition, *Advanced Materials*, 12 (2000) 582-586.
[134] J.M. Macak, P.J. Barczuk, H. Tsuchiya, M.Z. Nowakowska, A. Ghicov, M. Chojak, S. Bauer, S. Virtanen, P.J. Kulesza, P. Schmuki, Self-organized nanotubular TiO_2 matrix as support for dispersed Pt/Ru nanoparticles: Enhancement of the electrocatalytic oxidation of methanol, *Electrochemistry Communications*, 7 (2005) 1417-1422.
[135] R.S. Ray, B. Sarma, A.L. Jurovitzki, M. Misra, Fabrication and characterization of titania nanotube/cobalt sulfide supercapacitor electrode in various electrolytes, *Chemical Engineering Journal*, 260 (2015) 671-683.
[136] K.M. Susanta, B. Subarna, M. Mano, Synthesis of Fe_2O_3 / TiO_2 nanorod–nanotube arrays by filling TiO 2 nanotubes with Fe, *Nanotechnology*, 19 (2008) 315601.
[137] T. Gandhi, K.S. Raja, M. Misra, Synthesis of ZnTe nanowires onto TiO_2 nanotubular arrays by pulse-reverse electrodeposition, *Thin Solid Films*, 517 (2009) 4527-4533.
[138] D. Fang, K. Huang, S. Liu, D. Qin, High density copper nanowire arrays deposition inside ordered titania pores by electrodeposition, *Electrochemistry Communications*, 11 (2009) 901-904.
[139] J.M. Macak, B.G. Gong, M. Hueppe, P. Schmuki, Filling of TiO_2 Nanotubes by Self-Doping and Electrodeposition, *Advanced Materials*, 19 (2007) 3027-3031.
[140] I.R. Christie, B.P. Cameron, Gold electrodeposition within the electronics industry, *Gold Bulletin*, 27 (1994) 12-20.
[141] M. Clarke, *13.1 - Electroplating A2 - Shreir, L.L*, in: Corrosion, Newnes, 1976, pp. 13:13-13:47.
[142] J.W. Dini, *Electrodeposition: The Materials Science of Coatings and Substrates*, Noyes Publications, 1993.
[143] Y. Marcus, Ionic liquid properties : from molten salts to RTILs, in, 2016.
[144] D.M. F. Endres, A. Abbott, *Electrodeposition from Ionic Liquids*, WILEY-VCH Verlag GmbH & Co. KGaA, Weinheim, 2008.
[145] T. Welton, Room-Temperature Ionic Liquids. Solvents for Synthesis and Catalysis, *Chemical Reviews*, 99 (1999) 2071-2084.
[146] J.S. Wilkes, M.J. Zaworotko, Air and water stable 1-ethyl-3-methylimidazolium based ionic liquids, *Journal of the Chemical Society, Chemical Communications*, (1992) 965-967.
[147] J. Fuller, R.T. Carlin, R.A. Osteryoung, The Room Temperature Ionic Liquid 1- Ethyl- 3-methylimidazolium Tetrafluoroborate: Electrochemical Couples and Physical Properties, *Journal of The Electrochemical Society*, 144 (1997) 3881-3886.
[148] R.P. Swatloski, J.D. Holbrey, R.D. Rogers, Ionic liquids are not always green: hydrolysis of 1-butyl-3-methylimidazolium hexafluorophosphate, *Green Chemistry*, 5 (2003) 361-363.
[149] P. Bonhôte, A.-P. Dias, N. Papageorgiou, K. Kalyanasundaram, M. Grätzel, Hydrophobic, Highly Conductive Ambient-Temperature Molten Salts, *Inorganic Chemistry*, 35 (1996) 1168-1178.
[150] P. Atkins, J. de Paula, *Elements of Physical Chemistry*, W. H. Freeman, 2009.
[151] A.P. Abbott, G. Capper, D.L. Davies, H.L. Munro, R.K. Rasheed, V. Tambyrajah, Preparation of novel, moisture-stable, Lewis-acidic ionic liquids containing quaternary ammonium salts with functional side chains, *Chemical Communications*, (2001) 2010-2011.
[152] Y.-F. Lin, I.W. Sun, Electrodeposition of zinc from a Lewis acidic zinc chloride-1-ethyl-3-methylimidazolium chloride molten salt, *Electrochimica Acta*, 44 (1999) 2771-2777.

[153] S.-I. Hsiu, J.-F. Huang, I.W. Sun, C.-H. Yuan, J. Shiea, Lewis acidity dependency of the electrochemical window of zinc chloride–1-ethyl-3-methylimidazolium chloride ionic liquids, *Electrochimica Acta*, 47 (2002) 4367-4372.
[154] E.L. Smith, A.P. Abbott, K.S. Ryder, Deep Eutectic Solvents (DESs) and Their Applications, *Chemical Reviews*, 114 (2014) 11060-11082.
[155] A.P. Abbott, G. Capper, D.L. Davies, R.K. Rasheed, V. Tambyrajah, Quaternary ammonium zinc- or tin-containing ionic liquids: water insensitive, recyclable catalysts for Diels-Alder reactions, *Green Chemistry*, 4 (2002) 24-26.
[156] M.S. Sitze, E.R. Schreiter, E.V. Patterson, R.G. Freeman, Ionic Liquids Based on FeCl3 and FeCl2. Raman Scattering and ab Initio Calculations, *Inorganic Chemistry*, 40 (2001) 2298-2304.
[157] J.-Z. Yang, Y. Jin, W.-G. Xu, Q.-G. Zhang, S.-L. Zang, Studies on mixture of ionic liquid EMIGaCl4 and EMIC, *Fluid Phase Equilibria*, 227 (2005) 41-46.
[158] S. Zein El Abedin, A.Y. Saad, H.K. Farag, N. Borisenko, Q.X. Liu, F. Endres, Electrodeposition of selenium, indium and copper in an air- and water-stable ionic liquid at variable temperatures, *Electrochimica Acta*, 52 (2007) 2746-2754.
[159] A.P. Abbott, G. Capper, D.L. Davies, R. Rasheed, Ionic Liquids Based upon Metal Halide/Substituted Quaternary Ammonium Salt Mixtures, *Inorganic Chemistry*, 43 (2004) 3447-3452.
[160] G.C.C. A.P. Abbott, D.L. Davies, R.R.V. Tambyrajah, , *Int. Pat.*, WO 0226701 (2001).
[161] H. Wang, Y. Jing, X. Wang, Y. Yao, Y. Jia, Ionic liquid analogous formed from magnesium chloride hexahydrate and its physico-chemical properties, *Journal of Molecular Liquids*, 163 (2011) 77-82.
[162] A.P. Abbott, G. Capper, D.L. Davies, R.K. Rasheed, Ionic Liquid Analogues Formed from Hydrated Metal Salts, *Chemistry – A European Journal*, 10 (2004) 3769-3774.
[163] L.S. Bobrova, F.I. Danilov, V.S. Protsenko, Effects of temperature and water content on physicochemical properties of ionic liquids containing $CrCl_3 \cdot xH_2O$ and choline chloride, *Journal of Molecular Liquids*, 223 (2016) 48-53.
[164] V.S. Protsenko, L.S. Bobrova, F.I. Danilov, Physicochemical properties of ionic liquid mixtures containing choline chloride, chromium (III) chloride and water: effects of temperature and water content, *Ionics*, (2016) 1-7.
[165] A.P. Abbott, K.J. McKenzie, Application of ionic liquids to the electrodeposition of metals, *Physical Chemistry Chemical Physics*, 8 (2006) 4265-4279.
[166] A.P. Abbott, D. Boothby, G. Capper, D.L. Davies, R.K. Rasheed, Deep Eutectic Solvents Formed between Choline Chloride and Carboxylic Acids: Versatile Alternatives to Ionic Liquids, *Journal of the American Chemical Society*, 126 (2004) 9142-9147.
[167] A.P. Abbott, G. Capper, D.L. Davies, R.K. Rasheed, V. Tambyrajah, Novel solvent properties of choline chloride/urea mixtures, *Chemical Communications*, (2003) 70-71.
[168] A.P. Abbott, J.C. Barron, K.S. Ryder, D. Wilson, Eutectic-Based Ionic Liquids with Metal-Containing Anions and Cations, *Chemistry – A European Journal*, 13 (2007) 6495-6501.
[169] P. Wasserscheid, T. Welton, *Ionic Liquids in Synthesis, 2 Volume Set*, Wiley, 2007.
[170] Q. Dong, C.D. Muzny, A. Kazakov, V. Diky, J.W. Magee, J.A. Widegren, R.D. Chirico, K.N. Marsh, M. Frenkel, ILThermo: A Free-Access Web Database for Thermodynamic Properties of Ionic Liquids, *Journal of Chemical & Engineering Data*, 52 (2007) 1151-1159.
[171] M. Galiński, A. Lewandowski, I. Stępniak, Ionic liquids as electrolytes, *Electrochimica Acta*, 51 (2006) 5567-5580.
[172] W. Ochędzan-Siodłak, K. Dziubek, D. Siodłak, Densities and viscosities of imidazolium and pyridinium chloroaluminate ionic liquids, *Journal of Molecular Liquids*, 177 (2013) 85-93.
[173] J.S. Wilkes, J.A. Levisky, R.A. Wilson, C.L. Hussey, Dialkylimidazolium chloroaluminate melts: a new class of room-temperature ionic liquids for electrochemistry, spectroscopy and synthesis, *Inorganic Chemistry*, 21 (1982) 1263-1264.
[174] S. Carda–Broch, A. Berthod, D.W. Armstrong, Solvent properties of the 1-butyl-3-methylimidazolium hexafluorophosphate ionic liquid, *Analytical and Bioanalytical Chemistry*, 375 (2003) 191-199.
[175] R. Taguchi, H. Machida, Y. Sato, R.L. Smith, High-Pressure Densities of 1-Alkyl-3-methylimidazolium Hexafluorophosphates and 1-Alkyl-3-methylimidazolium Tetrafluoroborates at Temperatures from (313 to 473) K and at Pressures up to 200 MPa, *Journal of Chemical & Engineering Data*, 54 (2009) 22-27.
[176] D. Tomida, A. Kumagai, K. Qiao, C. Yokoyama, Viscosity of 1-Butyl-3-methylimidazolium Hexafluorophosphate + CO_2 Mixture, *Journal of Chemical & Engineering Data*, 52 (2007) 1638-1640.

[177] D. Tomida, A. Kumagai, S. Kenmochi, K. Qiao, C. Yokoyama, Viscosity of 1-Hexyl-3-methylimidazolium Hexafluorophosphate and 1-Octyl-3-methylimidazolium Hexafluorophosphate at High Pressure, *Journal of Chemical & Engineering Data,* 52 (2007) 577-579.
[178] H.L. Ngo, K. LeCompte, L. Hargens, A.B. McEwen, Thermal properties of imidazolium ionic liquids, *Thermochimica Acta,* 357–358 (2000) 97-102.
[179] J.G. Huddleston, A.E. Visser, W.M. Reichert, H.D. Willauer, G.A. Broker, R.D. Rogers, Characterization and comparison of hydrophilic and hydrophobic room temperature ionic liquids incorporating the imidazolium cation, *Green Chemistry,* 3 (2001) 156-164.
[180] J. Vila, B. Fernández-Castro, E. Rilo, J. Carrete, M. Domínguez-Pérez, J.R. Rodríguez, M. García, L.M. Varela, O. Cabeza, Liquid–solid–liquid phase transition hysteresis loops in the ionic conductivity of ten imidazolium-based ionic liquids, *Fluid Phase Equilibria,* 320 (2012) 1-10.
[181] K.R. Harris, M. Kanakubo, N. Tsuchihashi, K. Ibuki, M. Ueno, Effect of Pressure on the Transport Properties of Ionic Liquids: 1-Alkyl-3-methylimidazolium Salts, *The Journal of Physical Chemistry B,* 112 (2008) 9830-9840.
[182] A.J.L. Costa, J.M.S.S. Esperança, I.M. Marrucho, L.P.N. Rebelo, Densities and Viscosities of 1-Ethyl-3-methylimidazolium n-Alkyl Sulfates, *Journal of Chemical & Engineering Data,* 56 (2011) 3433-3441.
[183] H. Rodríguez, J.F. Brennecke, Temperature and Composition Dependence of the Density and Viscosity of Binary Mixtures of Water + Ionic Liquid, *Journal of Chemical & Engineering Data,* 51 (2006) 2145-2155.
[184] B.E. Mbondo Tsamba, S. Sarraute, M. Traïkia, P. Husson, Transport Properties and Ionic Association in Pure Imidazolium-Based Ionic Liquids as a Function of Temperature, *Journal of Chemical & Engineering Data,* 59 (2014) 1747-1754.
[185] A.P. Abbott, J.C. Barron, G. Frisch, S. Gurman, K.S. Ryder, A. Fernando Silva, Double layer effects on metal nucleation in deep eutectic solvents, *Physical Chemistry Chemical Physics,* 13 (2011) 10224-10231.
[186] S.V. Dzyuba, R.A. Bartsch, Influence of Structural Variations in 1-Alkyl(aralkyl)-3-Methylimidazolium Hexafluorophosphates and Bis(trifluoromethylsulfonyl)imides on Physical Properties of the Ionic Liquids, *ChemPhysChem,* 3 (2002) 161-166.
[187] A.P. Abbott, Model for the Conductivity of Ionic Liquids Based on an Infinite Dilution of Holes, *ChemPhysChem,* 6 (2005) 2502-2505.
[188] S.N. Baker, G.A. Baker, M.A. Kane, F.V. Bright, The Cybotactic Region Surrounding Fluorescent Probes Dissolved in 1-Butyl-3-methylimidazolium Hexafluorophosphate: Effects of Temperature and Added Carbon Dioxide, *The Journal of Physical Chemistry B,* 105 (2001) 9663-9668.
[189] K.R. Harris, M. Kanakubo, L.A. Woolf, Temperature and Pressure Dependence of the Viscosity of the Ionic Liquid 1-Butyl-3-methylimidazolium Tetrafluoroborate: Viscosity and Density Relationships in Ionic Liquids, *Journal of Chemical & Engineering Data,* 52 (2007) 2425-2430.
[190] K.R. Harris, M. Kanakubo, L.A. Woolf, Temperature and Pressure Dependence of the Viscosity of the Ionic Liquids 1-Hexyl-3-methylimidazolium Hexafluorophosphate and 1-Butyl-3-methylimidazolium Bis(trifluoromethylsulfonyl)imide, *Journal of Chemical & Engineering Data,* 52 (2007) 1080-1085.
[191] K.R. Harris, M. Kanakubo, L.A. Woolf, Temperature and Pressure Dependence of the Viscosity of the Ionic Liquids 1-Methyl-3-octylimidazolium Hexafluorophosphate and 1-Methyl-3-octylimidazolium Tetrafluoroborate, *Journal of Chemical & Engineering Data,* 51 (2006) 1161-1167.
[192] K.R. Harris, L.A. Woolf, M. Kanakubo, Temperature and Pressure Dependence of the Viscosity of the Ionic Liquid 1-Butyl-3-methylimidazolium Hexafluorophosphate, *Journal of Chemical & Engineering Data,* 50 (2005) 1777-1782.
[193] R. Aranowski, I. Cichowska-Kopczyńska, B. Dębski, P. Jasiński, Conductivity and viscosity changes of imidazolium ionic liquids induced by H_2O and CO_2, *Journal of Molecular Liquids,* 221 (2016) 541-546.
[194] J.A. Widegren, A. Laesecke, J.W. Magee, The effect of dissolved water on the viscosities of hydrophobic room-temperature ionic liquids, *Chemical Communications,* (2005) 1610-1612.
[195] J. Zhang, W. Wu, T. Jiang, H. Gao, Z. Liu, J. He, B. Han, Conductivities and Viscosities of the Ionic Liquid [bmim][PF_6] + Water + Ethanol and [bmim][PF_6] + Water + Acetone Ternary Mixtures, *Journal of Chemical & Engineering Data,* 48 (2003) 1315-1317.
[196] Q. Liao, C.L. Hussey, Densities, Viscosities, and Conductivities of Mixtures of Benzene with the Lewis Acidic Aluminum Chloride + 1-Methyl-3-ethylimidazolium Chloride Molten Salt, *Journal of Chemical & Engineering Data,* 41 (1996) 1126-1130.
[197] R.L. Perry, K.M. Jones, W.D. Scott, Q. Liao, C.L. Hussey, Densities, Viscosities, and Conductivities of Mixtures of Selected Organic Cosolvents with the Lewis Basic Aluminum Chloride + 1-Methyl-3-ethylimidazolium Chloride Molten Salt, *Journal of Chemical & Engineering Data,* 40 (1995) 615-619.

[198] S. Ibrahim, A. Bakkar, E. Ahmed, A. Selim, Effect of additives and current mode on zinc electrodeposition from deep eutectic ionic liquids, *Electrochimica Acta*, 191 (2016) 724-732.
[199] A.P. Abbott, J.C. Barron, G. Frisch, K.S. Ryder, A.F. Silva, The effect of additives on zinc electrodeposition from deep eutectic solvents, *Electrochimica Acta*, 56 (2011) 5272-5279.
[200] C.P. Fredlake, J.M. Crosthwaite, D.G. Hert, S.N.V.K. Aki, J.F. Brennecke, Thermophysical Properties of Imidazolium-Based Ionic Liquids, *Journal of Chemical & Engineering Data*, 49 (2004) 954-964.
[201] S.I. Smedley, The Interpretation of Ionic Conductivity in Liquids, in, Springer US, Boston, MA, 1980.
[202] C. Schreiner, S. Zugmann, R. Hartl, H.J. Gores, Fractional Walden Rule for Ionic Liquids: Examples from Recent Measurements and a Critique of the So-Called Ideal KCl Line for the Walden Plot, *Journal of Chemical & Engineering Data*, 55 (2010) 1784-1788.
[203] H. Ohno, *Electrochemical Aspects of Ionic Liquids*, Wiley, 2005.
[204] N.V. Ignat'ev, U. Welz-Biermann, A. Kucheryna, G. Bissky, H. Willner, New ionic liquids with tris(perfluoroalkyl)trifluorophosphate (FAP) anions, *Journal of Fluorine Chemistry*, 126 (2005) 1150-1159.
[205] P.R. Gifford, J.B. Palmisano, A Substituted Imidazolium Chloroaluminate Molten Salt Possessing an Increased Electrochemical Window, *Journal of The Electrochemical Society*, 134 (1987) 610-614.
[206] A. Noda, M. Watanabe, Highly conductive polymer electrolytes prepared by in situ polymerization of vinyl monomers in room temperature molten salts, *Electrochimica Acta*, 45 (2000) 1265-1270.
[207] J. Bridges Nicholas, E. Visser Ann, J. Williamson Mark, I. Mickalonis John, M. Adams Thad, Effects of gamma radiation on electrochemical properties of ionic liquids, in: Radiochimica Acta International journal for chemical aspects of nuclear science and technology, vol. 98, 2010, pp. 243.
[208] A.P. Abbott, G. Capper, K.J. McKenzie, K.S. Ryder, Electrodeposition of zinc–tin alloys from deep eutectic solvents based on choline chloride, *Journal of Electroanalytical Chemistry*, 599 (2007) 288-294.
[209] A.P. Abbott, G. Frisch, K.S. Ryder, Electroplating Using Ionic Liquids, *Annual Review of Materials Research*, 43 (2013) 335-358.
[210] G. Inzelt, A. Lewenstam, F. Scholz, *Handbook of Reference Electrodes*, Springer Berlin Heidelberg, 2013.
[211] M. Armand, F. Endres, D.R. MacFarlane, H. Ohno, B. Scrosati, Ionic-liquid materials for the electrochemical challenges of the future, *Nat Mater*, 8 (2009) 621-629.
[212] F. Liu, Y. Deng, X. Han, W. Hu, C. Zhong, Electrodeposition of metals and alloys from ionic liquids, *Journal of Alloys and Compounds*, 654 (2016) 163-170.
[213] W. Simka, D. Puszczyk, G. Nawrat, Electrodeposition of metals from non-aqueous solutions, *Electrochimica Acta*, 54 (2009) 5307-5319.
[214] T. Jiang, M.J. Chollier Brym, G. Dubé, A. Lasia, G.M. Brisard, Electrodeposition of aluminium from ionic liquids: Part I—electrodeposition and surface morphology of aluminium from aluminium chloride ($AlCl_3$)–1-ethyl-3-methylimidazolium chloride ([EMIm]Cl) ionic liquids, *Surface and Coatings Technology*, 201 (2006) 1-9.
[215] A. Bakkar, V. Neubert, Electrodeposition and corrosion characterisation of micro- and nano-crystalline aluminium from $AlCl_3$/1-ethyl-3-methylimidazolium chloride ionic liquid, *Electrochimica Acta*, 103 (2013) 211-218.
[216] Q. Zhang, Q. Wang, S. Zhang, X. Lu, Effect of nicotinamide on electrodeposition of Al from aluminium chloride ($AlCl_3$)-1-butyl-3-methylimidazolium chloride ([Bmim]Cl) ionic liquids, *Journal of Solid State Electrochemistry*, 18 (2014) 257-267.
[217] Y. Chao-Cheng, Electrodeposition of aluminum in molten $AlCl_3$-n-butylpyridinium chloride electrolyte, *Materials Chemistry and Physics*, 37 (1994) 355-361.
[218] A.P. Abbott, C.A. Eardley, N.R.S. Farley, G.A. Griffith, A. Pratt, Electrodeposition of aluminium and aluminium/platinum alloys from AlCl3/benzyltrimethylammonium chloride room temperature ionic liquids, *Journal of Applied Electrochemistry*, 31 (2001) 1345-1350.
[219] M. Lipsztajn, R.A. Osteryoung, Electrochemistry in neutral ambient-temperature ionic liquids. 1. Studies of iron(III), neodymium(III), and lithium(I), *Inorganic Chemistry*, 24 (1985) 716-719.
[220] G.E. Gray, P.A. Kohl, J. Winnick, Stability of Sodium Electrodeposited from a Room Temperature Chloroaluminate Molten Salt, *Journal of The Electrochemical Society*, 142 (1995) 3636-3642.
[221] B.J. Tierney, W.R. Pitner, J.A. Mitchell, C.L. Hussey, G.R. Stafford, Electrodeposition of Copper and Copper-Aluminum Alloys from a Room-Temperature Chloroaluminate Molten Salt, *Journal of The Electrochemical Society*, 145 (1998) 3110-3116.
[222] J.S.Y. Liu, I.W. Sun, Electrochemical Study of the Properties of Indium in Room Temperature Chloroaluminate Molten Salts, *Journal of The Electrochemical Society*, 144 (1997) 140-145.

[223] J.A. Mitchell, W.R. Pitner, C.L. Hussey, G.R. Stafford, Electrodeposition of Cobalt and Cobalt-Aluminum Alloys from a Room Temperature Chloroaluminate Molten Salt, *Journal of The Electrochemical Society*, 143 (1996) 3448-3455.
[224] W.R. Pitner, C.L. Hussey, Electrodeposition of Zinc from the Lewis Acidic Aluminum Chloride-1- Methyl- 3- ethylimidazolium Chloride Room Temperature Molten Salt, *Journal of The Electrochemical Society*, 144 (1997) 3095-3103.
[225] P.Y. Chen, Y.F. Lin, I.W. Sun, Electrochemistry of Gallium in the Lewis Acidic Aluminum Chloride- 1- Methyl- 3- ethylimidazolium Chloride Room- Temperature Molten Salt, *Journal of The Electrochemical Society*, 146 (1999) 3290-3294.
[226] D.A. Habboush, R.A. Osteryoung, Electrochemical studies of antimony(III) and antimony(V) in molten mixtures of aluminum chloride and butylpyridinium chloride, *Inorganic Chemistry*, 23 (1984) 1726-1734.
[227] E.G.S. Jeng, I.W. Sun, Electrochemistry of Tellurium(IV) in the Basic Aluminum Chloride-1-Methyl-3-ethylimidazolium Chloride Room Temperature Molten Salt, *Journal of The Electrochemical Society*, 144 (1997) 2369-2374.
[228] X.H. Xu, C.L. Hussey, The Electrochemistry of Gold at Glassy Carbon in the Basic Aluminum Chloride-1-Methyl-3-ethylimidazolium Chloride Molten Salt, *Journal of The Electrochemical Society*, 139 (1992) 3103-3108.
[229] M. Masatsugu, T. Nobutada, M. Morio, Induced Codeposition of Al–Mg Alloys in Lewis Acidic AlCl3–EMIC Room Temperature Molten Salts, *Chemistry Letters*, 29 (2000) 1028-1029.
[230] T. Tsuda, C.L. Hussey, G.R. Stafford, J.E. Bonevich, Electrochemistry of Titanium and the Electrodeposition of Al-Ti Alloys in the Lewis Acidic Aluminum Chloride–1-Ethyl-3-methylimidazolium Chloride Melt, *Journal of The Electrochemical Society*, 150 (2003) C234-C243.
[231] P.-Y. Chen, I.W. Sun, Electrochemistry of Cd(II) in the basic 1-ethyl-3-methylimidazolium chloride/tetrafluoroborate room temperature molten salt, *Electrochimica Acta*, 45 (2000) 3163-3170.
[232] Y. Katayama, T. Endo, T. Miura, K. Toshima, Electrodeposition of Gold in an Amide-Type Ionic Liquid, *Journal of The Electrochemical Society*, 161 (2014) D87-D91.
[233] P.-Y. Chen, I.W. Sun, Electrochemical study of copper in a basic 1-ethyl-3-methylimidazolium tetrafluoroborate room temperature molten salt, *Electrochimica Acta*, 45 (1999) 441-450.
[234] S. Saha, N. Tachikawa, K. Yoshii, Y. Katayama, Electrodeposition of Selenium in a Hydrophobic Room-Temperature Ionic Liquid, *Journal of The Electrochemical Society*, 163 (2016) D259-D264.
[235] Y. NuLi, J. Yang, J. Wang, J. Xu, P. Wang, Electrochemical Magnesium Deposition and Dissolution with High Efficiency in Ionic Liquid, *Electrochemical and Solid-State Letters*, 8 (2005) C166-C169.
[236] I. Mukhopadhyay, C.L. Aravinda, D. Borissov, W. Freyland, Electrodeposition of Ti from $TiCl_4$ in the ionic liquid l-methyl-3-butyl-imidazolium bis (trifluoro methyl sulfone) imide at room temperature: study on phase formation by in situ electrochemical scanning tunneling microscopy, *Electrochimica Acta*, 50 (2005) 1275-1281.
[237] N. Borisenko, S. Zein El Abedin, F. Endres, In Situ STM Investigation of Gold Reconstruction and of Silicon Electrodeposition on Au(111) in the Room Temperature Ionic Liquid 1-Butyl-1-methylpyrrolidinium Bis(trifluoromethylsulfonyl)imide, *The Journal of Physical Chemistry B*, 110 (2006) 6250-6256.
[238] G. Pulletikurthi, A. Lahiri, T. Carstens, N. Borisenko, S. Zein El Abedin, F. Endres, Electrodeposition of silicon from three different ionic liquids: possible influence of the anion on the deposition process, *Journal of Solid State Electrochemistry*, 17 (2013) 2823-2832.
[239] P.-Y. Chen, C.L. Hussey, Electrodeposition of cesium at mercury electrodes in the tri-1-butylmethylammonium bis((trifluoromethyl)sulfonyl)imide room-temperature ionic liquid, *Electrochimica Acta*, 49 (2004) 5125-5138.
[240] J.-F. Huang, I.-W. Sun, Electrochemical Studies of Tin in Zinc Chloride-1-ethyl-3-methylimidazolium Chloride Ionic Liquids, *Journal of The Electrochemical Society*, 150 (2003) E299-E306.
[241] M.K. Carpenter, M.W. Verbrugge, Electrochemical Codeposition of Gallium and Arsenic from a Room Temperature Chlorogallate Melt, *Journal of The Electrochemical Society*, 137 (1990) 123-129.
[242] M.K. Carpenter, M.W. Verbrugge, Electrochemical codeposition of indium and antimony from a chloroindate molten salt, *Journal of Materials Research*, 9 (1994) 2584-2591.
[243] M.-C. Lin, P.-Y. Chen, I.-W. Sun, Electrodeposition of Zinc Telluride from a Zinc Chloride-1-Ethyl-3-methylimidazolium Chloride Molten Salt, *Journal of The Electrochemical Society*, 148 (2001) C653-C658.

[244] N.M. Pereira, P.M.V. Fernandes, C.M. Pereira, A. Fernando Silva, Electrodeposition of Zinc from Choline Chloride-Ethylene Glycol Deep Eutectic Solvent: Effect of the Tartrate Ion, *Journal of The Electrochemical Society*, 159 (2012) D501-D506.
[245] A. Bakkar, V. Neubert, Electrodeposition onto magnesium in air and water stable ionic liquids: From corrosion to successful plating, *Electrochemistry Communications*, 9 (2007) 2428-2435.
[246] A.H. Whitehead, M. Pölzler, B. Gollas, Zinc Electrodeposition from a Deep Eutectic System Containing Choline Chloride and Ethylene Glycol, *Journal of The Electrochemical Society*, 157 (2010) D328-D334.
[247] X. Xie, X. Zou, X. Lu, K. Zheng, H. Cheng, Q. Xu, Z. Zhou, Voltammetric Study and Electrodeposition of Cu from CuO in Deep Eutectic Solvents, *Journal of The Electrochemical Society*, 163 (2016) D537-D543.
[248] A.P. Abbott, K. El Ttaib, K.S. Ryder, E.L. Smith, Electrodeposition of nickel using eutectic based ionic liquids, *Transactions of the IMF*, 86 (2008) 234-240.
[249] H.Y. Yang, X.W. Guo, X.B. Chen, S.H. Wang, G.H. Wu, W.J. Ding, N. Birbilis, On the electrodeposition of nickel–zinc alloys from a eutectic-based ionic liquid, *Electrochimica Acta*, 63 (2012) 131-138.
[250] L. Vieira, A.H. Whitehead, B. Gollas, Mechanistic Studies of Zinc Electrodeposition from Deep Eutectic Electrolytes, *Journal of The Electrochemical Society*, 161 (2014) D7-D13.
[251] L. Vieira, R. Schennach, B. Gollas, The effect of the electrode material on the electrodeposition of zinc from deep eutectic solvents, *Electrochimica Acta*, 197 (2016) 344-352.
[252] R. Hayes, S. Imberti, G.G. Warr, R. Atkin, Amphiphilicity determines nanostructure in protic ionic liquids, *Physical Chemistry Chemical Physics*, 13 (2011) 3237-3247.
[253] R. Hayes, G.G. Warr, R. Atkin, At the interface: solvation and designing ionic liquids, *Physical Chemistry Chemical Physics*, 12 (2010) 1709-1723.
[254] R. Atkin, G.G. Warr, Structure in Confined Room-Temperature Ionic Liquids, *The Journal of Physical Chemistry C*, 111 (2007) 5162-5168.
[255] H. Li, F. Endres, R. Atkin, Effect of alkyl chain length and anion species on the interfacial nanostructure of ionic liquids at the Au(111)-ionic liquid interface as a function of potential, *Physical Chemistry Chemical Physics*, 15 (2013) 14624-14633.
[256] R. Atkin, N. Borisenko, M. Druschler, S.Z. El Abedin, F. Endres, R. Hayes, B. Huber, B. Roling, An in situ STM/AFM and impedance spectroscopy study of the extremely pure 1-butyl-1-methylpyrrolidinium tris(pentafluoroethyl)trifluorophosphate/Au(111) interface: potential dependent solvation layers and the herringbone reconstruction, *Physical Chemistry Chemical Physics*, 13 (2011) 6849-6857.
[257] H. Li, M.W. Rutland, R. Atkin, Ionic liquid lubrication: influence of ion structure, surface potential and sliding velocity, *Physical Chemistry Chemical Physics*, 15 (2013) 14616-14623.
[258] A.A. Kornyshev, Double-Layer in Ionic Liquids: Paradigm Change?, *The Journal of Physical Chemistry B*, 111 (2007) 5545-5557.
[259] M.V. Fedorov, N. Georgi, A.A. Kornyshev, Double layer in ionic liquids: The nature of the camel shape of capacitance, *Electrochemistry Communications*, 12 (2010) 296-299.
[260] N. Georgi, A.A. Kornyshev, M.V. Fedorov, The anatomy of the double layer and capacitance in ionic liquids with anisotropic ions: Electrostriction vs. lattice saturation, *Journal of Electroanalytical Chemistry*, 649 (2010) 261-267.
[261] K. Kirchner, T. Kirchner, V. Ivaništšev, M.V. Fedorov, Electrical double layer in ionic liquids: Structural transitions from multilayer to monolayer structure at the interface, *Electrochimica Acta*, 110 (2013) 762-771.
[262] M. Figueiredo, C. Gomes, R. Costa, A. Martins, C.M. Pereira, F. Silva, Differential capacity of a deep eutectic solvent based on choline chloride and glycerol on solid electrodes, *Electrochimica Acta*, 54 (2009) 2630-2634.
[263] R. Costa, M. Figueiredo, C.M. Pereira, F. Silva, Electrochemical double layer at the interfaces of Hg/choline chloride based solvents, *Electrochimica Acta*, 55 (2010) 8916-8920.

Chapter II

Experimental Section Summary

This chapter presents the general description of all experiments performed during the PhD work. A brief overview of the techniques used in the work is also done here. Besides, the experimental details are additionally described in each chapter of the Results.

The main objective of the work was electrodeposition of zinc in non-detached porous anodic templates. In the first step, investigation was performed on bulk anodic films. For this purpose, dense anodic layers of various thickness on titanium and aluminium were prepared and characterized. Then, porous templates on the same metals were prepared and studied. In the following step, electrochemical behavior of the anodic films in deep eutectic solvent was considered. Finally, the results obtained for the planar anodic layers were analyzed and applied to the porous templates. The essential parameters of the electrodeposition process have been established and modification of the templates for successful Zn filling (where applicable) have been performed. The full scheme of the PhD work is schematically depicted on the Figure II. 1.

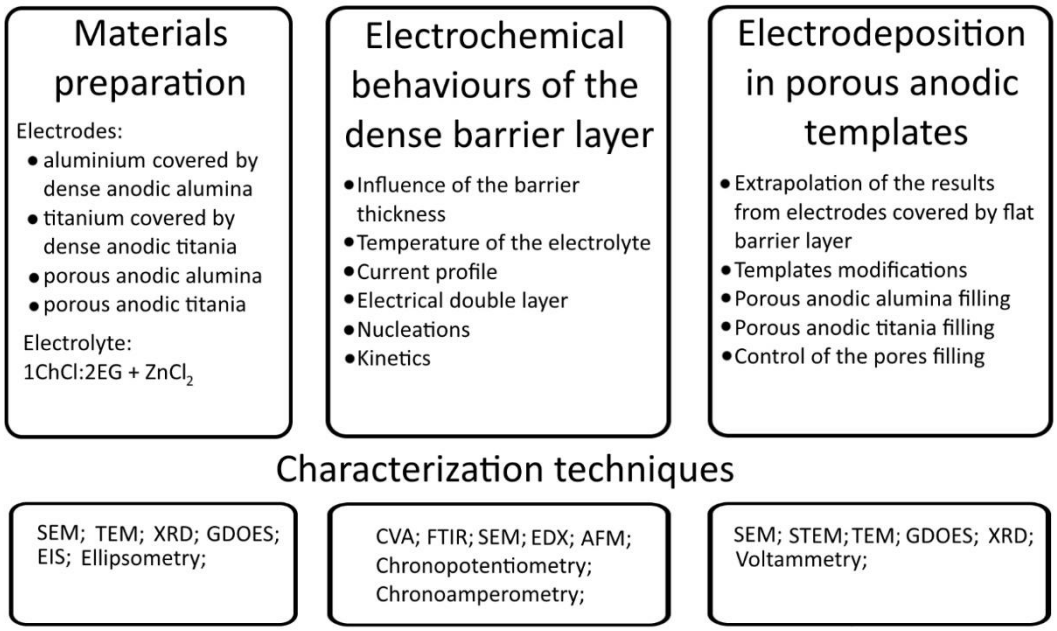

Figure II. 1 Summary of the experimental research performed during the PhD work.

1. Procedures description

The first stage of the work consists in the electrodes and electrolyte preparation. As it was mentioned above, the deep eutectic solvent based on the choline chloride was chosen as electrolyte. This type of ionic liquids can be prepared by simple mixing of the choline chloride and the hydrogen bond donor. In our case, the latter was ethylene glycol. The molar ratio of the components was 1 ChCl to 2 EG that corresponds to the eutectic point of the mixture. An appropriate amount of zinc was dissolved in the eutectic at 60^{o}C and then the electrolyte was kept under vacuum for 24 hours. Between the experiments, the solution was stored in desiccator over P_2O_5.

Initially, the metallic substrate was polished at suitable conditions and then anodized in two electrode cells. In this system, the chosen substrate (aluminium or titanium) was used as the working electrode and platinum foil was used as the counter electrode. Two types of electrolyte, with and without aggressive ions, were used for preparation of porous and dense anodic films, correspondingly. The dense barrier layer was formed in neutral solution (ammonium pentaborate), because alumina is sensitive to pH and easily dissolves in an acidic solution. As opposed to bulk layers, the porous oxides were produced in acidic electrolyte (oxalic acid) because of the same reason of the pH sensitivity of alumina. Since titania is indifferent to pH, the bulk titania anodic films can be obtained in many different of electrolytes. The sulfuric acid solution was used for that aim due to high reproducibility and stability of the obtaining layer. In the case of porous template formation, the ethylene glycol based electrolyte, with small amount of water and fluoride ions, has been used. The fact that the electrolyte is based on ethylene glycol allowed preparation of long pores with smooth walls. Presence of fluoride ions was important because exactly these ions promote dissolution of the barrier titania.

Commonly, bulk oxide layer preparation is carried out in one step (galvanostatic oxidation). However, the two-step technique is the most desirable way of formation of high-ordered porous anodic templates. Both steps are normally performed at the same conditions (electrolyte, temperature, voltage) and only the removal of the oxides (either chemical or mechanical) splits the steps. Detailed descriptions of the anodization mechanism and of the used parameters are presented in the State of the art and Results (papers), correspondingly.

The electrodes were fully characterized after preparation. The morphological properties, such as topography, pore diameter, interpore distance, pores ordering, thickness of the pores layer, and crystallinity of the templates were assessed using scanning and transmission electron microscopies. The barrier oxide layer thicknesses were estimated by several techniques, namely glow discharge optical emission spectroscopy, ellipsometry and electrochemical impedance spectroscopy.

At the second stage of the work, the electrochemical behavior of the electrodes covered by dense anodic alumina or titania was investigated. It has been done in three electrode cell to ensure a higher-precision control of the potential on the working electrode. In the frame of this step, influence of the film thickness and temperature of the solution on the kinetics of zinc reduction was studied using both cyclic and linear voltammetry as well as chronoamperometry. *I(t)* curves gave indication of the mechanism of nucleation which is an important factor for the electrodeposition process. SEM and AFM were used in order to confirm nucleation mechanism which was obtained by *I(t)* curves analyses.

Furthermore, strong influence of electrical double layer (EDL) on the zinc species reduction was observed during the electrochemical measurements, which increased interest in studying this phenomenon. The EDL was explored by attenuated total reflection Fourier transform infrared spectroscopy. Besides, the use of AC signal superimposed on a bias potential to avoid the blockage effect of the dense organic layer (EDL) at the electrodeposition to porous alumina templates was explored.

At the last stage, the parameters, and conditions revealed and then optimized for the dense anodic oxides were summarized and applied to the porous templates. It was decided to use two-step electrodeposition for filling of porous anodic alumina templates. The first step, a pulse electrodeposition, leads to zinc nucleation on bottoms of the pores. The second one results in the galvanostatic pores filling. Concerning the porous anodic titania, several modifications such as annealing and electrochemical selective crystallization were performed to achieve successful filling of the titania nanotubes by zinc in one step. Control of the pores filling was performed using SEM, TEM, EDX and GDOES techniques.

2. **Techniques overview**

Electron microscopy

Scanning and transmission electron microscopies are important tools for morphological characterization of materials. In these techniques, an electron beam is used for illumination, which allows a higher resolution than when using a visible light beam. Mathematically, the resolution can be described by Abbe's equation:

$$d = \frac{0.612\,\lambda}{n\,sin\alpha} \quad \text{(II.1)}$$

where (n sinα) is numerical aperture (NA), d is resolution and λ is wavelength of the imaging radiation. According to equation (II.1), the limit of optical resolution is about 2000 Å for the violet light (λ=4000 Å and NA = 1.25). The electron beam wavelength is much smaller that results in a higher resolution (d = 0.2 Å, by the same equation) [1].

The electron beam, emitted by electron gun, is accelerated and goes through the series of electromagnetic lenses which focus it on the sample. There are two groups of interactions of the electron beam with a sample: elastic and inelastic. The first group is characterised by wide-angle changes in electron trajectory and insignificant energy losses of the scattered electrons. Typical signal after elastic scattering, used for imaging, is contributed by backscattered electrons (BSE). BSE signal provides both topographical and compositional information. The compositional information is possible to receive because the intensity of the signal strongly depends on the atomic numbers of the elements in the sample [1, 2].

The second group, inelastic scattering, is characterized by significant amount of energy transferring from the incident beam to the specimen atoms. This interaction leads to excitation of the atoms and to generation of the secondary electrons with the energy less than 50 eV. Such a signal is widely used for visualization of surface texture of the sample. Another signal which also appears, when excited atom returns to ground state, is characteristic X-ray (EDX). EDX allows both qualitative and semi-quantitative analysis of the chemical composition [1, 2].

Besides the above-described signals, there are also other signals, such as continuum X-rays, Auger electrons, cathodoluminescence, and specimen current. All of them, except continuum X-rays, can be used for the specimen characterization [2, 3].

SEM was actively used during this PhD work for characterization of the deposits both on the dense anodic layers and inside the porous anodic templates. Moreover, the microstructure of the porous templates was also controlled by SEM. The deposits composition and distribution of the deposited particles over the electrode interface were controlled by EDX and BSE analyses.

The electrons from the incident beam can be transmitted through the sample if it is thin enough. Transmitted electrons participate in formation of electron diffraction image or TEM image. Two different modes are commonly applied for TEM analyses. The first and the most common one is a bright field imaging mode. In this mode, the contrast is formed "classically"; in other words, by direct occlusion and absorption of the electrons from the incident beam in the samples. It means that the thicker part of the sample or part containing heavier elements will be darker than the thinner region or area out of the sample. The second type is a dark field mode when unscattered (direct) beam is blocked by aperture. It leads to dark areas if there is no sample (beam passing without any interaction) and only scattered electrons make the bright places in the image. Dark field mode is very useful for particles size measurements and planar defects investigations [3].

Commonly TEM provides a higher resolution than SEM due to the use of the electron beam with a higher energy, but the sample preparation for TEM is more complicated. Nevertheless, presence and morphology of the secondary materials, crystallinity and structure of the tubes were studied by TEM.

Key benefits of these techniques are high resolution, possibility to measure a large variety of the materials characteristics, short analysis time *etc*. The drawbacks are the following: use of high vacuum in the electrode beam area, sampling (TEM), sample preparation (TEM), possible damage by electron beam and interpretation of the results (TEM).

Glow discharge optical emission spectroscopy

GDOES is an effective technique for elemental surface analysis and depth profiling of bulk solids and thin films. The working principle is based on the detection of

the photons which come from the highly-excited atoms during its de-excitation to a lower-energy state or to the ground state.

According to the quantum mechanics principles, in contrast to classical mechanics, electrons in the atoms can have only certain value of energy. Each pair of principal quantum number and azimuthal quantum number corresponds to only one specific energy level of electron. It is well known, that all atoms have a large number of possible energy levels, but not all of them are stable. Thus, excited atom returns to the ground state through one or several steps and, at each step, the energy difference releases in the form of radiation. The energy (E) and the frequency of the emitted photon (υ) are linked by the Planck–Einstein relation:

$$E=h\upsilon \quad \text{(II.2)}$$

where h is Plank constant (6.626 10^{-34} J·s).

Since the photon frequency is specific for each de-excitation step and for each different atom, it is possible to identify the atoms type and quantity the atoms from analysis of the emission spectra.

The sample should be atomized before excitation. The low-pressure plasma is used in the GDOES equipment for that aim. The plasma is induced by electrical current passed through the gas (argon is mostly used) under a low pressure. The electron flow interacts with inert argon atoms and forms a plasma. The plasma is not homogeneous and contains four different regions (Figure II. 2) [4].

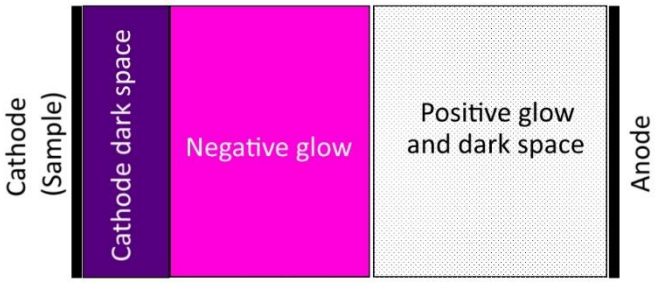

Figure II. 2 Schematic representation of the glow discharge plasma and distribution of light zones (adapted from Weston [4]).

The cathode dark space (CDS), also called the cathode fall, is about 1 mm length. Most of the potential differences between anode and cathode happen in this region.

Another region is called negative glow (NG) and its length has several millimeters. This region is almost field free and it is the biggest part of the plasma [4]. Formation of the similar zones (anode dark space and positive glow region) near anode has been also found in some sources. The phenomenon is irrelevant for our system because of the small distance between anode and cathode [5, 6].

The positive species (mostly Ar) are accelerated in the CDS region by electrical field and bombard the cathode (sample) surface. Moreover, significant part of ions regains electrons by means of collisions with neutral atoms. It leads to conversion of the neutral atoms and ions to the slow ions and fast neutral atoms, correspondingly. Both ions and the fast neutral atoms have enough kinetic energy for the sample sputtering [6].

The sputtered atoms move away from the sample surface to the NG region, which contains enough electrons with the energies sufficient to excite these atoms. Finally, excited atoms de-excite with emitting of the characteristic photons [6].

The GDOES technique has been used along all the work for determination of both the thicknesses and the composition qualitative characterization of the anodic films. Besides, GDOES has been applied to study the mechanism of the pore filling. The possibility to control the sputtering rate by the plasma energy allowed carrying the soft plasma polishing of the samples before SEM studies that broadens significantly opportunity of the SEM analyses.

The disadvantages of GDOES are the following: a strong influence of the surface condition, obligatory calibration for quantification, difficulties to analyse rough surfaces. Nevertheless, the GDOES technique offers a low-cost and rapid analysis with high sensitivity (1-10 ppm), high depth resolution (nm) and a possibility to measure all elements including the light ones (H, B, Li *etc*.).

Electrochemical techniques

Typical electrochemical measurements are performed in electrochemical cells which can contain two or more electrodes. In the simplest cell, the potential difference is measured between two electrodes, namely the working electrode and the counter one. Main drawback of this type of electrochemical cell is the lack of precise control of the working electrode potential. The problem can be solved by entering additional (third) electrode, so-called the reference electrode. The third electrode has a constant potential

and the potential difference is measured between the working and the reference electrode (in contrast to the two-electrode cell) that allows to make precise potential changes.

During electrochemical measurements, it is impossible to control the current and the potential simultaneously. Therefore, only two basic experiments can be performed: when the potential is controlled while the current is measured and, the opposite, when the potential is measured while current is controlled. The most known electrochemical techniques are presented in Figure II. 3.

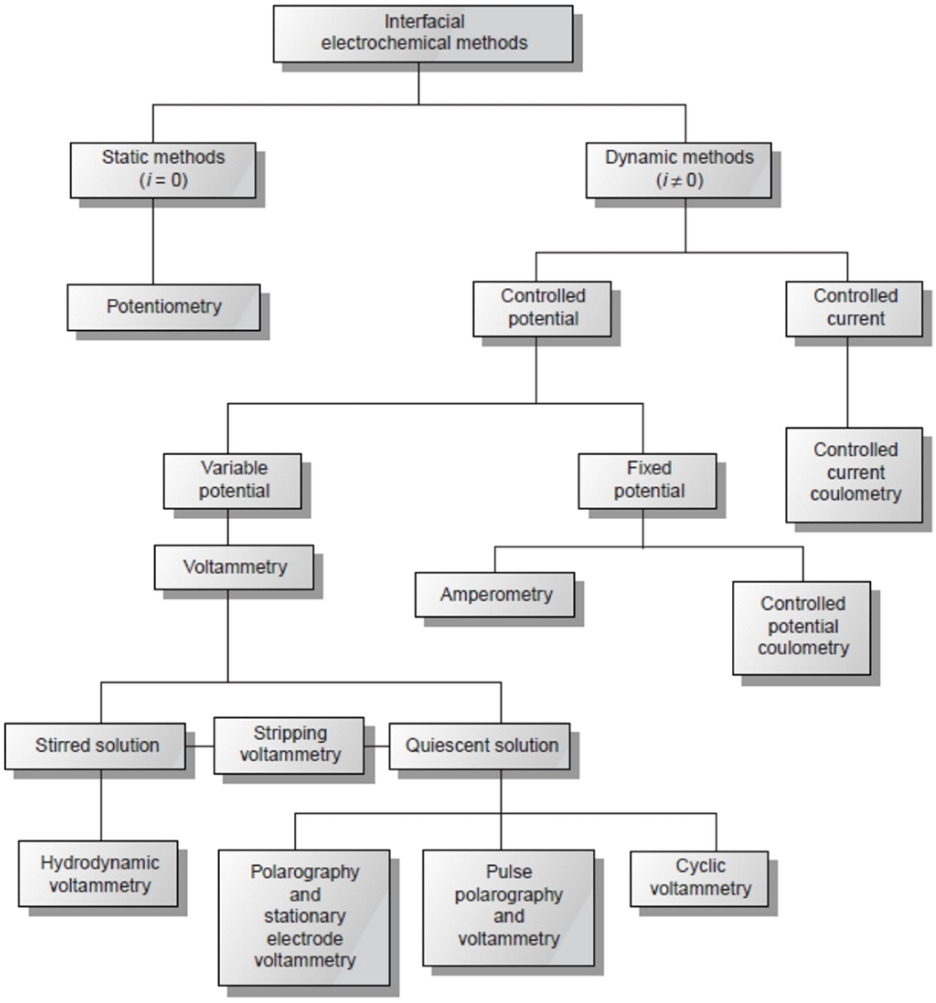

Figure II. 3 Family tree of interfacial electrochemical techniques (taken from Harvey [7, 8]).

Only two electrochemical techniques from the list, namely voltammetry and chronoamperometry were applied in this PhD work, because they are the main methods to study the electrode kinetics. It is possible to obtain information about nature of

electrode processes, based on the shape of curves and the shape changing in different solutions, temperature and other physico-chemical parameters [9, 10].

One of the most widely used technique is voltammetry. The method consists in application of a continuously time-varying potential to the working electrode and registration of the corresponding current.

In the electrochemical system, the resulting current contains faradaic and nonfaradaic parts. The most important example of nonfaradaic part is current of the EDL charging. This small current depends on the potential value due to reorganization of the EDL structure [8].

The faradaic current appears as a result of redox reactions on the electrode which mostly occur under polarization. Polarization is necessary for equilibrium changing in the system. The relationship between the electrode potential (E) and the equilibrium concentration of ions is described by the Nernst equation:

$$E = E^0 + \frac{RT}{nF}\ln(\frac{\alpha_{ox}}{\alpha_{red}}) \qquad \text{(II.3)}$$

where E^0 is standard potential (V), R – universal gas constant (8.314 J K^{-1} mol^{-1}), T – temperature (K), F – Faraday constant (96485 C mol^{-1}), n – number of moles of electrons transferred in the reaction, $\alpha_{red/ox}$ is a chemical activity for the relevant species (can be simplified by replacing for concentration of the species) [8, 11].

It is obvious from equation II.3 that any changes in E result in changing the concentration ratio (α_{ox}/α_{red}) of the species on the electrode interface according to the scheme:

$$Ox + ne = Red \qquad \text{(II.4)}$$

This particular electrons flow appears in the I(E) curve as a current. There are two main factors influencing the current density during the electrochemical experiments, namely mass-transport and kinetics of the electron transfer. The charge-transfer rate can be enhanced by applying potential until the moment, when the mass-transport becomes a limiting factor. The mass-transport is contributed by three independent mechanisms: migration, convection and diffusion. The driving forces are electric field in solution,

external energy (for example mechanical stirring) and chemical potential caused by concentration gradient, correspondingly [11].

The cyclic voltammetry (CVA) is a particular case of voltammetry. It is a very powerful technique for initial analysis of the system and occurring processes. As it was told by E. Gileady: "Cyclic voltammetry should always be the first experiment performed in a new system, but never the last" [11]. The advantage of the CVA, in comparison with the linear sweep voltammetry, is that scan of the potential is performed in both directions. It gives an opportunity to investigate species generated on the electrode. [7, 8, 11].

Additional information about electrochemical processes in the systems studied in the current work was obtained from the chronoamperometry measurements, where the potential was kept constant and the current response was studied. In particular, this technique has been used for determination of the nucleation mechanism, critical size of the nuclei, nucleation rate and also for quantification of the deposit amount using the Faraday equation (V.2) [9, 10].

References

[1] W. Zhou, Z.L. Wang, *Scanning Microscopy for Nanotechnology: Techniques and Applications*, Springer New York, 2007.
[2] J.I. Goldstein, D.E. Newbury, P. Echlin, D.C. Joy, C.E. Lyman, E. Lifshin, L. Sawyer, J.R. Michael, Scanning Electron Microscopy and X-ray Microanalysis, in, Springer US, Boston, MA, 2003.
[3] D.B. Williams, C.B. Carter, Transmission Electron Microscopy : a Textbook for Materials Science, in, Springer US, Boston, MA, 1996.
[4] G.F. Weston, Cold cathode glow discharge tubes, (1968).
[5] B.N. Chapman, *Glow discharge processes*, Wiley, 1980.
[6] T. Nelis, R. Payling, Glow discharge optical emission spectroscopy : a practical guide, in, Royal Society of Chemistry, Cambridge, 2003.
[7] D. Harvey, Analytical Chemistry 2.0, in, http://dpuadweb.depauw.edu/harvey_web/eTextProject/version_2.0.html, 2010.
[8] D. Harvey, *Modern analytical chemistry*, McGraw-Hill New York, 2000.
[9] L.I. Antropov, *Theoretical electrochemistry*, Mir, Moscow, 1972.
[10] C.M.A. Brett, A.M.O. Brett, *Electrochemistry : principles, methods, and applications*, Oxford University Press, Oxford; New York, 1993.
[11] E. Gileadi, *Electrode kinetics for chemists, chemical engineers, and materials scientists*, VCH, New York, 1993.

Chapter III

Electrodeposition of zinc nanorods from ionic liquid into porous anodic alumina

---

CHEMELECTROCHEM
COMMUNICATIONS

ChemPubSoc Europe

DOI: 10.1002/celc.201402130

Electrodeposition of Zinc Nanorods from Ionic Liquid into Porous Anodic Alumina

Maksim Starykevich,[a] Aleksey D. Lisenkov,[a] Andrei N. Salak,[a] Mario G. S. Ferreira,[a] and Mikhail L. Zheludkevich*[a, b]

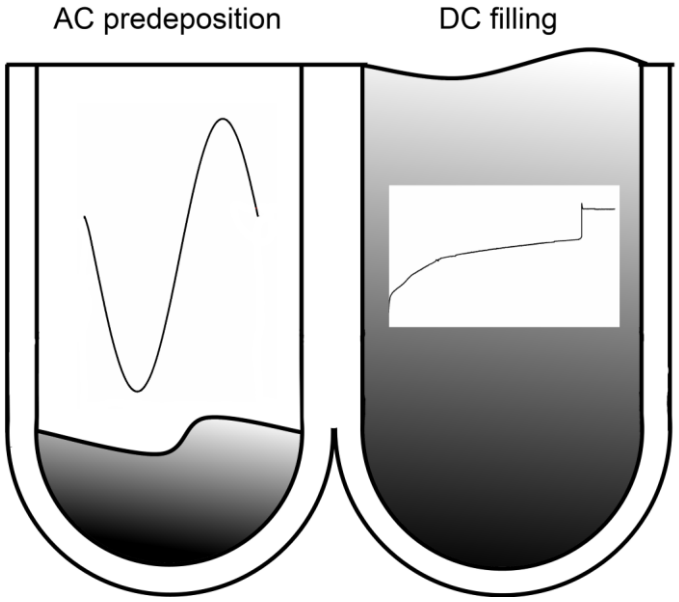

Abstract

Electrochemical deposition of zinc nanorods into the anodic aluminium-oxide template from ionic-liquid electrolyte is reported. For the first time, the electrodeposition from an ionic liquid is performed in a porous alumina template, anodically grown on the aluminium substrate without complete removal of the barrier layer. The two-step process was applied; first, with alternating-current pulse nucleation of zinc nanoparticles on the bottom of the pores, followed by direct-current growth of the rods. The electrolyte consisted of 0.5M $ZnCl_2$ in choline chloride and ethylene glycol in a 1:2 molar ratio. The resulting zinc nanorods are approximately 3 μm in length and 70 nm in diameter. The achieved fill factor of the pores is in the 70–80% range.

Keywords: anodic alumina, electrodeposition, ionic liquid, nanorods, porous template.

Introduction

In recent years, 1D nanostructured metal materials, such as nanowires and nanorods, have attracted more and more attention, owing to their applications and uses in photonics [1], nanoelectronics [2], catalysis, sensors [3], and so forth. Metallic nanorods have been intensively studied for potential use in the fields of high-density data storage [4] and biosensing [5]. The deposition of metallic nanorods into pores with a dielectric barrier layer has also opened new perspectives for the development of metal–dielectric–metal subwavelength plasmonic waveguides [6, 7] and, specifically, the one-end-sealed metal–insulator–metal waveguides [8] when the bottom of the pore is sealed by a dielectric material. Metallic nanorods can be considered as precursors for various inorganic compounds after relevant post-treatment. For example, metallic zinc nanomaterials can be converted to the semiconducting oxide or sulfide forms, keeping the original shape [9].

Electrodeposition into porous templates is a relatively simple and cheap method for the synthesis of metallic nanomaterials [10-13]. However, the uniform electrodeposition of metals into the pores from conventional water-based electrolytes is often complicated by number of limiting factors. The electrochemical window of water is rather limited, and hydrogen evolution can occur in parallel to the reduction of metal cations. It is especially critical when the pores in the template demonstrate a different geometry and different local iR drops. Thus, the real applied potential can vary from pore

to pore, causing hydrogen generation in the wider ones. The issue of hydrogen evolution can affect the deposited material if the hydrogen is dissolved in the nanorods. This process can also cause blocking of the pores, because of the formation of gas bubbles or through secondary effects in electrolyte, owing to local alkalinization [14].

Electrosynthesis from ionic liquids becomes attractive, owing to the unique properties of these electrolytes [15]. Ionic liquids demonstrate significantly wider electrochemical windows and higher thermal stability than standard electrolytes. Utilization of ionic liquids also allows electrosynthesis of active metallic materials, which are impossible in aqueous electrolytes. Several types of metallic nanorods have recently been obtained through electrodeposition from ionic liquid into porous polycarbonate and oxide templates [16-18]. The electrodeposition of free-standing zinc nanowires from an ionic liquid has also been reported recently [19]. The zinc nanostructures were grown in the pores of track-etched polycarbonate membranes, which contained a sputtered metallic layer, closing the end of the pores from one side and ensuring electrical contact. In the case of well-ordered nanostructures, the track-etched membranes cannot be employed, because of the random distribution of pores. The oxide templates are usually used in such situations. These templates are normally prepared as free-standing membranes with the barrier layer removed, and a metallic film is sputtered on the back side to establish an effective electrical contact by using a multistage complex process [20]. To the best of our knowledge, direct electrodeposition from ionic liquids into alumina templates without the removal of the barrier layer has not yet been reported.

The main aim of this work was to directly electrodeposit metallic nanorods from deep eutectic solvents into a porous anodic alumina template on aluminum substrates without the removal of the barrier layer. Zinc is used herein as a model system for growing the nanorods. Until now, no successful electrodeposition of zinc has been proven in this type of template. Moreover, zinc was selected here because of the ease of possible sulfurization or oxidation post-treatments, which can confer an ordered array of semiconductive nanorods. The obtained results can also be transferred to other metallic systems, especially those that are hard to electrodeposit from waterbased solutions.

A two stage AC/DC process, recently suggested for aqueous electrolytes [21], was employed in this work aiming at uniform filling of the pores with metal. In this paper, deposition of relatively noble metals such as copper, silver, and cobalt was shown. Zinc deposition from aqueous electrolytes was also tried, but without convincing proof of metallic zinc deposition.

Experimental

The annealed aluminium (99.0%) foil was used for preparation of porous template. The substrate was mechanically polished (down to grid 4000) followed by the chemical polishing in a mixture of phosphoric acid, nitric acid and acetic acid at 70-90^{o}C. Finally, the samples were washed with acetone, ethanol and distilled water, and then dried in air.

Two-step anodization of the samples was used in order to form a well-ordered alumina template [22]. The first anodization step was performed at constant potential of 40 V in oxalic acid (0.3M) for 1 hour at temperature about 3°C. The pre-structured aluminum surface was obtained after dissolution of the formed oxide in a mixture of phosphoric acid and CrO_3 at 70-80°C for 5 minutes. The second anodization stage was performed at similar condition as the first one with potential drop from 40V to 0V with sweep rate 1.3V min^{-1} after 30 or 60 minutes of potentiostatic polarization. Post-anodization wall thinning was carried out in 0.3M $(COOH)_2$ at 40^{o}C for 2.5 hours resulting in formation of the template with a pore size of 70 nm and wall thickness between the pores in the range of 15-20 nm. The obtained template had 3μm and 1.3μm pore length (by SEM measurements) for 60 min and 30 min anodization respectively.

Preparation of the ionic liquid electrolyte and following electrodeposition experiments were held in air. Eutectic solution was prepared by adding 0.5M of anhydrous zinc chloride (99.99%) to the mixture of choline chloride (98%) and ethylene glycol (99+%) in the molar ratio 1:2. Then the mixture was heated to 60°C and kept at this temperature in vacuum during 24 hours in order to dry the electrolyte.

Electrochemical studies were performed employing a Bio-Logic SAS SP-300 potentiostat using a two electrode cell with graphite rod as a counter electrode. Microscopic investigations were carried out using Hitachi S-4100 scanning electron microscope (SEM) coupled with energy dispersive spectroscopy (EDS). X-ray diffraction (XRD) data of the samples were obtained employing a PANalytical X'Pert PRO diffractometer (Bragg-Brentano geometry, CuKα-radiation).

Results and discussion

A uniform electrodeposition of Zn nanorods in the porous alumina template with thin barrier layer is not possible in DC mode. The potentiostatic polarization leads to high drop of potential across the barrier film. Therefore the electrochemical reduction of the

metal cations occurs only in some defective zones causing formation of large unordered lumps which are growing through porous oxide while most of the pores stay unfilled. The dissolution of alumina in the studied ionic liquid does not occur as observed by electrochemical impedance spectroscopy (not shown).

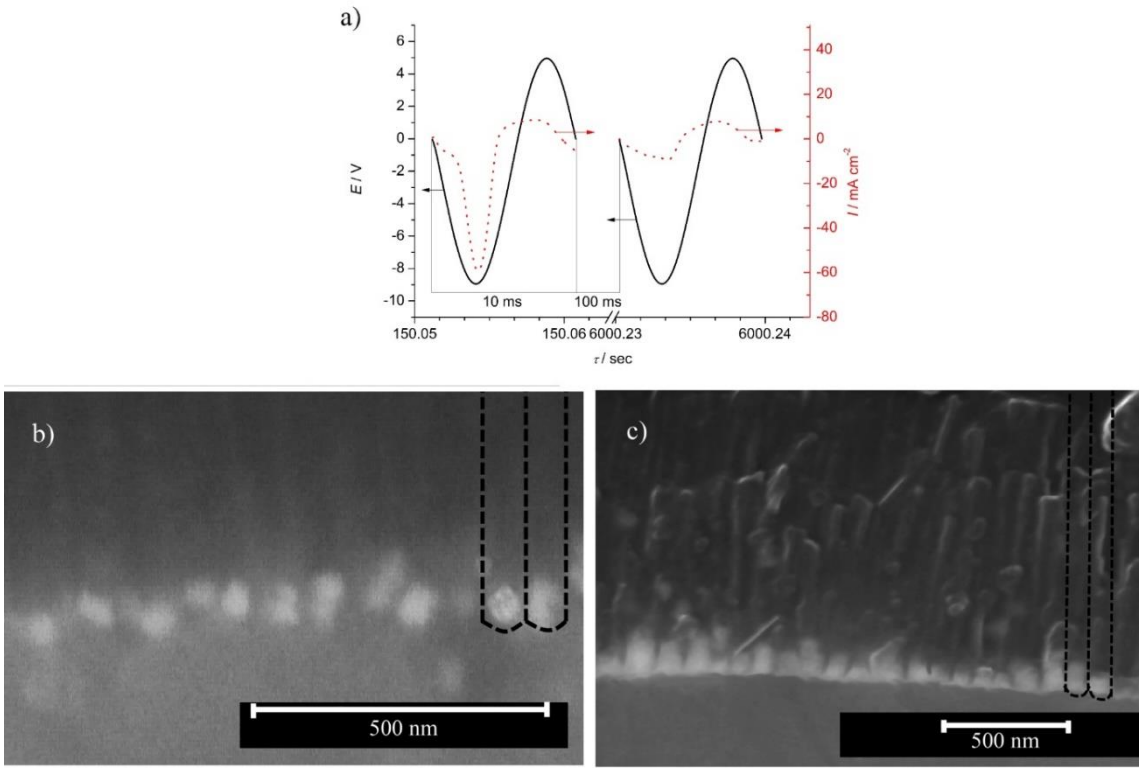

Figure III. 1 a) Typical shapes of voltage/current pulses applied during the first nucleation stage; b) and c) cross-sectional SEM micrographs obtained after first stage pulsed electrodeposition from 0.5M $ZnCl_2$ in 1ChCl:2EG for 10 and 30 min respectively.

Another strategy based on high-frequency pulsed electrodeposition with asymmetric pulse modulation was employed. The idea was to apply higher frequencies at which the impedance modulus of the system decreases at least below 10^3 Ohm cm^{-2} in order to achieve a reasonable current density. The desirable values of the impedance are achieved at frequencies above 10 Hz. Therefore the electrodeposition was performed at 50, 100 and 200 Hz in order to find an optimal frequency for uniform filling of the pores. The application of highest frequency (200 Hz) leads to formation of unordered deposits on top of the oxide without filling the pores. This fact can be caused by relatively low impedance of the total system including barrier and porous part at such frequencies. Thus

no preferential deposition into pores can be achieved. No clear filling of pores was also observed using 50 Hz perturbation. The optimal electrodeposition of Zn was achieved at 100 Hz as described below.

A non-symmetric pulsed AC signal with the shape shown in Figure III. 1 was applied. The signal was composed by the -9V – +5V sin-wave with total duration (t reduction + t oxidation) equal to 10 ms. 100 ms off time was kept between the pulses. The strong reduction potential applied to the anodized electrode leads to 'bridging' the barrier oxide layer. The integral impedance modulus of the oxide film decreases at such polarizations by several orders of magnitude (not shown) and make deposition in the pores possible. The anodic part of the pulse partially dissolves the deposited Zn. At the beginning of the electrodeposition a high Zn electrodeposition current and relatively low Zn dissolution current are observed. The reduction/oxidation charge ratio is 4 during the period from 120s to 180s. With time the ratio decreases and achieves values close to 1 after about 6000s (Figure III. 1). The situation when reduction current is equal to the oxidation one leads to situation when the amount of electrodeposited zinc is equal to the amount of metal dissolved at anodic part of the wave. The steady state is achieved and the growth of zinc particles terminates.

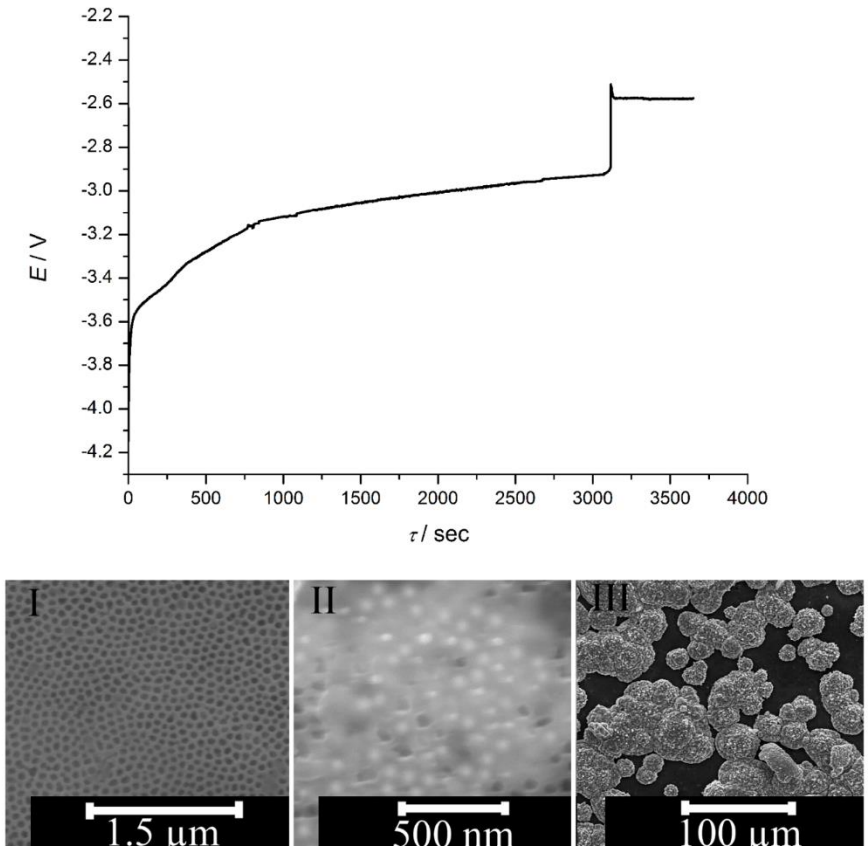

Figure III. 2 Chronopotentiometric curve obtained at galvanostatic electrodeposition at 5 mA/cm^2. The insets show SEM top-view of the sample after different times of galvanostatic polarization.

The zinc nanoparticles are formed at the bottom of all pores as a result of the pulsed electrodeposition during 10 minutes (Figure III. 1 b). The nanoparticles do not grow significantly when longer pulsed polarization is applied (Figure III. 1 c) since the steady state conditions are achieved.

A second galvanostatic step with 5 mA/cm^2 current density was applied to drive further growth of zinc nanorods inside the pores. Figure III. 2 demonstrates a chronopotentiometric curve during the galvanostatic electrodeposition. The initial potential at this stage had value of -4.1V and becomes less negative with time showing that electrochemical reduction process is initiated at the bottom of pores. The potential value demonstrates a sharp change in the beginning followed by a lower slope transformed with time into a plateau-like zone on the curve. This behaviour is associated with a steady state electrodeposition process controlled by the diffusion of metallic cations into the pores. The continuous slow decrease of polarization is caused by the decrease of the diffusion path of cations from the bulk electrolyte to the metal surface in

pores because of continuous filling of the pores with metallic Zn. The uniform filling of the pores can be observed at this stage (left inset on Figure III. 2) leading to the situation when zinc nanorods reach the surface of template and begin to fuse because of started multidirectional growth (middle inset on Figure III. 2). The next stage is formation of bulky deposits over whole surface with consequent drop of polarization (Figure III. 2) because of increased electroactive surface (Figure III. 2).

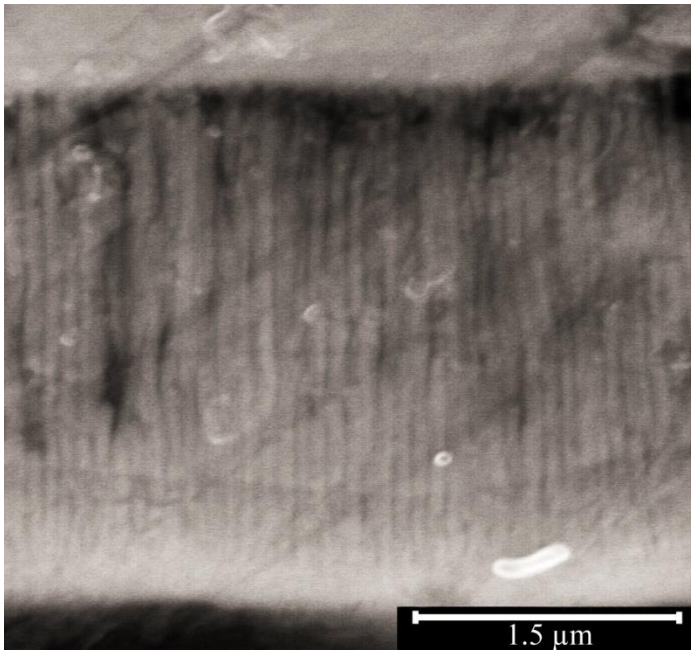

Figure III. 3 Cross-sectional SEM micrograph of porous alumina template filled with zinc after two-stage electrochemical deposition.

Figure III. 3 shows cross-sectional SEM image of the sample after the complete 2 steps of the deposition. Uniform complete filling of the pores with zinc nanorods of 3 µm length and 70 nm in diameter is observed. The XRD data (not shown) indicate that the phase appeared in the anodic template as a result of the deposition is metallic zinc. It also does not show any signs of post-oxidation. At least no respective crystalline products are observed.

Conclusions

The zinc nanorods were deposited from $ZnCl_2$/ChCl:EG ionic deep eutectic solvents into porous anodic alumina template without removal the barrier layer. A two-step electrodeposition process was developed with pulsed AC pre-deposition nucleation

stage followed by the galvanostatic growth. Highly uniform filling of the pores was achieved resulting in formation of nanorods with reproducible geometrical parameters. The method allows fabrication of highly-ordered metal-dielectric nanoassemblies utilizing fully wet and simple template preparation method as well as non-expensive ionic liquids with low sensitivity to humidity.

Acknowledgements

The financial support of the European Commission and Portuguese Foundation for Science and Technology (FCT) in frame of PIRSES-GA-2011-295273 – NANEL and PTDC/CTM-NAN/113570/2009 projects, respectively, is gratefully acknowledged.

References:

[1] V. Colvin, M. Schlamp, A.P. Alivisatos, Light-emitting-diodes made from cadmium selenide nanocrystals and a semiconducting polymer, *Nature*, 370 (1994) 354-357.
[2] Y. Huang, X. Duan, Y. Cui, L.J. Lauhon, K.-H. Kim, C.M. Lieber, Logic gates and computation from assembled nanowire building blocks, *Science*, 294 (2001) 1313-1317.
[3] M. Valden, X. Lai, D.W. Goodman, Onset of catalytic activity of gold clusters on titania with the appearance of nonmetallic properties, *science*, 281 (1998) 1647-1650.
[4] P. Zijlstra, J.W. Chon, M. Gu, Five-dimensional optical recording mediated by surface plasmons in gold nanorods, *Nature*, 459 (2009) 410-413.
[5] W.-C. Law, K.-T. Yong, A. Baev, R. Hu, P.N. Prasad, Nanoparticle enhanced surface plasmon resonance biosensing: application of gold nanorods, *Optics express*, 17 (2009) 19041-19046.
[6] R.F. Oulton, V.J. Sorger, D. Genov, D. Pile, X. Zhang, A hybrid plasmonic waveguide for subwavelength confinement and long-range propagation, *Nature Photonics*, 2 (2008) 496-500.
[7] G. Veronis, S. Fan, Bends and splitters in metal-dielectric-metal subwavelength plasmonic waveguides, *Applied physics letters*, 87 (2005) 131102.
[8] Z. Zhang, H. Wang, Y. Zhao, D. Lu, Z. Zhang, Transmission properties of the one-end-sealed metal–insulator–metal waveguide, *Optik-International Journal for Light and Electron Optics*, 124 (2013) 177-179.
[9] P.J. Dale, A.P. Samantilleke, D.D. Shivagan, L.M. Peter, Synthesis of cadmium and zinc semiconductor compounds from an ionic liquid containing choline chloride and urea, *Thin Solid Films*, 515 (2007) 5751-5754.
[10] J. Ustarroz, U. Gupta, A. Hubin, S. Bals, H. Terryn, Electrodeposition of Ag nanoparticles onto carbon coated TEM grids: a direct approach to study early stages of nucleation, *Electrochemistry Communications*, 12 (2010) 1706-1709.
[11] Y.A. Ivanova, D. Ivanou, E. Streltsov, A. Fedotov, Electrochemical deposition of Te and electroless deposition of Se nanoparticles in etched tracks of Au^+ ions in SiO_2 layer on n-Si (100) wafers, *Materials Science and Engineering: B*, 147 (2008) 271-275.
[12] A.M.M. Jani, D. Losic, N.H. Voelcker, Nanoporous anodic aluminium oxide: advances in surface engineering and emerging applications, *Progress in Materials Science*, 58 (2013) 636-704.
[13] D. Ivanou, Y.A. Ivanova, A. Lisenkov, M. Zheludkevich, E. Streltsov, Electrochemical deposition of lead and tellurium into barrierless nanoporous anodic aluminium oxide, *Electrochimica Acta*, 77 (2012) 65-70.
[14] M. Schlesinger, M. Paunovic, *Modern electroplating*, John Wiley & Sons, 2011.
[15] D.M. F. Endres, A. Abbott, *Electrodeposition from Ionic Liquids*, WILEY-VCH Verlag GmbH & Co. KGaA, Weinheim, 2008.
[16] A.P. Abbott, G. Frisch, K.S. Ryder, Electroplating using ionic liquids, *Annual Review of Materials Research*, 43 (2013) 335-358.
[17] S. Zein El Abedin, F. Endres, Free- Standing Aluminium Nanowire Architectures Made in an Ionic Liquid, *ChemPhysChem*, 13 (2012) 250-255.
[18] G. Oltean, L. Nyholm, K. Edström, Galvanostatic electrodeposition of aluminium nano-rods for Li-ion three-dimensional micro-battery current collectors, *Electrochimica Acta*, 56 (2011) 3203-3208.
[19] Z. Liu, S.Z. El Abedin, M. Ghazvini, F. Endres, Electrochemical synthesis of vertically aligned zinc nanowires using track-etched polycarbonate membranes as templates, *Physical Chemistry Chemical Physics*, 15 (2013) 11362-11367.
[20] C. Chan, H. Lam, K. Leung, C. Surya, Growth of copper zinc tin sulfide nano-rods by electrodeposition using anodized aluminum as the growth mask, *Journal of Nonlinear Optical Physics & Materials*, 18 (2009) 599-603.

[21] A. Belov, S. Gavrilov, V. Shevyakov, E. Redichev, Pulsed electrodeposition of metals into porous anodic alumina, *Applied physics A: materials science & processing*, 102 (2011) 219-223.
[22] H. Masuda, K. Fukuda, Ordered Metal Nanohole Arrays Made by a Two-Step Replication of Honeycomb Structures of Anodic Alumina, *Science*, 268 (1995) 1466-1468.

Chapter IV

Electrochemical deposition of zinc from deep eutectic solvent on barrier alumina layers

---

Electrochimica Acta 170 (2015) 284–291

Contents lists available at ScienceDirect

Electrochimica Acta

journal homepage: www.elsevier.com/locate/electacta

Electrochemical deposition of zinc from deep eutectic solvent on barrier alumina layers

M. Starykevich [a], A.N. Salak [a], D.K. Ivanou [b,c], A.D. Lisenkov [a], M.L. Zheludkevich [a,d], M.G.S. Ferreira [a,*]

[a] Department of Materials and Ceramic Engineering, CICECO-Aveiro Institute of Materials, University of Aveiro, 3810-193 Aveiro, Portugal
[b] Faculty of Engineering, University of Porto, 4200-465 Porto, Portugal
[c] Chemistry Department, Belarusian State University, 220050 Minsk, Belarus
[d] Institute of Materials Research, Helmholtz-Zentrum Geesthacht, 21502 Geesthacht, Germany

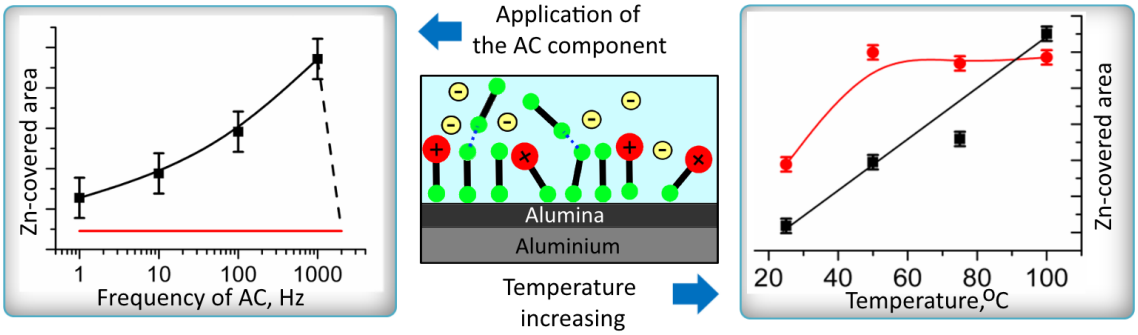

Abstract

The direct use of high-ordered porous templates of anodic aluminium oxide for formation of nanostructures via electrochemical deposition is difficult because the presence of the of barrier alumina layer in the bottom of pores. In this paper, zinc electrodeposition from a solution of $ZnCl_2$ in a choline chloride / ethylene glycol eutectic mixture on dense alumina layers of different thicknesses was studied. In a potentiostatic regime, the deposition on a barrier layer was found to be hardly possible even when the layer is a native alumina film (about 2 nm thick). Choline and ethylene glycol form an adsorbed stable layer at the alumina/electrolyte interface and thereby block the access of zinc chloride anions to the electrode.

It has been shown that zinc can be directly deposited on a barrier layer by means of application of a combined potential mode in which an AC component of 50 mV superimposed on the DC potential of -1.6 V. Increasing the temperature of the eutectic solution allows zinc electrodeposition in a potentiostatic regime already at 50^{o}C. By application of any of these conditions, zinc can be deposited on a barrier alumina layer up to about 60 nm thick. The range of frequencies of the AC component and the temperature range where the deposition is optimal were considered. The mechanism of unblocking of the electrode by the alternating potential and by the temperature rise has been suggested.

Keywords: barrier alumina layer, deep eutectic solvent, choline chloride, electrochemical deposition

Introduction

In the last decade the high-ordered porous templates of anodic aluminium oxide (AAO) have widely been used for preparation of 1-D nanostructures [1]. Nanorods and other nanostructures are produced using electrochemical deposition that is the most conventional and cheap method. However, there is a limitation for application of AAO templates that arises from the presence of a barrier layer at the bottom of pores. The alumina film formed as a result of anodization or immediate oxidation of aluminium acts as a high resistive medium impairing the flow of current.

Generally, a detached AAO membrane (free AAO) with sputtered metallic contact is used for electrofilling of the pores [2-4]. A multi-stage process of removal of both substrate and the barrier layer followed by contact deposition is typically applied [5].

Both stages are time-consuming, require expensive equipment and have a poor scalability. In this respect, preparation of 1-D nanostructures by means of direct deposition in pores AAO template has a good practical potential. The method is much cheaper and faster than a deposition using a detached membrane. A number of ways to thin the barrier layer have been reported. The decrease of potential at the end of anodizing process [6-8] and dissolution of the oxide layer are the most promising of them. Unfortunately, the layer cannot be completely removed by any of these methods, and results in difficulties in electrochemical deposition into pores. The direct growth of nanostructured materials on barrier alumina layers opens new possibilities, as to create different metal-insulator-metal and metal-insulator-semiconductor devices, which can be used as sub-wavelength plasmonic waveguides [9, 10] and supercapacitors [11, 12].

It is well-known that ionic liquids (ILs) demonstrate a number of important properties such as negligible vapour pressure, wide electrochemical window and high thermal stability [13]. Deep eutectic solvents (DESs) have similar properties but, in contrast to the conventional ILs, DESs are much cheaper, non-toxic, water-/ air- stable, and therefore have a good potential for use in industrial scale [14]. Abbott *et al*. have widely studied properties of DESs based on choline chloride namely viscosity and conductivity [15, 16]. Electrodeposition of metals [17, 18] and particularly zinc [19-24] and Zn-containing alloys [25] from these solvents was explored as well.

In our previous work [26], we formed zinc nanorods in an AAO template through zinc electrodeposition from DES based on choline chloride. Zinc was chosen as a model metal for deposition due to possibility of subsequent transformation into semiconductor materials such as zinc oxide and zinc sulphide [27]. It is known that the use of DES prevents a chemical destruction of the barrier which is typical for acidic/basic aqueous electrolytes. An ordered porous template was prepared by anodization of aluminium substrate without complete removal of the barrier layer. A two-step process was used; pulse nucleation of zinc nanoparticles on the bottom of the pores followed by a growth of the rods in a potentiostatic mode. Application of the alternating current [28] (AC) stage in the beginning of the process allowed us to deposit zinc in presence of the barrier [26]. It has been demonstrated that electrofilling of an AAO template without removal of the barrier layer is also feasible as well in aqueous electrolytes [29, 30]. An AC mode method or a pulse deposition [31] were shown to be the most promising methods in this respect. However, no systematic study of electrodeposition over an aluminium oxide layer has

been reported. The mechanisms of nucleation at the bottom of pores are also not fully understood.

The study of nucleation processes in porous templates is not easy because of the fact that the interface is buried. Besides, the diffusion limitations in the pores can create interfering effects. In this respect, electrodeposition on flat samples allows to avoid these limitations and can serve as an appropriate model process for such study. This work aims at investigating ways of zinc electrodeposition from DES based on choline chloride over barrier alumina layers in terms of temperature, oxide layer thickness, and potential profile applied. Effects of Zn deposition using a potentiostatic (PS) regime and a PS regime modified with a small alternating potential (AC-PS) were considered.

Experimental

Coupons of aluminium foil (10×5×0.2mm, 99.990%, Goodfellow) and Fluorine doped Tin Oxide (FTO) glass (Sigma-Aldrich) were used for template preparation. Part of their surface was isolated with varnish, giving an electrode working area of about 0.5 cm^2. Before anodization, the metallic electrodes were chemically polished in a mixture of phosphoric acid, nitric acid and acetic acid at 70-90ºC. Finally, the samples were rinsed with acetone, ethanol and distilled water, and then dried in air.

Preparation of anodized samples

A Keithley 237 High Voltage Source-Measure Unit was used as a current source for sample oxidation. A 0.1 M ammonium pentaborate aqueous solution served as electrolyte. A two-step anodization procedure was applied at room temperature. The first anodization step was performed in a galvanostatic mode with a current density of 1 mA/cm^2. Platinum foil was used as counter electrode. The process was terminated after the desired voltage (10, 20, 40 V) was achieved. The second anodization step was done in a potentiostatic regime at the same voltages during 10 min. After the two steps of anodization the electrodes were stored in a desiccator for stabilization of the compact alumina layer.

Oxide layer thickness measurements

Thickness of the layers was measured by Electrochemical Impedance Spectroscopy (EIS) and Glow Discharge Optical Emission Spectroscopy (GDOES).

The EIS measurements were performed using a Gamry FAS2 Femtostat with a PCI4 Controller over a $10^5 – 10^{-2}$ Hz frequency range with a step of 7 points per decade. Impedance spectra were recorded applying a 10 mV (rms) sinusoidal perturbation at open circuit potential. The measurements were carried out in a three-electrode cell (consisting of a Mercury/Mercury sulphate reference electrode, a platinum foil as the counter electrode and the working electrode with an area of 0.5 cm^2). All measurements were performed in the Faraday cage to avoid interferences with external electromagnetic fields. A 0.1 M ammonium pentaborate aqueous solution was the working electrolyte. The impedance plots were fitted using the Echem Analyst software from Gamry Inc. All spectra were successfully fitted using a parallel R-C network.

GDOES depth profile analysis of the coatings was completed using a HORIBA GD-Profiler 2 with an anode of 4 mm in diameter and operating at a pressure of 650 Pa and a power of 10 W.

Both EIS and GDOES methods gave the same thickness values (Table IV. 1).

Table IV. 1 Thickness of the barrier alumina layers

Voltage	Thickness
0 V	2 nm
10 V	15 nm
20 V	27 nm
40 V	54 nm

Electrodeposition study

Preparation of DES electrolytes and the electrodeposition experiments were done in air atmosphere. The eutectic system was prepared by mixing choline chloride (ChCl, 98%) and ethylene glycol (EG, 99+%) in the molar ratio of 1:2. Anhydrous zinc chloride (99.99%) was added to the DES to obtain a 0.1 M solution which was then heated and kept at 60 °C under vacuum during 24 h. As-prepared solution (hereafter DES:Zn) was either used for electrodeposition or stored in desiccator over P_2O_5.

Cyclic voltammograms (CVs) were obtained using a Bio-Logic SAS SP-300 potentiostat. Measurements were performed in a Faraday cage. A three-electrode cell consisting of a platinum wire as reference electrode, graphite rod as counter electrode and the working electrode was used. All cyclic voltammetric curves were recorded starting in

the cathodic direction. The potential scan rate was 0.1 V/s in all potentiodynamic experiments.

Investigations of electrode surface morphology and elemental analysis were performed using a Hitachi S-4100 scanning electron microscope (SEM) coupled with energy dispersive spectroscope (EDS). An ImageJ 1.48v image processing software was applied for calculation of the electrode areas covered by the deposited zinc.

Fourier transform infrared (FTIR) spectra were recorded using a Bruker IFS55 spectrometer equipped with a single horizontal Golden Gate attenuated total reflectance (ATR) cell.

Results and discussion

Electrodeposition of zinc in potentiostatic (PS) regime

Initially, zinc electrodeposition from DES:Zn on an electrode with a good conductivity for characterization of electrochemical properties of the system was tested. Typical CV recorded on a FTO electrode in a blank DES as a background solution is shown in Figure IV. 1 (dotted line). No electrochemical process is observed in the potential range from 0 to -2 V. Such a wide electrochemical window suggests feasibility of zinc deposition from a Zn-containing DES. Then, the experiments were performed in DES:Zn. It is seen from Figure IV. 1 (solid line) that a cathodic current appears at about -1.4 V. Further increase of the cathodic potential leads to onset of a reduction process that can be associated with deposition of metallic zinc. Indeed, appearance and growth of a zinc layer were observed. The obtained CVs are typical for 3D nucleation followed by diffusion limited growth. Similar CVs were previously reported for the case of Zn electrodeposition from DES on the different templates [22-24] The anodic process responsible for zinc dissolution was detected in the reverse potential scan at -1.25 V. The forward-reverse scan after the reduction peak demonstrates a current loop that is typical for the nucleation process, with overpotential of 0.15 V.

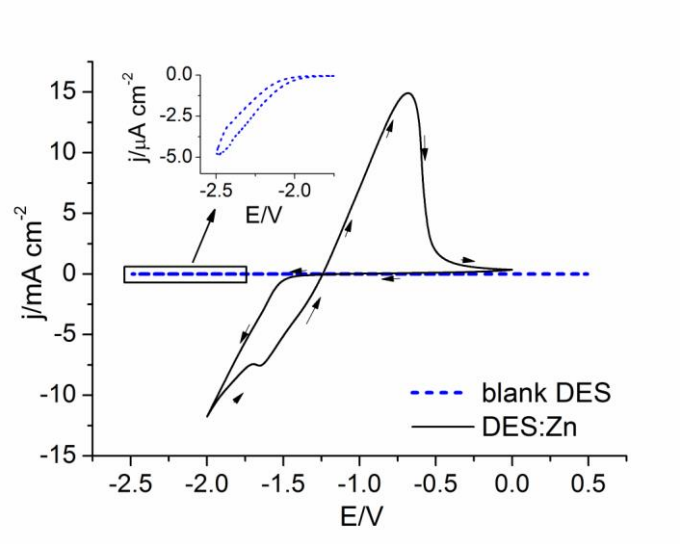

Figure IV. 1 Cyclic voltammetric curves recorded on an FTO coated glass electrode in blank Ch:EG DES and in DES:Zn. Notice the difference between the y-axis scales in the main plot and the inset.

It was observed that zinc electrodeposition from DES:Zn on FTO glass at -1.4 V resulted in an island-type metallic layer (3D nucleation) with poor adhesion. When deposition was undertaken at -2 V, gas evolution accompanying zinc reduction was detected. Hence, both potentials, -1.4 and -2 V, turned out to be not suitable for the compact zinc deposition. A mirror-like, solid zinc coating with a strong adhesion was obtained at -1.6 V. Therefore this value was used then as a base potential in all deposition experiments.

Zinc electrodeposition on aluminium surface with a native alumina film was expected to be different from that on FTO glass due to the presence of barrier layer. Indeed, the cathodic current at -1.4 V was much smaller (Figure IV. 2) as compared with that on FTO electrode at the same potential value (Figure IV. 1). Keeping the potential at -1.6 V for 30 min, zinc was not deposited on the electrode surface. (Figure IV. 3 A). Electrodeposition at -2 V and even at -5 V was tried as well. Intense gas evolution was observed but no metallic zinc on the electrode surface was found. It was shown in literature that trimethylamine [32, 33], hydrogen [24] as well as (in minor amounts) chloromethane, dichloromethane and chloroform [32] are the most likely gaseous products of cathodic reduction of DES based on ChCl.

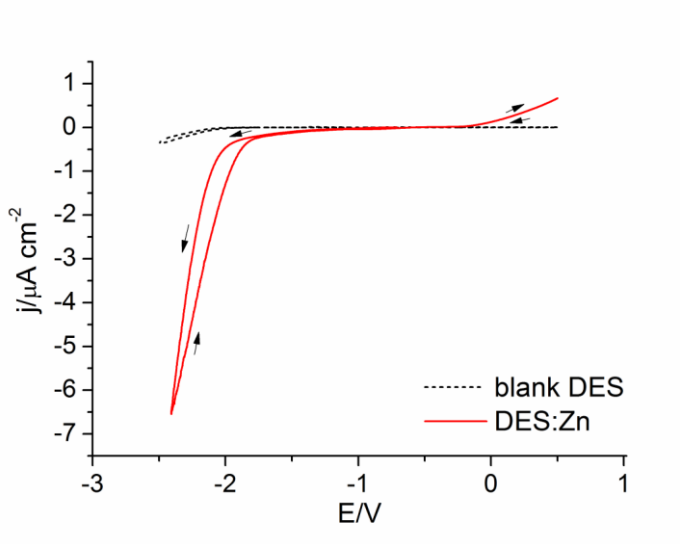

Figure IV. 2 Cyclic voltammetric curves recorded on aluminium electrode with native alumina film in blank Ch:EG DES and in DES:Zn.

These results suggested that the failure in the electrodeposition comes from large potential drop at the interface although other electrochemical processes could occur.

It has been reported that the DES components can form layers on an electrode surface [34-36]. Structure and composition of such a layer evidently depend on chemical nature of both DES and material of electrode. Based on the research conducted in ChCl:EG DESs, it has been suggested that the organic layer is formed by ethylene glycol molecules. However, one should notice that the above mentioned studies were performed using the electrodes that are free of oxide films, namely Au, Pt, Hg, and glassy carbon. Characteristics of the organic layer formed by DES components on an electrode with oxide film can differ from that formed on a pure metal (or carbon) electrode. Likely variations in composition and/or structure of such a layer can be also caused by the oxide film thickness and density. For example, in the case of aluminium electrode, the alumina film can be considered as either dielectric or semiconductor depending on thickness and defect concentration. Moreover, due to specificity of the oxidation mechanism, the oxide film on an aluminium surface is chemically inhomogeneous. The outer interface of such a film is rich in oxygen [37] that certainly favours formation of bonds with organic species that have OH groups as a constituent. In DES:Zn, such species are choline (Ch cation) and ethylene glycol (EG molecule). Therefore, Ch and EG seem to be likely species able to form a layer structure on the alumina/electrolyte interface (Figure IV. 4 A). Moreover,

these organic species are able to create strong hydrogen bonds among themselves thereby making the layer structure more stable.

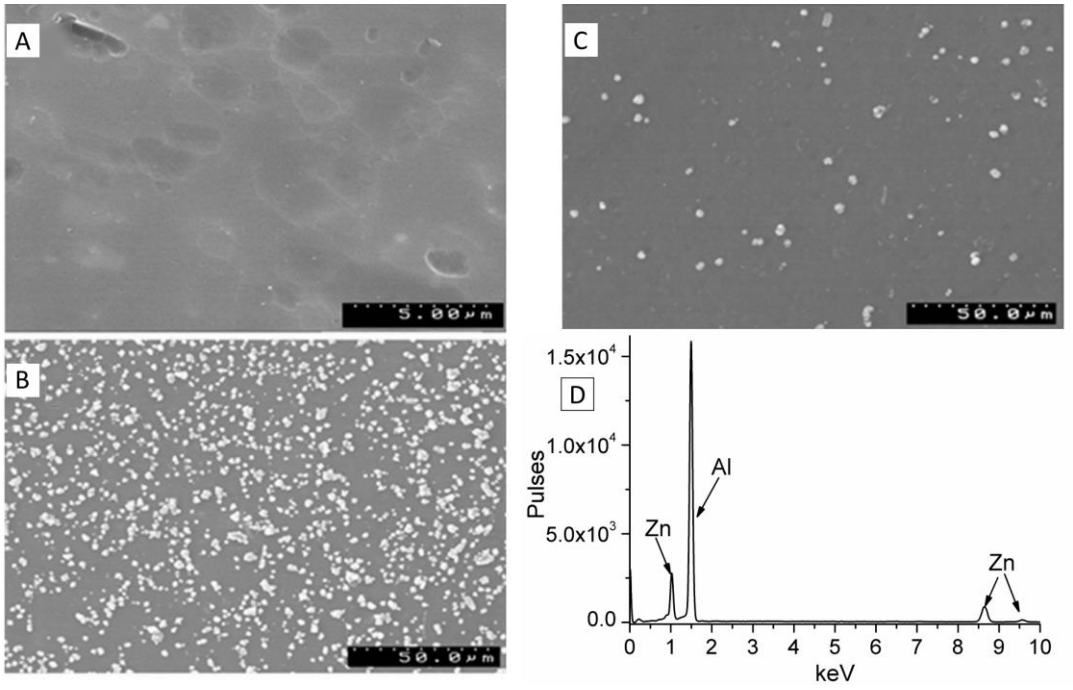

Figure IV. 3 SEM images of aluminium electrode surface with native alumina film after zinc deposition from DES:Zn in a PS mode (A) and after the deposition an AC-PS mode at 1 kHz (B). SEM image of aluminium electrode with a 15 nm anodic film after zinc deposition in an AC-PS mode at 1 kHz (C). The EDS spectrum recorded from the sample surface after zinc deposition in an AC-PS mode (15 nm anodic film, 1 kHz) (D). The deposition time was 30 min.

It has been found by Abbott *et al*. [25, 34] that zinc in DES:Zn exists in an anionic form as $ZnCl_4^{2-}$. Therefore application of a constant cathodic potential lowers concentration of zinc in a vicinity of the alumina/DES:Zn interface. In $ZnCl_4^{2-}$, zinc is coordinated by four chlorines forming a tetrahedron with the minimal dimension of ~0.7 nm. Such a big ion can hardly pass through the stable layer of organic species on the electrode. As a result, in a PS regime, no zinc deposition occurs (Figure IV. 4 B).

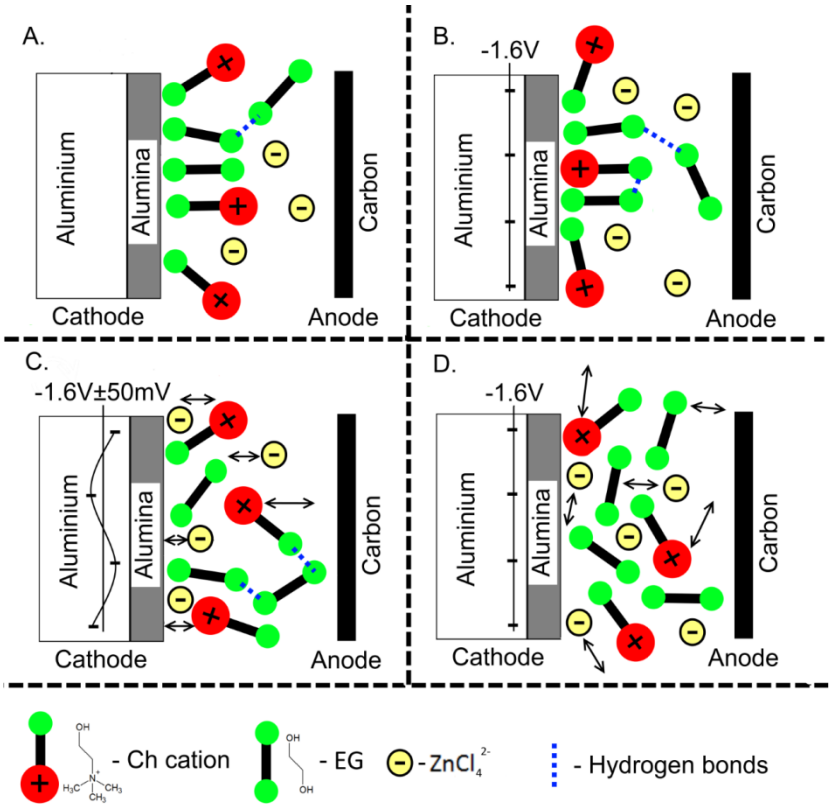

Figure IV. 4 Stable layer structured of choline / ethylene glycol on the electrode surface in absence of potential (A) and at constant potential (PS mode) (B). Destabilization of the layer as a result of application of an AC-PS mode (C) or/and increasing temperature (D).

Infrared spectroscopy study

Nature of the organic layer formed in DES:Zn on aluminium electrode with barrier alumina film and its characteristic features as compared with such a layer on a noble metal electrode were studied using infrared spectroscopy. FTIR-ATR spectrum of DES:Zn in contact with platinum electrode is in Figure IV. 5. The respective spectra of blank DES:Zn and blank platinum are shown for comparison. The observed bands in the DES:Zn spectra correlate well with the reference spectroscopic data for ethylene glycol and choline chloride. One can see that contact of DES:Zn with platinum surface results in no shift of the bands characteristic of the blank DES:Zn spectrum thereby suggesting that no chemical bonds between the organic species and platinum electrode form.

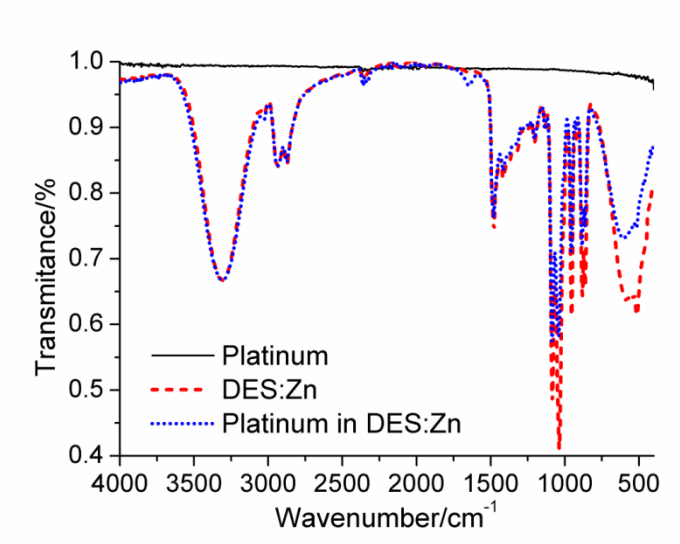

Figure IV. 5 FTIR-ATR spectra of platinum surface, blank DES:Zn and platinum surface in contact with DES:Zn.

Prior to the infrared spectroscopy study, aluminium electrode with a 15 nm anodic alumina layer was immersed in DES:Zn for 5 min, rinsed in distilled water and then dried in nitrogen gas flow. For comparison, an electrode with as-prepared (blank) 15 nm alumina layer and an electrode with the 15 nm layer in contact with DES:Zn were studied as well. Figure IV. 6 represents the respective FTIR-ATR spectra. The only band at about 1000 cm^{-1} associated with longitudinal optical vibrations of the Al-O bonds in alumina is seen in the blank alumina spectrum [38]. In the spectra of the alumina films either in contact with DES:Zn or after the 5 min immersion in DES:Zn, in addition to this band, the modes that are characteristic of the infrared spectrum of this eutectic solution are observed, although less intense. In blank DES:Zn, the mode that corresponds to the O-H stretching in alcohols is observed at 3310 cm^{-1}, while the same mode for alumina after immersion in this eutectic solution is at 3445 cm^{-1} (Inset A in Figure IV. 6). Such a shift in the mode position suggests some interaction between OH groups of the organic species in DES and defect outer surface of the anodic alumina film. This shift is considered to indicate the formation of a layer of adsorbed organic species on the alumina film surface. In the spectrum of alumina in contact with DES:Zn, the O-H stretching mode is also shifted in comparison with that of the blank DES:Zn and it is centered at 3357 cm^{-1}. We consider that this band has the contribution of the respective modes of both adsorbed species and free species, and the contribution from the former is definitely smaller than

that from the latter. Hence, the band position for the alumina in contact with DES:Zn is close to that for the blank DES:Zn.

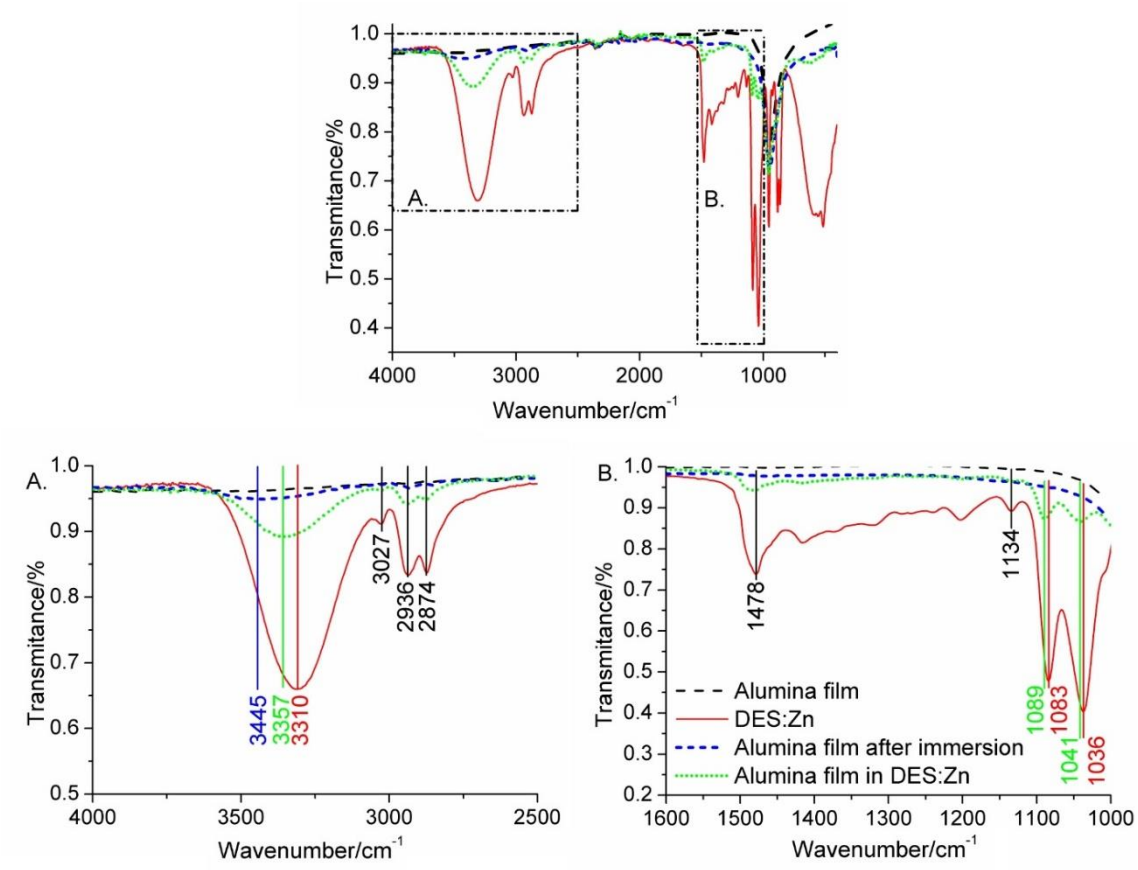

Figure IV. 6 FTIR-ATR spectra of blank DES:Zn, blank anodic alumina film, anodic alumina film after a 5 min immersion in DES:Zn and anodic alumina film in contact with DES:Zn. Magnified areas of the spectra in the ranges of 2500-4000 cm^{-1} (A) and 1000-1600 cm^{-1} (B).

The modes associated with C-O vibrations in blank DES:Zn (at 1083 and 1036 cm^{-1}) are shifted to 1089 and 1041 cm^{-1}, respectively, in DES:Zn in contact with alumina (Inset B in Figure IV. 6). As regards the modes related to C-H vibrations that are present in the spectra as well, changes in their positions were found to be below the experimental error. This suggests that the interaction between the alumina surface and choline / ethylene glycol occurs through OH groups of these organic species.

Electrodeposition of zinc in AC-PS regime

Zinc electrodeposition in the AC-PS regime was studied using the anodized samples with a 15 nm alumina layer. A sinusoidal potential of 50 mV amplitude was superposed on above the DC potential of -1.6 V at the following frequencies: 1, 10, 10 Hz; 1, 2, 5, 10, 50, 100 kHz.

We found out that blocking effect of the choline / ethylene glycol layer can be diminished by application of such a combined potential. Indeed, zinc reduction was detected in the frequency range of 1 Hz - 1 kHz. It was revealed from SEM/EDS study that the observed isolated particles on the electrode surface are metallic zinc (Figure IV. 3 B, C, and D). Both number and size of the particles were found to increase as the AC-PS frequency is increased from 1 Hz to 1 kHz. The maximal deposited zinc amount was obtained when electrodeposition was performed at 1 kHz (Figure IV. 7).

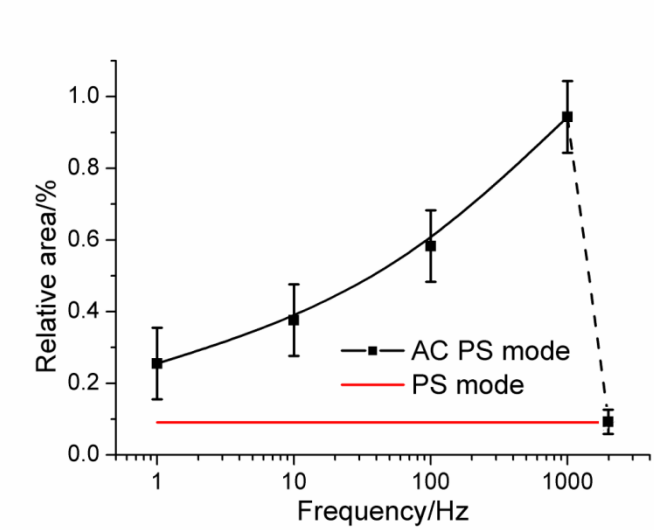

Figure IV. 7 Relative surface area of aluminium electrode with a 15 nm anodic alumina layer covered by the deposited zinc particles after electrodeposition in AC-PS mode at different frequencies of the alternating component of the applied potential. The deposition in the frequency range between 1 kHz and 2 kHz has not been explored. The lines are used to guide eyes.

Periodic variations of the potential are assumed to disturb the stationary state established in the vicinity of cathode as a result of application of the PS regime only. Specifically, field-induced vibrations of polar choline cations make the respective organic layer on the alumina/electrolyte interface less compact (Figure IV. 4 C). It opens a way

for zinc chloride anions to reach the cathode followed by zinc reduction. Zinc deposition was more efficient when the frequency of the alternating component was 1 kHz (Figure IV. 3 B, C and Figure IV. 7). When the frequency increases the relatively heavy choline ions are not able to move substantially during the potential cycles. Thus, due to inertia of the choline cations the respective layer keeps compact. Periodic variations of the applied potential with frequency of 2 kHz and above do not disturb the stationary state and zinc deposition remains impossible.

Effect of temperature

The process of zinc electrodeposition on a barrier alumina layer was also studied as a function of the electrolyte temperature. Deposition experiments in the PS regime and AC-PS regime with the applied potentials of -1.6 V and -1.6 V overlaid with a sinusoidal potential of 50 mV at 1 kHz, respectively, on a 15 nm alumina layer at 25, 50, 75 and 100°C were performed.

The electrical properties of alumina layers before and after 30 min immersion in DES:Zn at each temperature was controlled by EIS. No significant change in EIS spectra of barrier layers has been observed. The high-frequency part of the spectra was found to be the same for all samples regardless of the temperature.

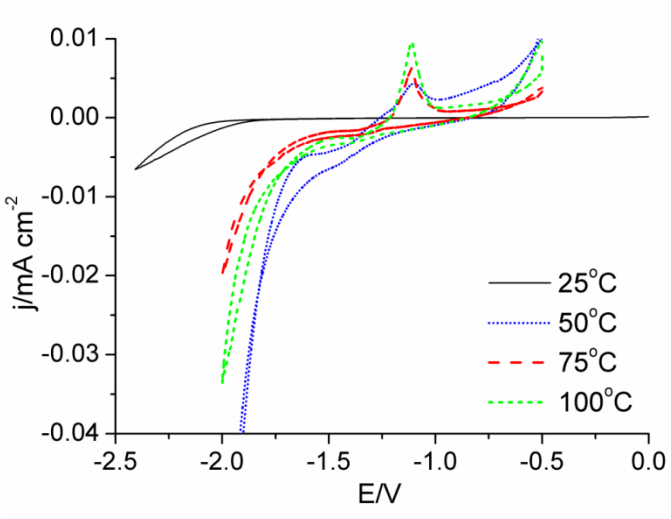

Figure IV. 8 Cyclic voltammetric curves recorded on aluminium electrode with a 15 nm anodic alumina layer in DES:Zn at 25, 50, 75 and 100°C.

Increasing temperature was found to allow zinc electrodeposition from DES:Zn even in the potentiostatic regime. It is seen from the CV curves in Figure IV. 8 that already at 50°C a zinc oxidation peak appears and increases with temperature. Indeed, a PS electrodeposition at 50°C resulted in formation of isolated particles of zinc on the electrode surface while no deposit was detected in the same experiments at room temperature (Figure IV. 9). It should be noticed that application of the alternating component at this temperature still enhanced the deposition: the zinc coated area after AC-PS-mode deposition was almost two times larger than that when the PS regime was only applied. However, at 100°C, the amount of the deposited zinc turned out to be the same regardless of the deposition regime (either PS or AC-PS) used (Figure IV. 9).

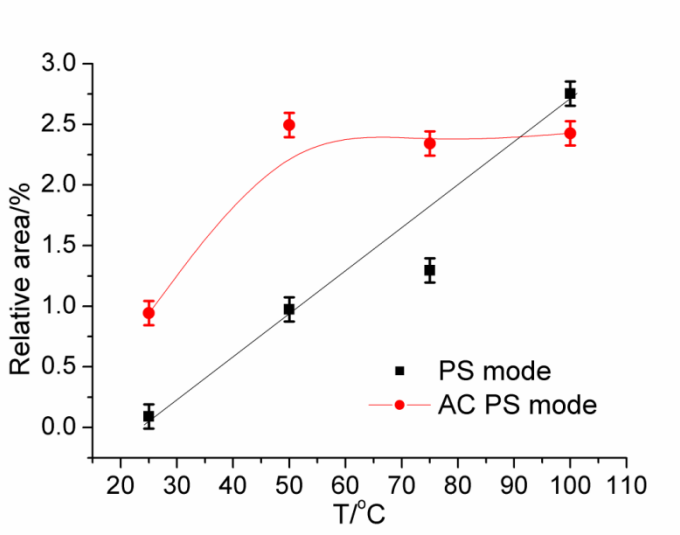

Figure IV. 9 Relative surface area of aluminium electrode with a 15 nm anodic alumina layer covered by the deposited zinc particles after electrodeposition either in PS mode or in AC-PS mode at different temperatures. Solid lines are used to guide eyes.

Therefore, increasing temperature gives qualitatively the same result as that caused by application of an alternating potential component. In fact, in both cases the zinc deposition on a barrier alumina layer can be described using the same mechanism. Vibrations of choline cations and ethylene glycol molecules, which make the blocking layer of the organic species permeable to zinc chloride anions, can be induced both by alternating applied potential and by thermal agitation (Figure IV. 4 D).

Effect of the alumina barrier layer thickness

Effect of the barrier layer thickness was studied at room temperature using either samples with a native alumina film (~2 nm thick) or anodized samples with barrier layers of 15, 27 and 54 nm thick. Experiments were performed in the AC-PS regime at 1 kHz for 30 min.

It was found from SEM study that the morphology of the zinc particles and their quantity per unit area are approximately the same in cases of deposition on a native layer and on a 15 nm alumina layer. However, the particles deposited on the thicker layer were rather smaller. Therefore, one can suggest that the zinc nucleation rate was equal in both cases while the particle growth rate was bigger when zinc was deposited on a native layer. Figure IV. 10 shows the relative electrode area covered by zinc particles as a function of the alumina layer thickness. One can see that the deposition rate decreases strongly when crossing from a native alumina film to a 15 nm layer. Deposition on a 54 nm layer is still possible but with much smaller amount of zinc particles.

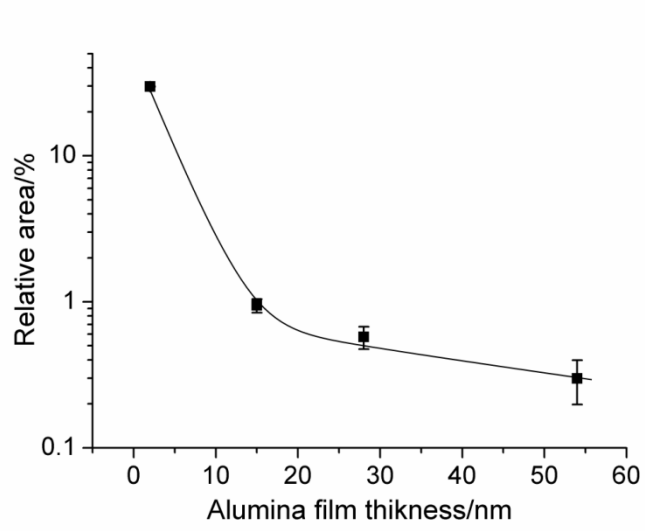

Figure IV. 10 Relative surface area of aluminium electrode either with native alumina layer or with anodic alumina layers of different thicknesses covered by the deposited zinc particles after electrodeposition in AC-PS mode at 1 kHz. Solid lines are used to guide eyes.

Further experiments have revealed that zinc deposition on barrier layers is possible when frequency of the alternating component of the applied potential is within the range of 1 Hz - 1 kHz regardless of the barrier layer thickness unless it exceeds ~60

nm. The difficulty in depositing zinc on a thicker barrier layer is caused by increasing resistance of the layer.

Conclusions

Potentiostatic deposition of zinc from a 0.1 M $ZnCl_2$ solution in a choline chloride/ethylene glycol eutectic mixture on an alumina barrier layer at room temperature is impossible even if the layer thickness does not exceed ~2 nm (a native alumina film), although zinc is easily deposited at -1.4 V from the same solution on a FTO glass electrode. In the case of deposition on alumina layers, the cathodic current is negligible at the same potential. Intense gas evolution is observed when -2 V and higher potentials are applied but no zinc deposition occurs.

Choline and ethylene glycol adsorb on alumina surface. Due to interaction between OH groups of these organic species with the oxygen-reach outer part of the alumina film, stable layer structures in the alumina/electrolyte interface are formed which block the access of zinc chloride anions to the cathode in a potentiostatic regime.

Application of the potential of -1.6 V superimposed with alternating sinusoidal component of 50 mV allows to deposit zinc both on native alumina film and on anodic layers up to about 60 nm thick when the frequency of the alternating component is within the range of 1 Hz - 1 kHz. Periodic variations of the potential disturb the stationary state of the choline cations making the respective organic layer in the alumina/electrolyte interface less compact and permeable to zinc chloride anions. The deposition rate decreases when the potential frequency is 2 kHz and above - relatively heavy organic species are not able to follow the cycling potential variations.

Increasing the temperature has the same effect as the use of an alternating component over the DC potential. Electrodeposition of zinc on a barrier layer at 100^{o}C is possible even in potentiostatic regime.

Acknowledgements

The financial support of the European Commission and Portuguese Foundation for Science and Technology (FCT) in frame of the projects PIRSES-GA-2011-295273 – NANEL and PTDC/CTM-NAN/113570/2009, respectively, is gratefully acknowledged.

References:

[1] A.M. Md Jani, D. Losic, N.H. Voelcker, Nanoporous anodic aluminium oxide: Advances in surface engineering and emerging applications, *Progress in Materials Science*, 58 (2013) 636-704.
[2] R. Chen, D. Xu, G. Guo, L. Gui, Preparation of Ag_2Se and $Ag_2Se_{1-x}Te_x$ nanowires by electrodeposition from DMSO baths, *Electrochemistry Communications*, 5 (2003) 579-583.
[3] A.P. Leontiev, O.A. Brylev, K.S. Napolskii, Arrays of rhodium nanowires based on anodic alumina: Preparation and electrocatalytic activity for nitrate reduction, *Electrochimica Acta*, 155 (2015) 466-473.
[4] S.-H. Yoo, L. Liu, S. Park, Nanoparticle films as a conducting layer for anodic aluminum oxide template-assisted nanorod synthesis, *Journal of Colloid and Interface Science*, 339 (2009) 183-186.
[5] C.P. Chan, H. Lam, K.K. Leung, C. Surya, Growth Of Copper Zinc Tin Sulfide Nano-Rods By Eelectrodeposition Using Anodized Aluminium As The Growth Mask, *Journal of Nonlinear Optical Physics & Materials*, 18 (2009) 599-603.
[6] J.M. Montero-Moreno, M. Belenguer, M. Sarret, C.M. Müller, Production of alumina templates suitable for electrodeposition of nanostructures using stepped techniques, *Electrochimica Acta*, 54 (2009) 2529-2535.
[7] R.C. Furneaux, W.R. Rigby, A.P. Davidson, The formation of controlled-porosity membranes from anodically oxidized aluminium, *Nature*, 337 (1989) 147-149.
[8] A. Santos, L. Vojkuvka, J. Pallarés, J. Ferré-Borrull, L.F. Marsal, In situ electrochemical dissolution of the oxide barrier layer of porous anodic alumina fabricated by hard anodization, *Journal of Electroanalytical Chemistry*, 632 (2009) 139-142.
[9] D.F.P. Pile, Two-dimensionally localized modes of a nanoscale gap plasmon waveguide, *Appl. Phys. Lett.*, 87 (2005) 261114.
[10] R.F. Oulton, V.J. Sorger, D.A. Genov, D.F.P. Pile, X. Zhang, A hybrid plasmonic waveguide for subwavelength confinement and long-range propagation, *Nat Photon*, 2 (2008) 496-500.
[11] E. Hourdakis, A.G. Nassiopoulou, High performance MIM capacitor using anodic alumina dielectric, *Microelectronic Engineering*, 90 (2012) 12-14.
[12] E. Hourdakis, A.G. Nassiopoulou, High-Density MIM Capacitors With Porous Anodic Alumina Dielectric, *Electron Devices, IEEE Transactions on*, 57 (2010) 2679-2683.
[13] D.M. F. Endres, A. Abbott, *Electrodeposition from Ionic Liquids*, WILEY-VCH Verlag GmbH & Co. KGaA, Weinheim, 2008.
[14] E.L. Smith, A.P. Abbott, K.S. Ryder, Deep Eutectic Solvents (DESs) and Their Applications, *Chemical Reviews*, 114 (2014) 11060-11082.
[15] A.P. Abbott, Model for the Conductivity of Ionic Liquids Based on an Infinite Dilution of Holes, *ChemPhysChem*, 6 (2005) 2502-2505.
[16] A.P. Abbott, R.C. Harris, K.S. Ryder, Application of Hole Theory to Define Ionic Liquids by their Transport Properties†, *The Journal of Physical Chemistry B*, 111 (2007) 4910-4913.
[17] A.P. Abbott, K.E. Ttaib, G. Frisch, K.S. Ryder, D. Weston, The electrodeposition of silver composites using deep eutectic solvents, *Physical Chemistry Chemical Physics*, 14 (2012) 2443-2449.
[18] S. Salomé, N.M. Pereira, E.S. Ferreira, C.M. Pereira, A.F. Silva, Tin electrodeposition from choline chloride based solvent: Influence of the hydrogen bond donors, *Journal of Electroanalytical Chemistry*, 703 (2013) 80-87.
[19] A.P. Abbott, J.C. Barron, K.S. Ryder, Electrolytic deposition of Zn coatings from ionic liquids based on choline chloride, *Transactions of the IMF*, 87 (2009) 201-207.
[20] N.M. Pereira, P.M.V. Fernandes, C.M. Pereira, A. Fernando Silva, Electrodeposition of Zinc from Choline Chloride-Ethylene Glycol Deep Eutectic Solvent: Effect of the Tartrate Ion, *Journal of The Electrochemical Society*, 159 (2012) D501-D506.

[21] A.P. Abbott, J.C. Barron, G. Frisch, K.S. Ryder, A.F. Silva, The effect of additives on zinc electrodeposition from deep eutectic solvents, *Electrochimica Acta,* 56 (2011) 5272-5279.
[22] A.H. Whitehead, M. Pölzler, B. Gollas, Zinc Electrodeposition from a Deep Eutectic System Containing Choline Chloride and Ethylene Glycol, *Journal of The Electrochemical Society,* 157 (2010) D328-D334.
[23] A. Bakkar, V. Neubert, Electrodeposition onto magnesium in air and water stable ionic liquids: From corrosion to successful plating, *Electrochemistry Communications,* 9 (2007) 2428-2435.
[24] H. Yang, R.G. Reddy, Electrochemical deposition of zinc from zinc oxide in 2:1 urea/choline chloride ionic liquid, *Electrochimica Acta,* 147 (2014) 513-519.
[25] A.P. Abbott, G. Capper, K.J. McKenzie, K.S. Ryder, Electrodeposition of zinc–tin alloys from deep eutectic solvents based on choline chloride, *Journal of Electroanalytical Chemistry,* 599 (2007) 288-294.
[26] M. Starykevich, A.D. Lisenkov, A.N. Salak, M.G.S. Ferreira, M.L. Zheludkevich, Electrodeposition of Zinc Nanorods from Ionic Liquid into Porous Anodic Alumina, *ChemElectroChem,* 1 (2014) 1484-1487.
[27] P.J. Dale, A.P. Samantilleke, D.D. Shivagan, L.M. Peter, Synthesis of cadmium and zinc semiconductor compounds from an ionic liquid containing choline chloride and urea, *Thin Solid Films,* 515 (2007) 5751-5754.
[28] M.S. Chandrasekar, M. Pushpavanam, Pulse and pulse reverse plating—Conceptual, advantages and applications, *Electrochimica Acta,* 53 (2008) 3313-3322.
[29] D. Routkevitch, T. Bigioni, M. Moskovits, J.M. Xu, Electrochemical Fabrication of CdS Nanowire Arrays in Porous Anodic Aluminum Oxide Templates, *The Journal of Physical Chemistry,* 100 (1996) 14037-14047.
[30] G.D. Sulka, A. Brzózka, L. Zaraska, M. Jaskuła, Through-hole membranes of nanoporous alumina formed by anodizing in oxalic acid and their applications in fabrication of nanowire arrays, *Electrochimica Acta,* 55 (2010) 4368-4376.
[31] A. Ramazani, M. Almasi Kashi, M. Alikhani, S. Erfanifam, Fabrication of high aspect ratio Co nanowires with controlled magnetization direction using ac and pulse electrodeposition, *Materials Chemistry and Physics,* 112 (2008) 285-289.
[32] D. Yue, Y. Jia, Y. Yao, J. Sun, Y. Jing, Structure and electrochemical behavior of ionic liquid analogue based on choline chloride and urea, *Electrochimica Acta,* 65 (2012) 30-36.
[33] K. Haerens, E. Matthijs, K. Binnemans, B. Van der Bruggen, Electrochemical decomposition of choline chloride based ionic liquid analogues, *Green Chemistry,* 11 (2009) 1357-1365.
[34] A.P. Abbott, J.C. Barron, G. Frisch, S. Gurman, K.S. Ryder, A. Fernando Silva, Double layer effects on metal nucleation in deep eutectic solvents, *Physical Chemistry Chemical Physics,* 13 (2011) 10224-10231.
[35] R. Costa, M. Figueiredo, C.M. Pereira, F. Silva, Electrochemical double layer at the interfaces of Hg/choline chloride based solvents, *Electrochimica Acta,* 55 (2010) 8916-8920.
[36] M. Figueiredo, C. Gomes, R. Costa, A. Martins, C.M. Pereira, F. Silva, Differential capacity of a deep eutectic solvent based on choline chloride and glycerol on solid electrodes, *Electrochimica Acta,* 54 (2009) 2630-2634.
[37] K.A. Yasakau, A.N. Salak, M.L. Zheludkevich, M.r.G.S. Ferreira, Volta Potential of Oxidized Aluminum Studied by Scanning Kelvin Probe Force Microscopy, *The Journal of Physical Chemistry C,* 114 (2010) 8474-8484.
[38] M. Kaltchev, W.T. Tysoe, An infrared spectroscopic investigation of thin alumina films: measurement of acid sites and surface reactivity, *Surface Science,* 430 (1999) 29-36.

Chapter V

Effect of the anodic titania layer thickness on electrodeposition of zinc on Ti/TiO_2 from deep eutectic solvent

---

D88 *Journal of The Electrochemical Society*, **164** (2) D88-D94 (2017)
0013-4651/2017/164(2)/D88/7/$37.00 © The Electrochemical Society

Effect of the Anodic Titania Layer Thickness on Electrodeposition of Zinc on Ti/TiO_2 from Deep Eutectic Solvent

M. Starykevich,[a,z] A. N. Salak,[a] D. K. Ivanou,[b] K. A. Yasakau,[a] P. S. André,[c] R. A. S. Ferreira,[d] M. L. Zheludkevich,[a,e] and M. G. S. Ferreira[a,*]

[a] *Department of Materials and Ceramic Engineering, CICECO-Aveiro Institute of Materials, University of Aveiro, 3810-193 Aveiro, Portugal*
[b] *LEPABE, Faculty of Engineering, University of Porto, 4200-465 Porto, Portugal*
[c] *Instituto de Telecomunicações and Department of Electrical and Computer Engineering, Instituto Superior Técnico, Technical University of Lisbon, 1049-001 Lisbon, Portugal*
[d] *Physics Department, CICECO-Aveiro Institute of Materials, University of Aveiro, 3810-193 Aveiro, Portugal*
[e] *Institute of Materials Research, Helmholtz-Zentrum Geesthacht, 21502 Geesthacht, Germany*

Abstract

Zinc electrodeposition from a deep eutectic mixture of $ZnCl_2$ and choline chloride/ethylene glycol on titanium covered by an anodic titania film of different thicknesses was studied. It was shown that thin titanium dioxide layers work as high resistive media and the rate of zinc deposition decreases with film thickness. Thicker titania layers (23 nm and higher) have opposite properties and the zinc reduction rate starts gradually increasing with thickness. This happens because at the higher voltage necessary to grow thicker anodic films they become more crystalline and consequently more conductive.

There is also evidence that in deep eutectic solvent no dense organic layer forms on the titanium/titania electrodes. The application of an AC signal superimposed on a DC potential only marginally increases the amount of zinc deposited and FTIR measurements did not reveal the formation of any chemical bonds between the film and deep eutectic solvent.

Zn deposition onto titanium/titania at -1.6V is characterised by instantaneous three-dimensional nucleation mechanism, which is independent of the titania thickness.

Keywords: Titanium oxide, deep eutectic solvent, zinc electrodeposition.

Introduction

Electrochemical deposition is a conventional and cheap technique to form 1-D nanostructures. In most of the cases, porous anodic templates on the valve metals are used. Filling of the matrices by other materials is applied to produce solid state solar cells, photodetectors, magnetic sensors, metal–insulator–metal capacitors [1] *etc*. The major drawback of the porous anodic oxide templates is a barrier layer on the bottom of pores, which usually acts as a high resistive medium impairing the flow of current.

Direct investigation of deposition and nucleation processes in porous templates is challenging because the interface is hidden. Electrodeposition on flat samples allows to avoid these limitations and can serve as an appropriate model process for such study. However extrapolation of results found on a bare metal electrode to the processes on the bottom of pores is incorrect because of critical differences between metal/electrolyte and barrier oxide/electrolyte interfaces. Consequently, the use of a metallic electrode covered by the anodic oxide layer is one of the most convenient ways to study the bottom processes. In our previous work [2] zinc electrodeposition from a solution of $ZnCl_2$ in a

choline chloride / ethylene glycol eutectic mixture on dense alumina layers of different thicknesses was studied. It was shown that the potentiostatic deposition of zinc on an alumina barrier layer at -1.6V and room temperature is impossible even if the layer thickness does not exceed ~2 nm (a native alumina film). As a comparison, zinc is easily deposited at -1.4 V from the same solution on a fluorine doped tin oxide coated glass electrode. The formation of a dense organic layer due to interaction between OH groups of the organic species with the alumina film was demonstrated. Moreover deposition has been shown to be possible by superimposing an alternating sinusoidal voltage on DC potential (-1.6V) or alternatively increasing the solution temperature [2].

The current paper is devoted to studying of electrodeposition of zinc from choline based eutectic on anodic titanium oxide film. Bulk anodic titania has been investigated for more than 50 years. Several properties such as growth factors [3-8], crystallinity [1, 9-12], conductivity, influence of anodization solution and regime [13] were widely studied by different authors. Despite all these studies deposition over anodic titania is still hardly understood. Only works about deposition of copper on titanium oxide films from water solution were described in literature [14, 15]. Electrodeposition of metals from deep eutectic solvent (DES) on titania covered electrodes has not yet been analysed.

Titanium dioxide films both in pure state and after electrochemical modification have distinguished properties, for instance, catalytic and photocatalytic [16, 17], self-cleaning and wetting [18], use as solar cell [19] and optical devices [20]. Furthermore, anodic titania is a promising porous matrix to be filled by different materials [21-23].

Deep eutectic solvent based on choline chloride was selected as electrolyte for deposition due to its properties, such as negligible vapour pressure, wide electrochemical window and high thermal stability [24]. Choline eutectic is often called in literature as quasi ionic liquid since their behaviour is similar, for instance, low melting point, relatively wide liquid-range *etc*. However, in contrast to conventional ionic liquids, DESs are very cheap, not-toxic and have good potential for industrial usage [25]. Abbott *et al*. have widely studied properties of DESs based on choline chloride, namely viscosity and conductivity [26, 27]. Electrodeposition of metals [28, 29] and particularly zinc [30-36] and Zn-containing alloys [37] from these solvents was explored as well. Moreover the use of DES as electrolyte gives an opportunity to dissolve compounds which are insoluble in water (for example ZnO) and to make deposition from these solutions [35, 38].

In the present work zinc was chosen as a material to be deposited due to its capability to transform afterwards into semiconductor materials such as zinc oxide and

zinc sulphide [39] and for comparison of the results with previous work [2] where deposition of zinc on aluminium/alumina was reported.

Experimental

Coupons of titanium foil (100mm ×5mm ×1 mm, 99.2%, Alfa Aesar) were used as electrode material for sample preparation. The coupons were rinsed with acetone, ethanol and distilled water and then were dried in air. Before anodization, the electrodes were chemically polished in a HF:HNO_3 mixture (1:3 by volume) to mirror finish and finally were rinsed with deionized water. Part of their surface was isolated with chemically resistant varnish, giving an electrode working area of 0.5 cm^2. The sample with the thinnest barrier layer was prepared by activation in hydrofluoric acid. It is a common procedure before plating and it results in decrease of the native layer thickness due to formation of soluble titanium fluorides. Formation of titanium hydride takes also place [40] and this layer prevents generation of a new barrier layer [41]. The activation was performed in 5% HF during 30 seconds.

A Keithley 237 High Voltage Source-Measure Unit was used as a current source for the sample anodizing. A 1M sulphuric acid aqueous solution was used as electrolyte [12]. The anodization was performed in a galvanostatic mode with a current density of 10 mA/cm^2. The counter electrode was a platinum foil. The process was terminated after the desired voltage (3, 7, 10, 20, 40 V) was attained. The thinnest anodic film used in this work (12 nm) corresponds to 3V. Preparation of thinner anodic titania layers is hindered because of low reproducibility of the experiments and inhomogeneity of the films. After anodization the electrodes were stored in a desiccator for stabilization of the compact titania layer for 24 hours.

Thickness of the layers was measured by Ellipsometry and Glow Discharge Optical Emission Spectroscopy (GDOES). The spectroscopic ellipsometry measurements were made using an AutoSE ellipsometer (HORIBA Scientific) with a total of 250 points in the wavelength interval 450-850 nm, an incidence angle of 70º, a signal quality of 30 and a measurement spot area of 250×250 μm^2. The structural model used consists of a three-layered structure incorporating substrate, titania layer and air as ambient medium with a refractive index value of 1.00. The thickness of the substrate was considered infinite and the refractive index was obtained by direct inversion of the ellipsometric data.

To describe the refractive index values the Lorentz model was used, which expresses the relative complex dielectric constant as a function of the frequency (ω) described by:

$$\varepsilon = \varepsilon_\infty + \frac{(\varepsilon_s - \varepsilon_\infty) \times \omega_0^2}{(\omega_0^2 - \omega^2) + i\Gamma\omega} \quad \text{(V.1)}$$

where ε_∞, ε_s, ω_0 (eV), Γ (eV) are the high frequency relative dielectric constant, the static relative dielectric constant, the oscillator resonant frequency and the damping factor, respectively [42]. The fitting method has been described elsewhere [43]. The reported values for the thickness are the average of three measurements performed for each sample with a maximum standard deviation of 5%.

GDOES depth profile analysis of the coatings was done using a HORIBA GD-Profiler 2 with a copper anode of 4 mm in diameter. Argon sputtering of the sample surface occurred at a pressure of 900 Pa and power of 10 W. A minimum of three measurements were performed for each sample.

Preparation of DES electrolytes and the electrodeposition experiments have been done in contact with air. The eutectic system was prepared by mixing choline chloride (ChCl, 98%) and ethylene glycol (EG, 99+%) in the molar ratio of 1:2. Anhydrous zinc chloride (99.99%) was added to the DES to obtain a 0.3 M solution, which was heated and kept at 60 °C under vacuum during 24 h. The as-prepared solution (hereafter DES:Zn) was either used for electrodeposition or was stored in a desiccator over P_2O_5. All experiments were performed in open air because the DES is water and air stable and it is one of the main advantages of this electrolyte compared to ionic liquids. Moreover, it is not sensitive even to small amount of water [24]. When not in use the DES was stored in the desiccator with P_2O_5.

Voltammograms were recorded using a Bio-Logic SAS SP-300 potentiostat. Measurements were performed in a Faraday cage. A three-electrode cell consisting of a platinum wire as pseudo-reference electrode, graphite rod as counter electrode and the working electrode was used. All voltammetric curves were recorded starting in the cathodic direction. In all potentiodynamic experiments, the potential scan rate was 20 mV/s. Each measurement was repeated minimum twice for reproducibility checking.

Investigation of electrode surface morphology and elemental analysis were performed using a Hitachi S-4100 scanning electron microscope (SEM) coupled with an

energy dispersive spectroscope (EDS). An ImageJ 1.48v image processing software was applied for calculation of the electrode areas covered by the deposited zinc.

The Fourier transform infrared (FTIR) spectra were recorded with the use of a Bruker IFS55 spectrometer equipped with a single horizontal Golden Gate attenuated total reflectance (ATR) cell. In the optical range of 350-4000 cm^{-1}, 128 scans were performed for each measurement. The resolution of the equipment is 4 cm^{-1}. Templates were prepared on thin titanium substrate (0.1 mm) involving the procedure that has been described before. The samples were installed in contact with the DES:Zn and pressured to the crystal.

A Digital Instruments NanoScope III atomic force microscope (AFM) system with ExtenderTM Electronic Module was used for acquisition of topography. The measurements were performed with highly doped Si AFM probes purchased from App Nano (model ACT). The probes had the following characteristics: tip pyramid height 14-16 μm, tip radius <10 nm, 300 kHz resonance frequency, spring constant around 37 N/m.

Results and discussion

Titanium anodization

Figure V. 1 a shows the dependence of the signal intensity of the elements composing the titanium anodized layer (40 V) on its depth obtained by GDOES. It demonstrates homogeneity of the oxide film and uniformity of sulphur distribution. Sulphur is present in the titania film because sulphuric acid solution was used as an electrolyte. Deviation of the profiles at the beginning of sputtering can be explained by the presence of an adsorbed layer on the surface containing sulphur and oxygen, probably from the sulphuric acid. The oxygen concentration slightly decreases throughout the film because oxygen migration occurs during the anodization process, from the electrolyte to the electrode leading to higher concentration of oxygen on the titania/electrolyte surface than on titania/titanium interface. A well-defined interface between the anodic titania film and the titanium substrate was obtained. The plateau on the titanium and oxygen signal intensity curves during the glow discharge etching process corresponds to the oxide layer. Further growth of the titanium signal indicates that the metal sputtering started.

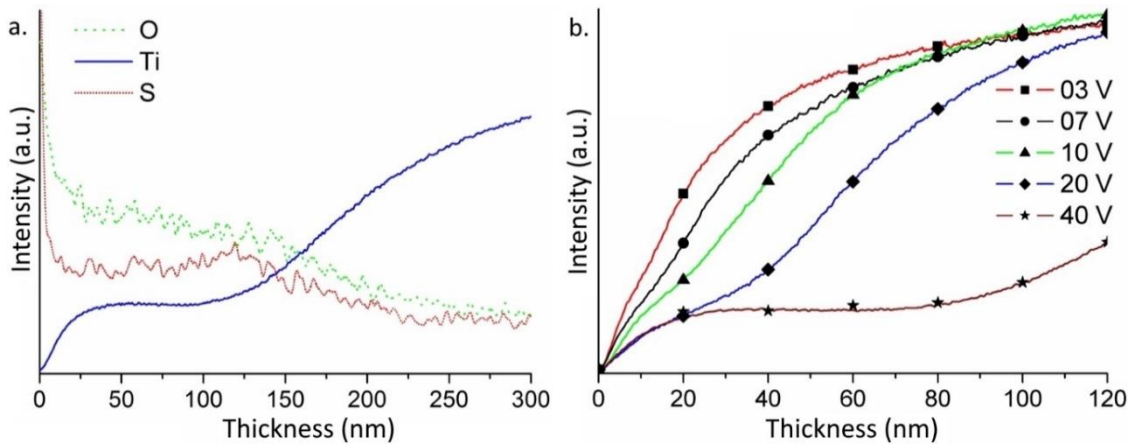

Figure V. 1 Qualitative GDOES depth profiles of titanium anodized at different voltages for Ti, O, S after anodization at 40 V (a), and for titanium after anodization at 3, 7, 10, 20 and 40 V (b).

Ellipsometry measurements were done in parallel to GDOES and data fitting were performed using the Lorentz model. Both the techniques showed similar results in terms of thickness/voltage ratio for instance at 5 and 20 volts the ellipsometry results are 15 nm and 44 nm respectively, whereas the GDOES technique estimates 12 and 43 nm. Routinely, the oxide thickness of the samples was controlled and presented (Figure V. 2) only for GDOES due to similarity of the results.

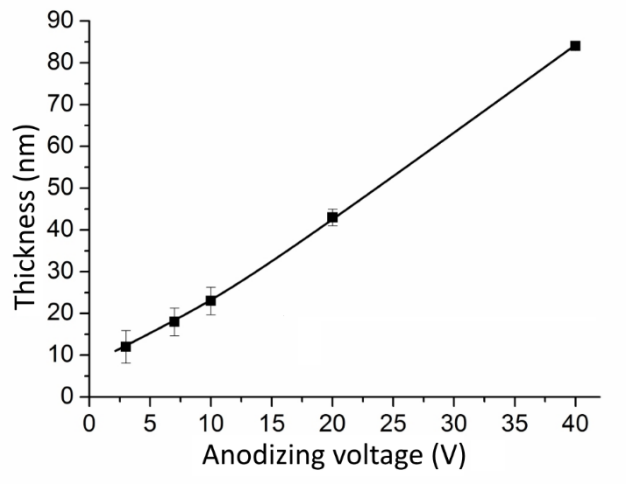

Figure V. 2 Film thickness vs anodizing potential of titanium in 1M sulphuric acid solution measured by GDOES equipment. Solid line is used to guide eyes.

The GDOES data of Figure V. 2 shows that the thickness-voltage ratio for the galvanostatic growth of anodic TiO_2 is in the range of 2–3 nm/V, which is in accordance

with the values commonly reported in literature for titania anodic films grown in sulphuric acid solutions [3-8].

Zinc electrodeposition on Ti/TiO_2 electrodes with different film thicknesses

Typical voltammograms that were obtained on zinc and on titanium electrode covered with compact titania film in DES:Zn are presented in Figure V. 3. The potential for reduction of zinc on zinc electrode is -1.1V (Figure V. 3). Nevertheless, the negative current was only detected at -1.2V on the titanium/titania electrode after pre-treatment (activation) in hydrofluoric acid, which evidences the existence of an overpotential for zinc reduction on the titania surface. Fast current increase followed by a plateau was observed for these electrodes. Strong cathodic current appears at -1.65V and corresponds to reduction of the electrolyte organic species. Decomposition occurs according to the mechanism described in literature [44, 45]. The small current that appears on the titania covered electrodes probably corresponds to reduction of titania [23] since zinc was not detected on the surface by SEM studies in this potential region. Electroreduction of zinc was performed in the range from -1.2V to -1.7V with a 100mV step to find the best physical properties of the deposit. The quality of the coating was evaluated visually. The deposition potential of -1.6V was selected because it gives solid zinc coating with the best adhesive properties.

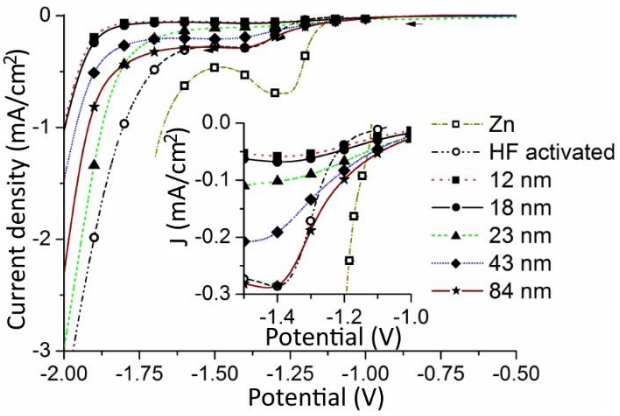

Figure V. 3 Voltammograms for zinc and titanium covered with anodic titania of different thicknesses electrodes (inset: magnification of -1.5 to -1.0 V zone).

Initial increase in the barrier layer thickness from the one corresponding to the HF activated electrode until 12 nm obtained by anodizing leads to a strong decrease of the reduction current (Figure V. 3). It is typical for valve metals because of low conductivity of the oxide film. Normally, the resistance of the film rises with its growth, which makes the deposition difficult. This situation was demonstrated for the like aluminium/alumina system in our previous work [2]. Increasing the alumina barrier thickness provides significant increase of the resistance and consequently decrease of the zinc reduction current. Nevertheless, in the present case, the negative current on the titanium/titania electrode with 18 nm titania film stays on the same level as with 12 nm thickness (Figure V. 3). Moreover, with further increment of thickness to 23 nm and thicker, the current rises, contrary to the case of alumina where the current decreases dramatically with growth of the film. The maximum current on titanium/titania electrode was obtained at maximal film thickness of 84 nm, and is similar to the current on the activated electrode (Figure V. 3). The phenomenon of current increase on thicker anodic titania films was demonstrated in Hyun Chang's work for copper deposition from water solution [15]. The authors modified the Ti cathode surface by temperature oxidation and anodization process. Both cases showed enhanced deposition rate because the film is more conductive in spite of the oxide layer is thicker. They explained this fact by better crystallinity of the anodic film at higher anodization voltage and correspondingly at higher film thickness. Similar conclusion was achieved by Shibata et Zhu [9]. The structure of the anodic oxide film on titanium was found to be dependent on the formation potential. Film crystallization occurs at potentials more positive than 7.0 V. In the present work it can be suggested an analogous explanation for the current increment. The oxide layer remains amorphous on the initial stage of the growth and the conductivity decreases with film thickness (12 and 18 nm films). After reaching a critical anodization voltage, the anodic layer starts crystallizing, which results in higher current for the 23 nm barrier film (limit voltage of 10V) compared to the 12 and 18 nm films (limit voltage of 3 and 7V, respectively). The film crystallinity and conductivity progressively increase with additional accretion of the barrier, which reflects on the voltammetric curves as increase of current (Figure V. 3). These results are in accordance with Shibata's work [9] where it was demonstrated that the crystallization starts after the anodization potential of 7 V.

Figure V. 4 a depicts the current-time transients resulting from chronoamperometric experiments on titanium electrode covered with titania of different thicknesses at -1.6 V. The maximum of current was not detected for the HF activated

specimen. The initial high current is decreasing according to the Cottrell equation [46]. It means that the nuclei formation in this case occurs fast and easily. The layer of titanium hydride formed on the electrode after activation is one of the conditions that probably promotes nucleation process due to the strong reducing ability of the compound. Zinc deposition on the activated electrode is much faster than on thin barrier layers (12, 18 nm thick). The total electric charge starts to increase for the 23 nm layer and rises as the layer thickness grows. In our previous work [2], it was demonstrated that electrodepostion of zinc on native alumina layer (around 2 nm) was impossible in standard potentiostatic regime. Even after shifting the potential into the deep cathodic region (-5V) where intense gas evolution was observed there was no deposition of zinc on the electrode surface.

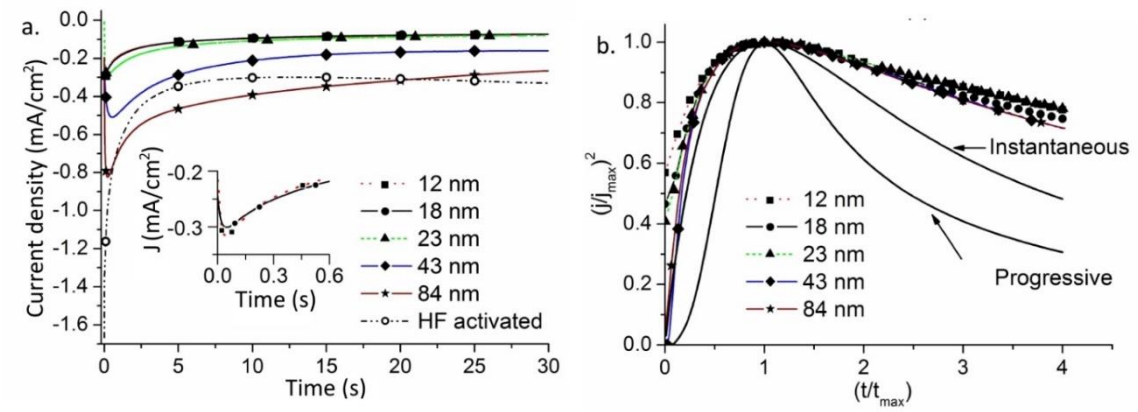

Figure V. 4 Current-time transients resulting from chronoamperometric experiments that were performed at a titanium electrode with different titania layer thicknesses in DES:Zn at -1.6V applied potential (inset: magnification of 0 to -0.6 s zone) (a). Comparison of experimental data obtained from current transients with instantaneous and progressive nucleation models (b).

The amount of zinc that was deposited during 30 seconds was calculated from Faraday's law:

$$n = \frac{Q}{zF} \text{ (V.2)}$$

where n is the chemical amount of zinc deposited, Q is the total electric charge passed, which is calculated from the above current-time curves, z = 2 is the number of

electrons transferred per ion and F is the Faraday constant. The results are shown in Figure V. 5 (red line).

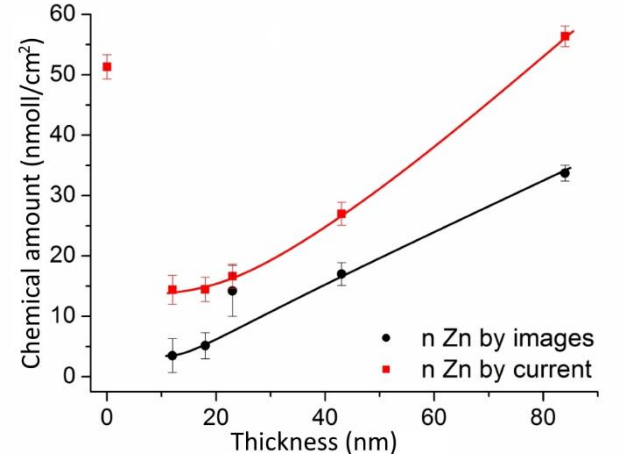

Figure V. 5 Chemical amount of zinc deposited on titanium electrode covered with titania calculated by ImageJ software (black line) and by Faraday's law (red line). Deposition dwell was 30 s. Solid lines are used to guide eyes.

Analysis of SEM images of the samples was performed to confirm that the current increase corresponds to the growth of the zinc deposition rate and not to additional competitive reactions (as in the case of aluminium/alumina). The typical image obtained for deposited zinc on titania film, 23nm thick, at E = −1.6V, is shown in Figure V. 6 a and in the inset after processing by ImageJ. At the early stages of Zn deposition (30 seconds) individual spherical particles with size d = 40 nm were formed. EDS analysis (Figure V. 6 c) shows the presence of Zn. The number and average size of the particles were determined in the same way for all the samples. For the sake of simplicity it was assumed that the particles are spherical. Then the zinc volume was calculated and the chemical amount of the deposit obtained. The results demonstrate that the quantity of zinc deposited on the surface increases with the barrier thickness growth (Figure V. 5, black line). The difference between the black and red lines could be because the deposition process efficiency is not 100% (around 60%).

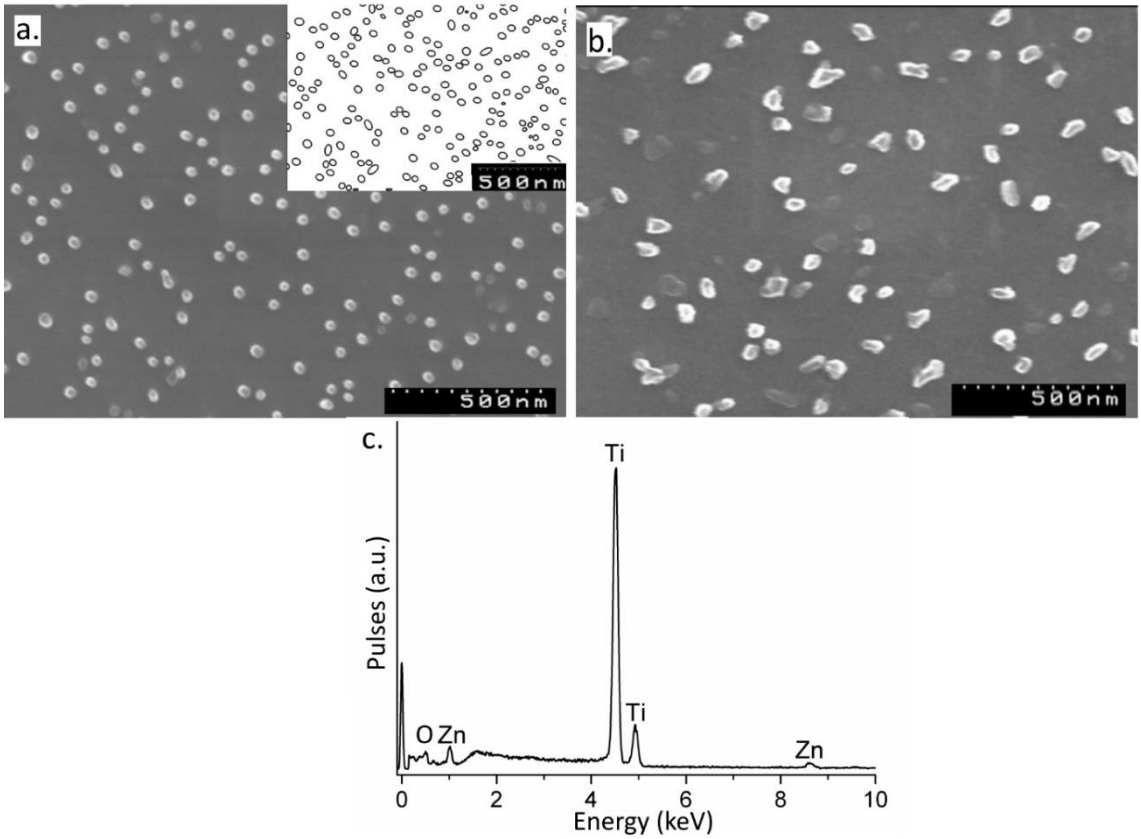

Figure V. 6 SEM images of titanium electrode surface covered with 23 nm titania film after zinc deposition at -1.6V from DES:Zn in PS mode (a) and in AC-PS mode (b) inset is a typical image obtained after processing by ImageJ. The EDS spectrum recorded from the sample surface after zinc deposition in DC mode (23 nm anodic film) (c). Deposition dwell was 30 s.

As it has been mentioned in the introduction a strong interaction between the solution eutectic components and alumina interface was observed during deposition on anodic alumina in our previous work [2]. Additional AC component superimposed on constant DC potential makes the organic layer on the alumina/electrolyte interface less compact and more permeable to zinc chloride anions. The positive influence of this regime, such as growth of zinc reduction rate, for electrodeposition on the aluminium/alumina system was demonstrated. Identical study in this work was performed using a sinusoidal potential of 50 mV amplitude superimposed on the DC potential of -1.6 V at the 1 kHz frequency. Specimens with titania layers of 12, 18, 23, 43 and 84 nm were used. Typical SEM images of the electrode surface after 30 seconds of zinc deposition on the titanium electrode covered with 23 nm titania film is presented in Figure V. 6 b.

The particles size on the electrode after AC-PS mode deposition is bigger than on DC (PS) mode, but the number of the particles is less. The quantity of deposited zinc in both modes was estimated by the same way using ImageJ and it is 1.5 times less in potentiostatic mode than in the AC-PS regime. Thus, it can be concluded that there is a small influence of the AC component on the deposition process. Increase of the zinc amount was much smaller in comparison with the aluminium/alumina system where it was found an increase of 10 times at the same conditions [2]. The small difference observed can be explained by additional "electro stirring" on the AC-PS mode, i.e., transport of charged species due to the alternating electric field. The dense organic layer formed in the case of alumina/aluminium system might not exist in the case of titanium/titania.

FTIR measurements were carried out to confirm that this organic layer does not form. FTIR-ATR spectra of DES:Zn in contact with titanium electrodes covered by titania are presented in Figure V. 7. The respective spectrum of blank DES:Zn is shown for comparison. The observed bands in the DES:Zn spectra correlate well with the reference spectroscopic data for ethylene glycol and choline chloride. One can see that contact of DES:Zn with the electrode surface results in no shift of the characteristic bands. It differs from the case of alumina/DES interface where a O-H stretching shift around 135 cm^{-1} was found [2]. Thereby we anticipate that no chemical bonds were formed between the organic species and the titanium/titania electrode. Titanium/titania and aluminium/alumina systems despite chemical similarity demonstrated different properties in terms of interaction with DES.

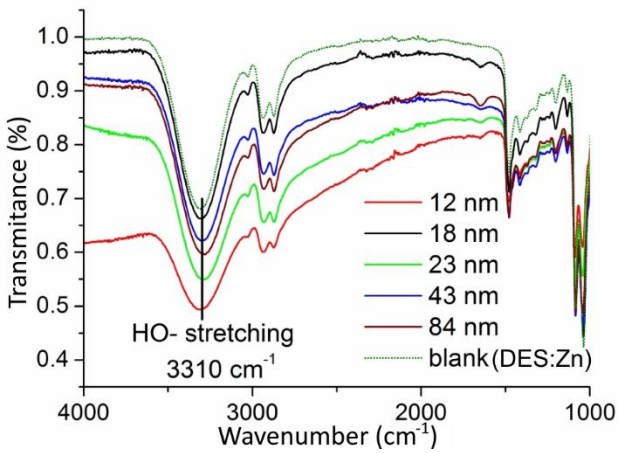

Figure V. 7 FTIR-ATR spectra of blank DES:Zn, and titanium covered with different thicknesses of anodic titania films in contact with DES:Zn.

Zinc nucleation mechanism

Electrodeposition of metals on an electrode with low chemical affinity to electrodeposited metal usually occurs with overvoltage and involves three-dimensional nucleation with hemispherical growth of the nuclei [47]. There are two limiting cases of three-dimensional nucleation: instantaneous and progressive. In the instantaneous model practically all nucleation sites are activated in a short time after potential is applied. Progressive model is the situation when the nucleation sites become activated during the experiment. In the description below, we use the expressions instantaneous and progressive models in the sense that it is closer to one or the other mechanism, although we are aware that these are limiting cases.

Deep understanding of the nucleation process and other processes, which occur in the beginning of the deposition, is extremely important since the initial stage of the process is crucial to the properties and structure of the deposited materials. For example, in the same titania matrix, inside and over the tubes is possible to obtain different structures such as nanowires, nanotubes, sandwich and coaxial multilayer structures.

The mechanism of nucleation and growth can be determined by graphical analysis of the current transients from chronoamperometric measurements. Such an approach has been commonly used in studies for metal nucleation on different substrates (Ge, Si, W, vitreous carbon, *etc*.) [36, 47-50]. Transition from instantaneous to progressive nucleation mechanism could occur with decrease of deposition overvoltage [51]. To detect the potential of this transition, current-time transients at different applied potentials were recorded on a titanium electrode covered with a 23 nm titania film (Figure V. 8 a). The transients are characterized by an initial increase of current followed by a drop at longer time. We believe, that the nucleation process matches to 3D mechanism due to the high deposition overpotential (about 100 mV) and is followed by diffusion-limited growth because of the transient shape [47]. The deposition transients acquired at different overvoltages were plotted in dimensionless form by normalizing the current (j) and time (t) respectively to the maximum current (j_{max}) and time (t_{max}) where the maximum current is reached, Figure V. 8 b.

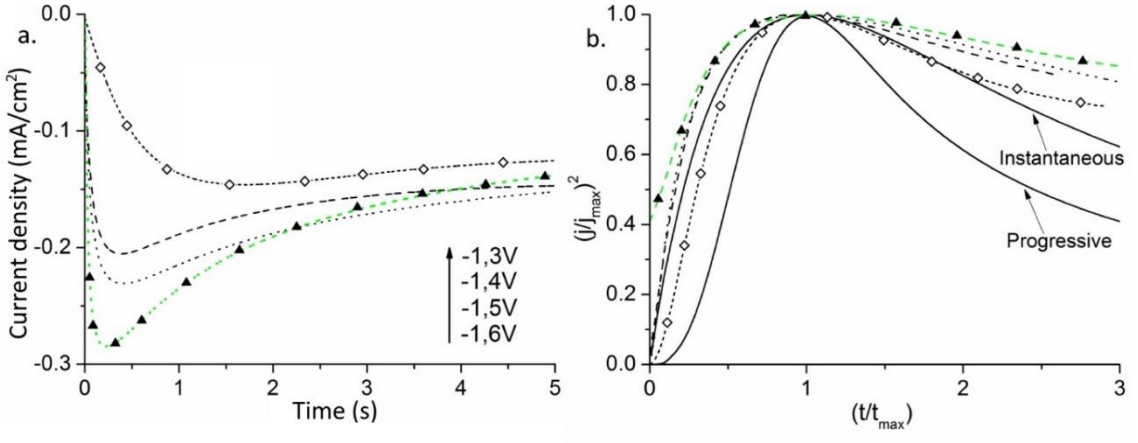

Figure V. 8 Current-time transients recorded at different potentials on a titanium electrode covered with 23 nm titania layer in DES:Zn (a) and the same transients replotted in dimensionless form (b).

According to literature [47, 48, 52] for instantaneous nucleation the theoretical transient is represented by:

$$\left(\frac{j}{j_{max}}\right)^2 = 1.9542\,\frac{t_{max}-t_0}{t-t_0}\left[1-exp\left(-1.2564\,\frac{t-t_0}{t_{max}-t_0}\right)\right]^2 \quad \text{(V.3)}$$

for progressive nucleation the theoretical transient is given by:

$$\left(\frac{j}{j_{max}}\right)^2 = 1.2254\,\frac{t_{max}-t_0}{t-t_0}\left[1-exp\left(-2.3367\,\frac{(t-t_0)^2}{(t_{max}-t_0)^2}\right)\right]^2 \quad \text{(V.4)}$$

where t_0 is the induction time, i.e. the time needed to form a nucleus larger than the critical nucleus size. The respective plots are also shown in Figure V. 8 b (solid lines). Electrocrystallization of zinc in the potential range from -1.4 to -1.6 V fits well the instantaneous mechanism. However, the curve recorded at more positive potential, -1.3 V, shifts towards to the progressive nucleation theoretical curve and it is situated between instantaneous and progressive theoretical curves. The mechanism determination at higher voltages (where it could be found better overlapping of the theoretical curve) is hindered because the peak maximum is not evident at potentials greater than -1.3 V.

Chronoamperometric curves in Figure V. 4 a were replotted in dimensionless form (Figure V. 4 b). The plot for the activated electrode is not in the figure since the maximum on current time transient is absent as already explained in previous section.

The theoretical plots are also shown in Figure V. 4 b. Comparing the theoretical plots for progressive and instantaneous nucleation with the experimental plots for zinc reduction, it can be concluded that Zn deposition onto titanium/titania electrode proceeds by instantaneous three-dimensional nucleation. The mechanism is independent of the titania thickness and denotes that practically all Zn nuclei on the electrode surface are formed at once and have the same size. These results correlate with the work of Abbott *et al.* [30] where they reported that the electrodeposition of electronegative metals such as aluminium and zinc in ionic liquids occurs by instantaneous nucleation mechanism irrespectively of the ions or substrate material. Deviation from the theoretical curves after $t_{max}>1$ is probably related to accessory processes such as hydrogen and dioxolanes formation [44, 45, 53]. This has been also reported for different deep eutectic solvents, as choline chloride and ethylene glycol DES [36]. Abbott *et al.* also demonstrated high mismatch between the experimental curves and the theoretical ones and explained it by specific adsorption of species on the electrode surface, apparently chloride ions [30]. In case of one side reaction, like hydrogen reduction, its contribution to the current could be mathematically extracted by using multiparametric model [54]. However, there is no unanimity in the origin and number of side reactions at low cathodic potentials in DES [36, 44, 45]. The impact of side reactions to overall current could be addressed in future studies.

The nucleation mechanism was additionally verified by AFM study. AFM measurements were performed on titanium electrode covered by 84 nm titania film at -1.6 V potential. Figure V. 9 shows AFM images of the electrode surface (area 5x5 μm) after different times of deposition. The blank surface before application of potential is shown in Figure V. 9 a. The surface is not perfectly flat, revealing big irregularities. After the initial 1.5 second of deposition formation of particles with sizes of *ca.* 85 nm on the electrode surface was observed (Figure V. 9 b). Increasing the deposition time results in gradual increase of particles sizes: 120 and 170 nm for deposition times of 4 and 9 seconds (Figure V. 9 c, d), respectively. Statistically insignificant variations in number of particles per unit surface area at the different deposition times indicate that nucleation rate is much lower than the growth rate, clearly pointing to instantaneous nucleation.

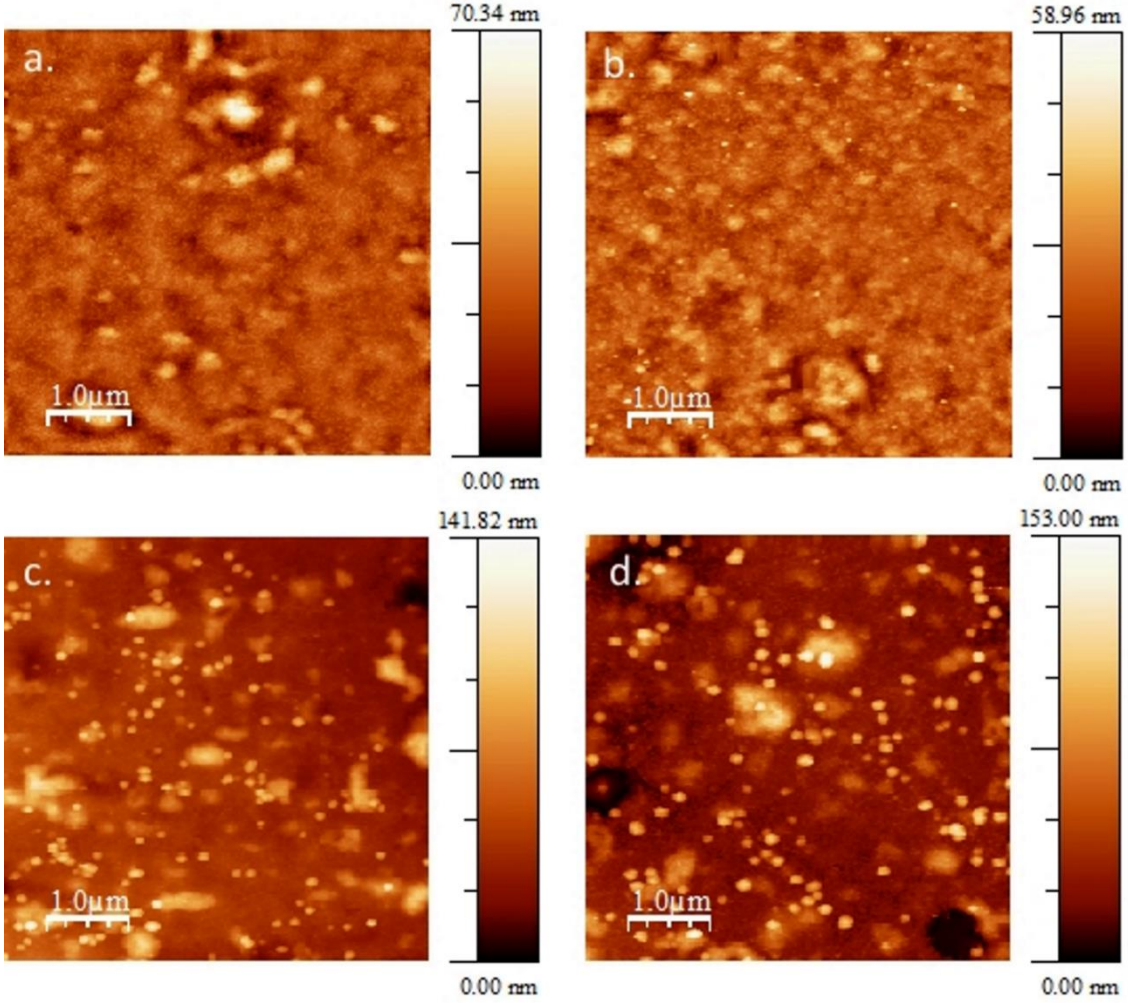

Figure V. 9 AFM images of titanium covered with 84 nm titania layer (a) and after zinc electrodeposition in DES:Zn at -1.6V: during 1.5 s (b); 4 s (c) and 9 s (d).

Conclusions

Electrodeposition of zinc from 0.3M $ZnCl_2$ solution in choline chloride/ethylene glycol eutectic solvent on titania barrier layer was successfully performed. Reduction of zinc species occurs much faster on thicker anodic films than on thinner ones. The chemical amount of reduced metallic zinc at -1.6 V during 30 seconds is 4 times higher on 84 nm thick films than on 12 nm ones. It happens because both film thickness and crystallinity grow with the anodization potential, the latter leading to higher oxide conductivity. Application of -1.6V DC potential, superimposed by an alternating sinusoidal component of 50 mV, leads to moderate increase of the amount of zinc reduced. Regarding this fact and additional FTIR results it is assumed that there is no

formation of a dense organic layer on titanium/titania electrode contrary to the aluminium/alumina system. Thus, zinc deposition becomes easier.

Electrodeposition of zinc at -1.6 V from DES occurs by the instantaneous three-dimensional nucleation mechanism and it is not influenced by the titania layer thickness. This result was confirmed by AFM studies. A trend for transition from instantaneous nucleation mechanism to progressive one seems to occur at deposition potential of -1.3 V.

Acknowledgements

The financial support of the European Commission and Portuguese Foundation for Science and Technology (FCT) in frame of the projects PIRSES-GA-2011-295273 – NANEL and PTDC/CTM-NAN/113570/2009, respectively, is gratefully acknowledged. The financial support of a Post-Doctoral grant (ref. SFRH/BPD/80754/2011) of the Portuguese Foundation for Science and Technology (FCT) and "Programa Operacional Capital Humano, comparticipado pelo Fundo Social Europeu e por fundos nacionais do MCTES" is greatly acknowledged by KY. M. Starykevich also thanks S.F.H.Correia (University of Aveiro) and A.Miranouskaya for helping with ellipsometry measurements and English revision correspondingly.

References:

[1] D. Kannadassan, R. Karthik, M. Shojaei Baghini, P.S. Mallick, Nanostructured metal–insulator–metal capacitor with anodic titania, *Materials Science in Semiconductor Processing,* 16 (2013) 274-281.
[2] M. Starykevich, A.N. Salak, D.K. Ivanou, A.D. Lisenkov, M.L. Zheludkevich, M.G.S. Ferreira, Electrochemical deposition of zinc from deep eutectic solvent on barrier alumina layers, *Electrochimica Acta,* 170 (2015) 284-291.
[3] J.L. Delplancke, R. Winand, Galvanostatic anodization of titanium—I. Structures and compositions of the anodic films, *Electrochimica Acta,* 33 (1988) 1539-1549.
[4] M. Kozlowski, W.H. Smyrl, L. Atanasoska, R. Atanasoski, Local film thickness and photoresponse of thin anodic TiO_2 films on polycrystalline titanium, *Electrochimica Acta,* 34 (1989) 1763-1768.
[5] T. Ohtsuka, M. Masuda, N. Sato, Ellipsometric Study of Anodic Oxide Films on Titanium in Hydrochloric Acid, Sulfuric Acid, and Phosphate Solution, *Journal of The Electrochemical Society,* 132 (1985) 787-792.
[6] S.K. Poznyak, A.D. Lisenkov, M.G.S. Ferreira, A.I. Kulak, M.L. Zheludkevich, Impedance behaviour of anodic TiO2 films prepared by galvanostatic anodisation and powerful pulsed discharge in electrolyte, *Electrochimica Acta,* 76 (2012) 453-461.
[7] M. Schneider, S. Schroth, J. Schilm, A. Michaelis, Micro-EIS of anodic thin oxide films on titanium for capacitor applications, *Electrochimica Acta,* 54 (2009) 2663-2671.
[8] J.W. Schultze, M.M. Lohrengel, Stability, reactivity and breakdown of passive films. Problems of recent and future research, *Electrochimica Acta,* 45 (2000) 2499-2513.
[9] T. Shibata, Y.C. Zhu, The effect of film formation conditions on the structure and composition of anodic oxide films on titanium, *Corrosion Science,* 37 (1995) 253-270.
[10] A.G. Mantzila, M.I. Prodromidis, Development and study of anodic Ti/TiO_2 electrodes and their potential use as impedimetric immunosensors, *Electrochimica Acta,* 51 (2006) 3537-3542.
[11] H. Habazaki, M. Uozumi, H. Konno, K. Shimizu, P. Skeldon, G.E. Thompson, Crystallization of anodic titania on titanium and its alloys, *Corrosion Science,* 45 (2003) 2063-2073.
[12] C. Jaeggi, P. Kern, J. Michler, T. Zehnder, H. Siegenthaler, Anodic thin films on titanium used as masks for surface micropatterning of biomedical devices, *Surface and Coatings Technology,* 200 (2005) 1913-1919.
[13] M.V. Diamanti, M.P. Pedeferri, Effect of anodic oxidation parameters on the titanium oxides formation, *Corrosion Science,* 49 (2007) 939-948.
[14] J.L. Delplancke, M. Sun, T.J. O'Keefe, R. Winand, Nucleation of electrodeposited copper on anodized titanium, *Hydrometallurgy,* 23 (1989) 47-66.
[15] H.K. Chang, B.-H. Choe, J.K. Lee, Influence of titanium oxide films on copper nucleation during electrodeposition, *Materials Science and Engineering: A,* 409 (2005) 317-328.

[16] M.V. Diamanti, M. Ormellese, E. Marin, A. Lanzutti, A. Mele, M.P. Pedeferri, Anodic titanium oxide as immobilized photocatalyst in UV or visible light devices, *Journal of Hazardous Materials*, 186 (2011) 2103-2109.
[17] M. Valden, X. Lai, D.W. Goodman, Onset of catalytic activity of gold clusters on titania with the appearance of nonmetallic properties, *Science*, 281 (1998) 1647-1650.
[18] R. Wang, K. Hashimoto, A. Fujishima, M. Chikuni, E. Kojima, A. Kitamura, M. Shimohigoshi, T. Watanabe, Light-induced amphiphilic surfaces, *Nature*, 388 (1997) 431-432.
[19] M. Gratzel, Photoelectrochemical cells, *Nature*, 414 (2001) 338-344.
[20] A.K. Sharma, Anodizing titanium for space applications, *Thin Solid Films*, 208 (1992) 48-54.
[21] T. Gandhi, K.S. Raja, M. Misra, Synthesis of ZnTe nanowires onto TiO_2 nanotubular arrays by pulse-reverse electrodeposition, *Thin Solid Films*, 517 (2009) 4527-4533.
[22] Y. Kang, J. Zhao, J. Tao, X. Wang, Y. Li, Electrochemical deposition of Co nanowire arrays into self-organized titania nanotubes, *Applied Surface Science*, 254 (2008) 3935-3938.
[23] J.M. Macak, B.G. Gong, M. Hueppe, P. Schmuki, Filling of TiO2 Nanotubes by Self-Doping and Electrodeposition, *Advanced Materials*, 19 (2007) 3027-3031.
[24] D.M. F. Endres, A. Abbott, *Electrodeposition from Ionic Liquids*, WILEY-VCH Verlag GmbH & Co. KGaA, Weinheim, 2008.
[25] E.L. Smith, A.P. Abbott, K.S. Ryder, Deep Eutectic Solvents (DESs) and Their Applications, *Chemical Reviews*, 114 (2014) 11060-11082.
[26] A.P. Abbott, Model for the Conductivity of Ionic Liquids Based on an Infinite Dilution of Holes, *ChemPhysChem*, 6 (2005) 2502-2505.
[27] A.P. Abbott, R.C. Harris, K.S. Ryder, Application of Hole Theory to Define Ionic Liquids by their Transport Properties, *The Journal of Physical Chemistry B*, 111 (2007) 4910-4913.
[28] A.P. Abbott, K.E. Ttaib, G. Frisch, K.S. Ryder, D. Weston, The electrodeposition of silver composites using deep eutectic solvents, *Physical Chemistry Chemical Physics*, 14 (2012) 2443-2449.
[29] S. Salomé, N.M. Pereira, E.S. Ferreira, C.M. Pereira, A.F. Silva, Tin electrodeposition from choline chloride based solvent: Influence of the hydrogen bond donors, *Journal of Electroanalytical Chemistry*, 703 (2013) 80-87.
[30] A.P. Abbott, J.C. Barron, G. Frisch, S. Gurman, K.S. Ryder, A. Fernando Silva, Double layer effects on metal nucleation in deep eutectic solvents, *Physical Chemistry Chemical Physics*, 13 (2011) 10224-10231.
[31] A.P. Abbott, J.C. Barron, G. Frisch, K.S. Ryder, A.F. Silva, The effect of additives on zinc electrodeposition from deep eutectic solvents, *Electrochimica Acta*, 56 (2011) 5272-5279.
[32] A. Bakkar, V. Neubert, Electrodeposition onto magnesium in air and water stable ionic liquids: From corrosion to successful plating, *Electrochemistry Communications*, 9 (2007) 2428-2435.
[33] N.M. Pereira, P.M.V. Fernandes, C.M. Pereira, A. Fernando Silva, Electrodeposition of Zinc from Choline Chloride-Ethylene Glycol Deep Eutectic Solvent: Effect of the Tartrate Ion, *Journal of The Electrochemical Society*, 159 (2012) D501-D506.
[34] A.H. Whitehead, M. Pölzler, B. Gollas, Zinc Electrodeposition from a Deep Eutectic System Containing Choline Chloride and Ethylene Glycol, *Journal of The Electrochemical Society*, 157 (2010) D328-D334.
[35] H. Yang, R.G. Reddy, Electrochemical deposition of zinc from zinc oxide in 2:1 urea/choline chloride ionic liquid, *Electrochimica Acta*, 147 (2014) 513-519.
[36] L. Vieira, R. Schennach, B. Gollas, The effect of the electrode material on the electrodeposition of zinc from deep eutectic solvents, *Electrochimica Acta*, 197 (2016) 344-352.
[37] A.P. Abbott, G. Capper, K.J. McKenzie, K.S. Ryder, Electrodeposition of zinc–tin alloys from deep eutectic solvents based on choline chloride, *Journal of Electroanalytical Chemistry*, 599 (2007) 288-294.
[38] H. Yang, R.G. Reddy, Electrochemical Kinetics of Reduction of Zinc Oxide to Zinc Using 2:1 Urea/ChCl Ionic Liquid, *Electrochimica Acta*, 178 (2015) 617-623.
[39] P.J. Dale, A.P. Samantilleke, D.D. Shivagan, L.M. Peter, Synthesis of cadmium and zinc semiconductor compounds from an ionic liquid containing choline chloride and urea, *Thin Solid Films*, 515 (2007) 5751-5754.
[40] S.F. Lamolle, M. Monjo, M. Rubert, H.J. Haugen, S.P. Lyngstadaas, J.E. Ellingsen, The effect of hydrofluoric acid treatment of titanium surface on nanostructural and chemical changes and the growth of MC3T3-E1 cells, *Biomaterials*, 30 (2009) 736-742.
[41] S. Szmukler-Moncler, M. Bischof, R. Nedir, M. Ermrich, Titanium hydride and hydrogen concentration in acid-etched commercially pure titanium and titanium alloy implants: a comparative analysis of five implant systems, *Clinical Oral Implants Research*, 21 (2010) 944-950.
[42] M. Fox, *Optical Properties of Solids*, OUP Oxford, 2010.

[43] V.R. Fernandes, C.M.S. Vicente, N. Wada, P.S. André, R.A.S. Ferreira, Multi-objective genetic algorithm applied to spectroscopic ellipsometry of organic-inorganic hybrid planar waveguides, *Optics Express*, 18 (2010) 16580-16586.
[44] K. Haerens, E. Matthijs, K. Binnemans, B. Van der Bruggen, Electrochemical decomposition of choline chloride based ionic liquid analogues, *Green Chemistry*, 11 (2009) 1357-1365.
[45] D. Yue, Y. Jia, Y. Yao, J. Sun, Y. Jing, Structure and electrochemical behavior of ionic liquid analogue based on choline chloride and urea, *Electrochimica Acta*, 65 (2012) 30-36.
[46] F.G. Cottrell, *Z. Phys. Chem.*, (1903) 385.
[47] E. Budevski, G. Staikov, W.J. Lorenz, *Frontmatter*, in: Electrochemical Phase Formation and Growth, Wiley-VCH Verlag GmbH, 2007.
[48] G. Gunawardena, G. Hills, I. Montenegro, B. Scharifker, Electrochemical nucleation: Part I. General considerations, *Journal of Electroanalytical Chemistry and Interfacial Electrochemistry*, 138 (1982) 225-239.
[49] M.-J. Deng, P.-C. Lin, J.-K. Chang, J.-M. Chen, K.-T. Lu, Electrochemistry of Zn(II)/Zn on Mg alloy from the N-butyl-N-methylpyrrolidinium dicyanamide ionic liquid, *Electrochimica Acta*, 56 (2011) 6071-6077.
[50] C. Ehlers, U. König, G. Staikov, J.W. Schultze, Role of surface states in electrodeposition of Pb on n-Ge(111), *Electrochimica Acta*, 47 (2001) 379-385.
[51] H.Y. Yang, X.W. Guo, X.B. Chen, S.H. Wang, G.H. Wu, W.J. Ding, N. Birbilis, On the electrodeposition of nickel–zinc alloys from a eutectic-based ionic liquid, *Electrochimica Acta*, 63 (2012) 131-138.
[52] B. Scharifker, G. Hills, Theoretical and experimental studies of multiple nucleation, *Electrochimica Acta*, 28 (1983) 879-889.
[53] M.Y. Abyaneh, M. Fleischmann, General Models for Surface Nucleation and Three-Dimensional Growth: the Effects of Concurrent Redox Reactions and of Diffusion, *Journal of The Electrochemical Society*, 138 (1991) 2491-2496.
[54] M. Palomar-Pardavé, B.R. Scharifker, E.M. Arce, M. Romero-Romo, Nucleation and diffusion-controlled growth of electroactive centers: Reduction of protons during cobalt electrodeposition, *Electrochimica Acta*, 50 (2005) 4736-4745.

Chapter VI

Modification of porous titania templates for uniform metal electrodeposition from deep eutectic solvent

---

Journal of The Electrochemical Society, **164** (6) D335-D341 (2017) D335
0013-4651/2017/164(6)/D335/7/$37.00 © The Electrochemical Society

Modification of Porous Titania Templates for Uniform Metal Electrodeposition from Deep Eutectic Solvent

M. Starykevich,[a,z] A. N. Salak,[a] M. L. Zheludkevich,[a,b] and M. G. S. Ferreira[a]

[a]*Department of Materials and Ceramic Engineering, CICECO-Aveiro Institute of Materials, University of Aveiro, 3810-193 Aveiro, Portugal*
[b]*Institute of Materials Research, Helmholtz-Zentrum Geesthacht, 21502 Geesthacht, Germany*

Abstract

Zinc electrochemical deposition in porous anodic titania from 0.5M $ZnCl_2$ solution in choline chloride based deep eutectic solvent is reported. Electroreduction is performed by a pulse method in titanium dioxide templates modified in three different ways. Titania nanotubes were formed in ethylene glycol based electrolyte with 0.38% (wt.) ammonium fluoride and 1.79% (wt.) of water. The first template has been used as-prepared, without any modification. Such a matrix shows a low fill-factor and zinc electrodeposition mainly occurs on the top of the tubes. The next template was annealed at 450^{o}C to complete crystallization of titania. It results in electrodeposition of zinc along the entire tube surface and consequently in formation of coaxial structure. The third template was modified based on selective crystallization of the pore bottoms using higher anodisation voltage (80 V) than the one used for tubes formation (40 V) in sulphuric acid electrolyte. The successful bottom-up filling of the titania nanotubes is demonstrated in this case. Investigation of the tubes filling is performed by a set of complementary techniques such as GDOES, SEM and TEM.

Keywords: Titanium dioxide, deep eutectic solvent, ionic liquids, electrodeposition, zinc, choline chloride.

Introduction

Recently, porous anodic films on valve metals such as aluminium [1], zirconium [2, 3], iron [4], titanium [3, 5] *etc*., attract great attention due to wide range of applications. One of the most important uses of the templates is electroformation of nanorods [6] and nanowires. The parameters of matrix such as length and diameter of the pores, wall thickness can be easily controlled [7] by composition of the anodisation solution [8-11], its temperature [12, 13] or the applied voltage [14, 15].

Titanium dioxide has semiconductive properties that advantageously differentiate it from many other porous anodic layers. Additionally, it reveals common porous anodic template characteristics such as high regularity, homogeneity of the layer *etc*. However, there is scant work on application of porous anodic titania (PAT) as a matrix for electropreparation of metallic or other conductive nanowires, when compared with a growing number of existing studies of the "sister material" porous alumina. Moreover, the majority of both templates studies was performed with detached oxide template

instead having them attached to the metal electrode [16-19]. The use of the detached template leads to increase of cost and time due to the additional step of substrate removal and evaporation of an electrical contact. There were several attempts to perform deposition directly in the pores without removing the original substrate. Macak *et al* [20] have reported increasing the conductivity of the bottom part of the tubes via proton intercalation ($Ti^{4+} + e^- + H^+ \rightleftarrows Ti^{3+}H^+$).

Porous titania template can be formed in a number of inorganic solutions containing sulphate [21], phosphate [10, 22], acetate [23] ions *etc*. or in organic solutions [5] which are based on glycerol [15], ethylene glycol *etc*. The presence of fluoride ions is mandatory for all these electrolytes, otherwise a dense oxide layer will form instead of a porous one. In the current work we have used ethylene glycol based electrolyte for formation of the pores with several micrometres length and with very smooth walls.

Electrodeposition of active metals from water based solutions is difficult or even impossible. Ionic liquids are promising electrolytes in this area, because they demonstrate unique properties such as wide electrochemical window, high thermal stability, conductivity, negligible vapour pressure, *etc* [24]. High price and water sensitivity are the biggest disadvantages of classical ionic liquids. Deep eutectic solvents [25] (DES) are a cheap alternative to common ionic liquids with similar physicochemical properties. DES are non-toxic, water-/air- stable and also have good potential to be scaled up to industrial level [25]. Choline chloride based DES is one of the alternative green solvents. Several groups have studied in detail the properties of the choline chloride DES. Abbott et al. has studied viscosity and conductivity [26, 27] and influence of different hydrogen bond donors [28, 29]. Moreover, electrodeposition of different metals such as zinc [30-36], tin [37], silver [38] and alloys [39] is under intensive investigation.

In our previous works we have studied zinc electrodeposition from choline chloride (ChCl):ethylene glycol (EG) DES on bulk anodic titania [40]. It was found that electrodeposition on a thick titanium dioxide layer occurred faster than on a thin film. Taking into account previous studies [41] it was suggested that crystallinity of the films formed at higher anodising voltage (and correspondingly thicker ones) is better.

The main aim of present work is the investigation of direct electrodeposition of metallic nanorods from deep eutectic solvent into porous anodic titania templates directly on the titanium substrate. Until now, there is no report on successful electrodeposition of zinc in PAT template. Zinc was chosen as a model metal to be electrodeposited because it is an attractive metal due to further possibilities to be oxidized leading to semiconductor

materials such a zinc oxide, zinc sulphide, zinc selenide, etc. Moreover, the similar approach can be used for electrodeposition of other metals.

Experimental

Materials

Titanium foil of 1 mm thick (99.2%, Alfa Aesar), Nitric acid (68-70%, Alfa Aesar), Hydrofluoric acid (48-51%, Alfa Aesar), Ammonium fluoride (Puriss p.a. Sigma-Aldrich) Ethylene glycol (99.8% anhydrous, Sigma-Aldrich), Choline chloride (>98%, Sigma), Ethanol (absolute anhydrous), Zinc chloride (98+%, Alfa Aesar), Sulphuric acid (95-98%, Alfa Aesar) were used as received. Deionized water was used as solvent.

Procedures

Coupons of titanium foil (100×5×1 mm) were used as electrode material for sample preparation. The coupons were consequently rinsed with acetone, ethanol, and distilled water and then they were dried in air. Before anodization, the electrodes were chemically polished in a HF:HNO_3 mixture (1:3 by volume) to mirror finish and finally were rinsed with deionized water. A part of their surface was isolated with chemically resistant varnish, giving defined electrode working area of about 1 cm^2.

A Keithley 237 High Voltage Source-Measure Unit was used as a current source for the sample anodizing. Ethylene glycol solution with 0.38% (wt.) ammonium fluoride and 1.79% (wt.) of water was used as electrolyte [42]. The anodization was performed in a potentiostatic mode with an applied voltage of 40 V applied for 1 hour. The counter electrode was a platinum foil. Anodization was carried out in two steps with intermediate removal of the oxide. The voltage and the electrolyte were the same for both steps and duration of the second step was 30 minutes. Removal of the anodic layer after the first step was done by ultra sonication in the distilled water during 5 minutes. After anodization the electrodes were washed in ethanol and stored in a desiccator for stabilization of the titania layer during 24 hours. Mechanism of pore formation allows preparation of highly-ordered template using the two-step technique [43].

The crystallization was performed in a furnace at 450^{o}C for 5 hours with 2^{o}C/min heating and cooling ramps.

Preparation of DES electrolytes and the electrodeposition experiments were carried out in contact with air. The eutectic system was prepared by mixing choline chloride (ChCl) and ethylene glycol (EG) in the molar ratio of 1:2. Anhydrous zinc chloride was added to the DES to obtain a 0.5 M solution, which was heated and kept at 60°C under vacuum for 24 hours. The as-prepared solution (hereafter DES:Zn) was either directly used for electrodeposition or was stored in desiccator over P_2O_5.

Electrodeposition was performed using a Bio-Logic SAS SP-300 potentiostat. All measurements were done in a Faraday cage. A three-electrode cell consisting of a platinum wire as a reference electrode, graphite rod as a counter electrode and titanium template as a working electrode was used in the experiments. All electrodes after deposition were rinsed in distilled water and then were stored in deionized water for several hours for physically adsorbed zinc species removal.

Investigation of the electrode surface morphology and elemental analysis was performed using a Hitachi SU-70 scanning electron microscope (SEM) coupled with an energy dispersive spectroscope (EDS). A Hitachi 9100 transmission electron microscope (TEM) with acceleration voltage 300kV was also used for the analysis.

The thickness of the layers was estimated by Glow Discharge Optical Emission Spectroscopy (GDOES). GDOES depth profile analysis of the coatings was done using a HORIBA GD-Profiler 2 with a copper anode of 4 mm in diameter. Argon sputtering of the sample surface occurred at a pressure of 650 Pa and power of 30 W. Plasma polishing was performed at a pressure of 900 Pa and power of 10 W. About 1 µm of the porous template have been removed during plasma polishing.

Results and discussion

Typical SEM image of porous anodic titania template after anodisation at the conditions indicated in *Experimental* is presented in Figure VI. 1a. An uniform porous layer is self-aligned and well-ordered forming tapered tubes array, wider at the top [44, 45]. It is also evident that the pores are open on the top. Diameter of the pores and wall thickness on the interface after 0.5 hour of anodisation are about 70 and 30 nm respectively. The thickness of the porous layer is in the range of 3-3.5 µm as shown in Figure VI. 1b. The tubes have a smooth wall morphology typical for the anodic layers grown in organic electrolytes [46]. Qualitative GDOES profile of the tubes is presented in Figure VI. 1c. There are two regions which belong to porous titania layer and titanium

substrate. After initiating sputtering the titanium and oxygen signals reach a plateau which corresponds to the porous titania part. The second region with the maximal titanium signal intensity and oxygen background level has been reached at the end of sputtering. It corresponds to metallic titanium (substrate) sputtering. The porous film has homogeneous composition along the entire length of the tubes.

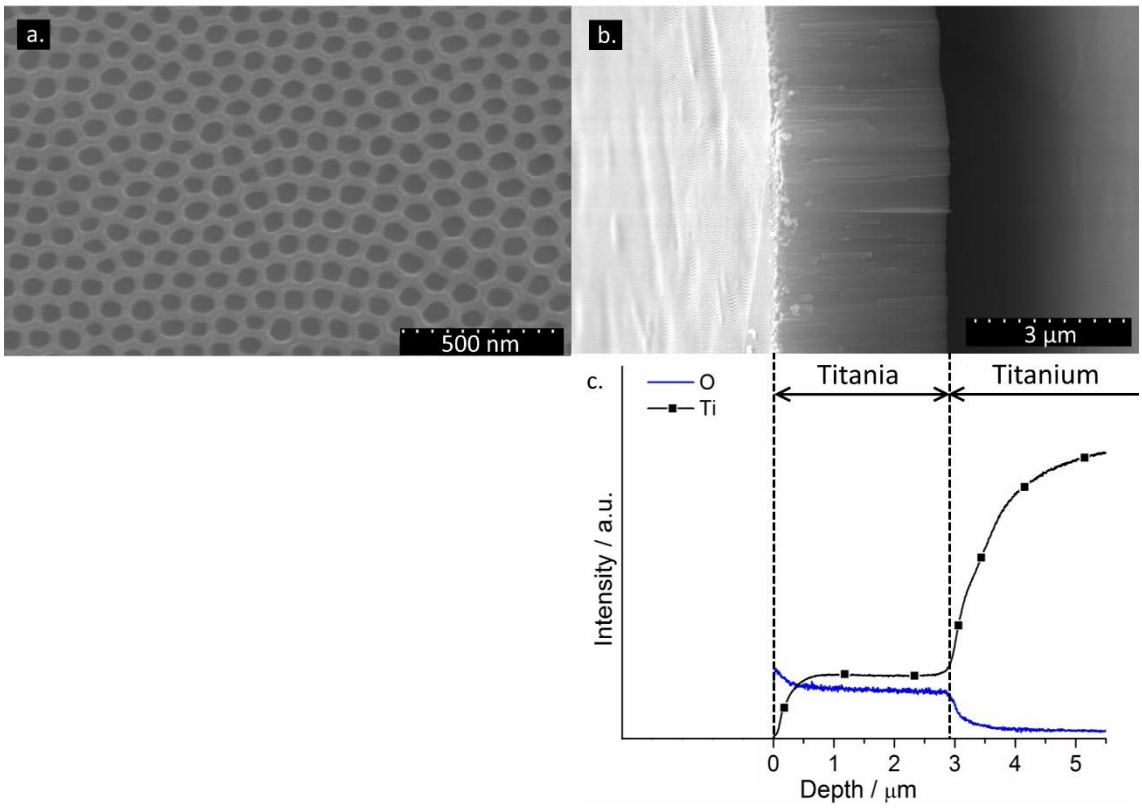

Figure VI. 1 SEM images of the titanium electrode surface (a), cross-section (b) and qualitative GDOES profile (c) obtained on electrode after 30 min of anodisation in ethylene glycol ammonium fluoride solution at 40V.

Figure VI. 2 TEM image of the porous titania layer with the barrier film on the bottom which was formed during anodization. It can be seen that the pores are closed by titania from the bottom. This compact layer on the pore bottom is named in literature barrier layer and its formation is typical for valve metals such as tungsten, aluminium *etc* [47]. In contrast to the majority of other barrier layers titanium dioxide is a semiconductor. Comparatively the high conductivity of the titania barrier layer facilitates the filling of the porous template. On the other hand, conductivity of the titanium dioxide is also a weakness of this template, because the deposition can occur not only on the bottom but also on the pore walls and on the electrode surface. The Zn electrodeposition

experiments were performed using the titania templates described above. Electrical parameters such as current profile and current distribution affect the quantity of reduced zinc at the interface and the uniformity of the deposition process. Optimal results were obtained with a pulsed technique at a current density of 100 mA/cm^2 (current applied in one step). Cathodic and anodic rectangular pulses with a dwell time of 10 μs and 2 μs, respectively, and the same absolute value of current density were applied sequentially. One cycle was applied every second. Anodic current is needed to remove metallic zinc from the electrode interface and opens access to the fresh electrolyte inside the pores. Moreover, a positive potential promotes electromigration of negatively charged zinc species ($ZnCl_3^-$, $Zn_2Cl_5^-$ [32, 39]) inside the tubes. Enrichment of the electrolyte in zinc species also occurs during intervals between the pulses. The relatively long waiting time between the pulses was chosen to allow partial relaxation of the system taking into account the length of the pores and high viscosity of the electrolyte.

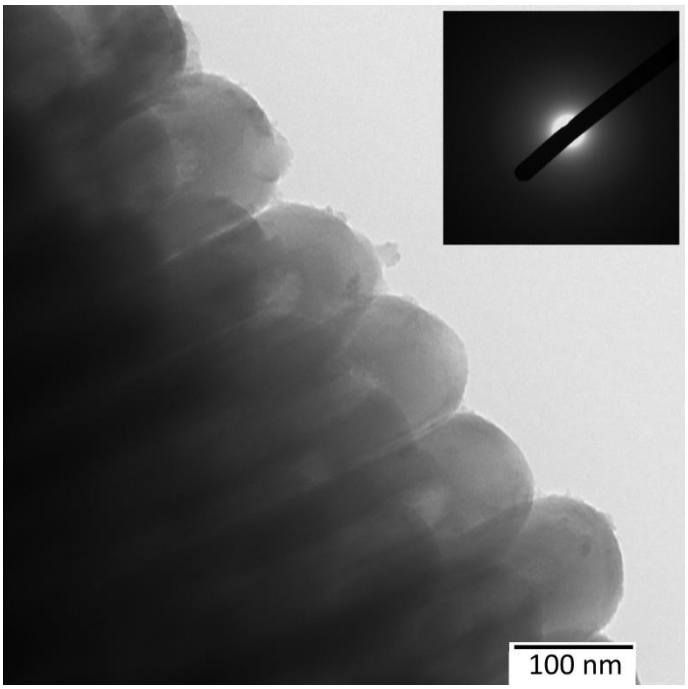

Figure VI. 2 TEM image of as-prepared titanium dioxide tube, the inset shows selected area electron diffraction pattern.

Electrodeposition in as-prepared PAT

The inset in Figure VI. 2 presents an electron diffraction image of as-prepared titanium dioxide tubes. Diffuse ring without separate reflections suggests that the as-

prepared porous titania layer is amorphous. The conductivity of the amorphous titania is lower than conductivity of the crystalline titania. This causes difficulties during deposition, but even so in this condition electroreduction occurs.

In this work the filling of the pores along their length was controlled by GDOES technique. The elemental depth profile of the sample obtained after one hour of deposition in as-prepared template is presented in Figure VI. 3a. The position of the interface between the porous titania and substrate was assessed through Ti profile. After initiating sputtering the titanium signal reaches a plateau which corresponds to porous titania part. The maximum of the intensity has been reached in the end of sputtering that corresponds to metallic titanium (substrate). Zinc signal has very high intensity in the beginning of the electrode sputtering, but it is followed by a sharp decrease. It is evident that the zinc layer was formed mainly on the top of the pores with only minor penetration into pores. The zinc signal goes down to the background at the titania/titanium interface that means almost no zinc deposition occurs at the pores bottom.

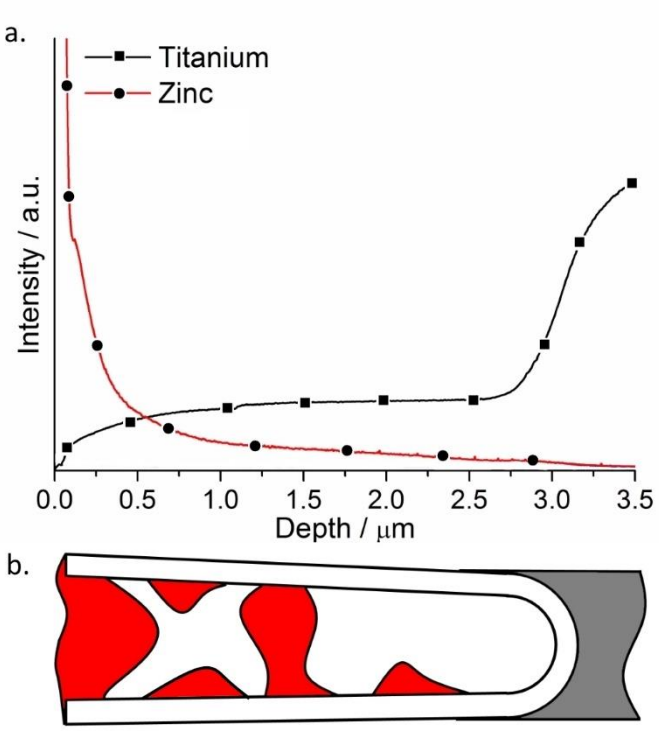

Figure VI. 3 Qualitative depth profile of a porous titanium oxide measured by GDOES after zinc deposition during 1 h (a) and schematic representation of the pores filling (b).

This result was confirmed by the electron microscopy as well. Figure VI. 4a depicts a top view of the porous template after 1 hour of deposition. The upper part of the template (around 1 µm here and after) was removed by soft plasma polishing using the GDOES equipment. The pores fill-factor (ratio between the numbers of filled pores to the total number) at this depth is very low, about 5-10%, and decreases closer to the bottom (GDOES results). Additional STEM investigation (Figure VI. 4b) demonstrates that the pores, besides being covered by the zinc layer on the top, are also sealed in random places as it is schematically demonstrated in Figure VI. 3b. Sealing the pores at the middle blocks the access of fresh electrolyte and impairs their filling. Changing the electrodeposition parameters does not solve this issue. Therefore, the next step was to modify the template in order to improve the electrodeposition inside the pores.

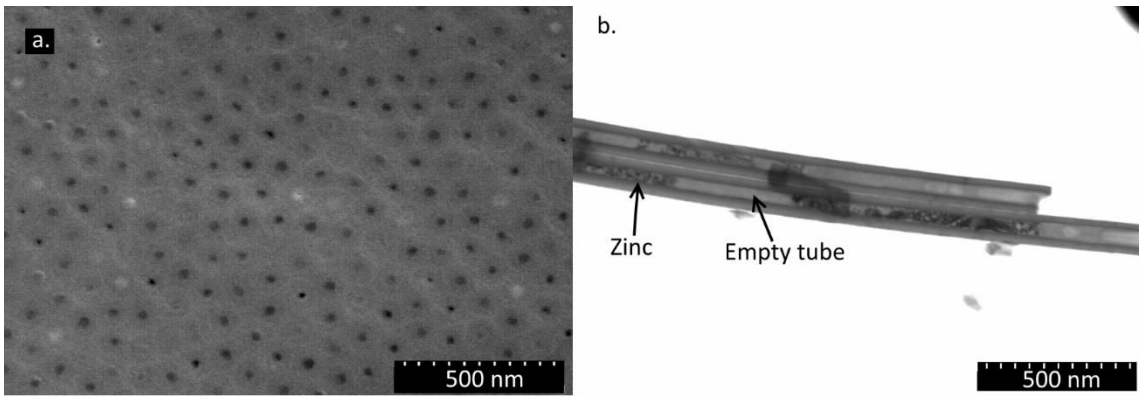

Figure VI. 4 SEM (after plasma polishing) (a) and STEM (b) micrographs obtained after electrodeposition in as-prepared template for 1 h.

Electrodeposition in annealed PAT

Increase of the conductivity of the porous titania template achieved via annealing in air at 450^{o}C. In these conditions the amorphous titania converts into anatase phase that leading to increase of electrical conductivity and, as a result, to more uniform electrodeposition along the whole pore surface. Figure VI. 5 depicts TEM micrograph of porous titania film after annealing. Electron diffraction pattern (insert in Figure VI. 5) demonstrates discrete rings with bright spots and it indicates the anatase crystalline structure.

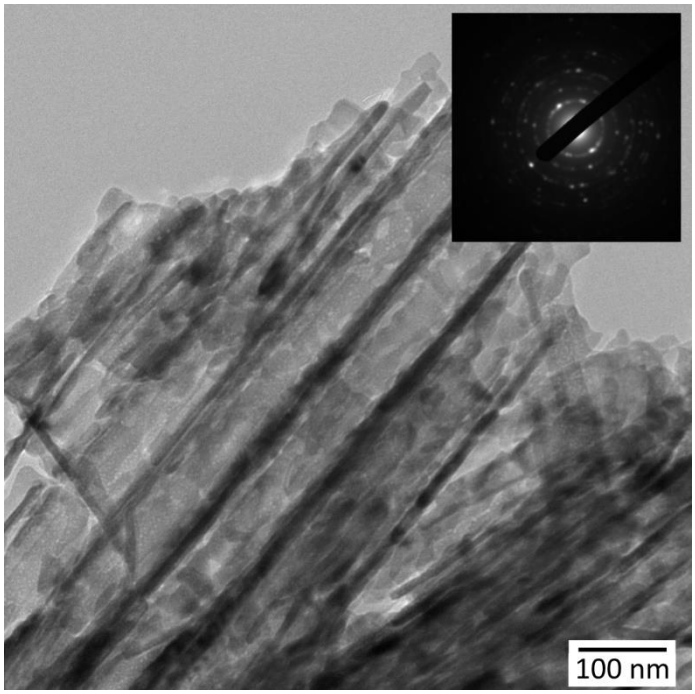

Figure VI. 5 TEM image of annealed titanium dioxide tube, the inset shows selected area electron diffraction pattern.

Electrodeposition of zinc was performed at the same conditions as those applied in the as-prepared template. GDOES profile for such sample is presented in Figure VI. 6a. Only one titanium profile is shown because of similarity of templates. With the help of this profile the transition from anodic titania to titanium has been demonstrated. The depth profiles for Zn is also presented for two different electrodeposition times, namely 1 hour and 10 minutes. The zinc signal after one hour of deposition in annealed template has a peak in the beginning of sputtering, and then it decreases and reaches a plateau followed by a second decrease until the background level at the titania/titanium interface. The template can be divided in three main zones according to the shape of the zinc signal curve. The first zone, in the beginning of sputtering, is the electrode surface and it has a high zinc signal because of a deposit formed on the electrode surface. The middle part of the template (zone II) shows a plateau which means that pores are successfully and homogeneously filled along the length. Then, near the interface between the anodic film and substrate (zone III), a small zinc peak appears and it can be explained by the presence of empty space next to the bottom as schematically shown in Figure VI. 6b. This irregularity forms due to strong diffusion limitation, which originates concentration gradient of zinc species and consequently results in different zinc deposition rate along the length of pores. The faster deposition rate on the wall surface at the pore opening

leads to the situation that after a certain time the pore fully closes leaving a void with entrapped electrolyte closer to the pore bottom. High homogeneity (geometrical shape and distribution) of the tubes ensures sealing of the pores mainly at specific depth depending on solution concentration, pore length and diameter. A noteworthy detail is that regular sealing (at the same distance from the surface) is only possible if growth occurs through the whole length of the tube simultaneously, otherwise the pores close randomly as it was shown for the as-prepared templates.

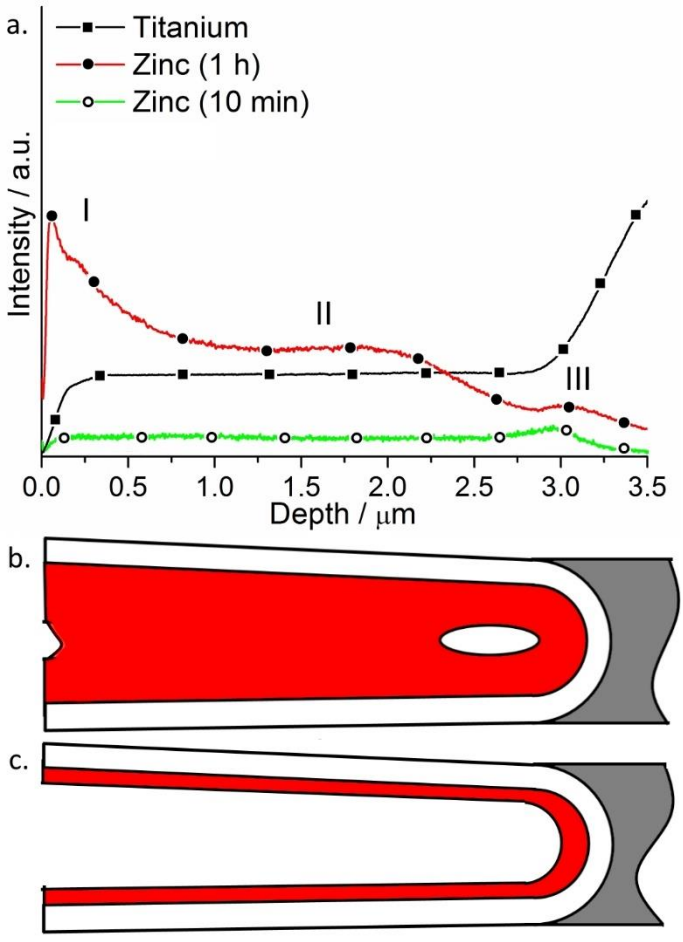

Figure VI. 6 Qualitative depth profile of a porous titanium oxide measured by GDOES after zinc deposition during 10 min and 1 h (a) and schematic representation of the pores filling after 1 h (b) and 10 min (c) of deposition.

Analysing the depth profiles after shorter deposition times can provide important information on the kinetics of pore filling. The profile after 10 minutes was chosen since this time ensures a detectable signal, but at the same time the sealing doesn't occur yet (green curve in Figure VI. 6a). The zinc signal reaches a plateau at the beginning of

sputtering and remains at the same level until pore bottoms are reached. It is reasonable to suggest that, in this zone, the walls of the pores are homogeneously covered with a thin layer of zinc as schematically represented in Figure VI. 6c. The peak on the zinc signal appears near the titania/titanium interface presumably because the higher quantity of zinc deposited in this plane.

In support of GDOES results, SEM studies were also performed. Figure VI. 7 demonstrates templates surfaces after 1 hour and after 10 minutes of deposition (GDOES polishing was also carried out). Zinc nanowires inside the template are clearly seen after 1 hour of deposition (Figure VI. 7a). The fill-factor at this plane is near 90% which is much higher than in the as-prepared templates. The SEM image after a short-time deposition indicates formation of zinc precipitates on the tubes walls (Figure VI. 7b).

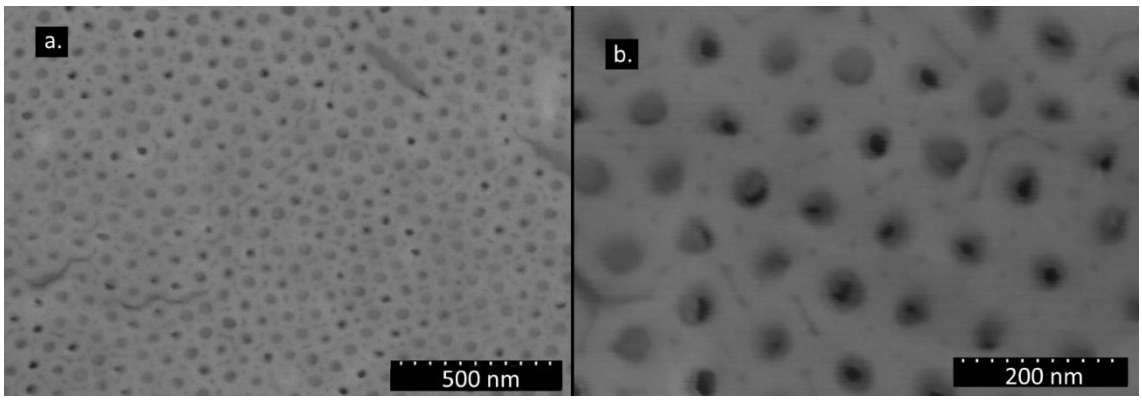

Figure VI. 7 SEM (after plasma polishing) micrographs obtained after electrodeposition in annealed template for 1 h (a) and 10 min (b).

Based on both GDOES measurements (1 hour and 10 minutes) and SEM results we suggest that zinc deposition occurs simultaneously on the whole titania surface and in the beginning of growth zinc forms coaxial tubes (titania outer layer and zinc inner). Longer deposition leads to sealing the tubes and filling of the template from these seals until interface (Figure VI. 6b).

Electrodeposition in PAT after bottom crystallization.

As it was shown above, electrodeposition in the as-prepared and in the annealed templates occurs on the whole tube length. Based on this result one can assume that bottom-up filling of the tubes requires higher conductivity of the bottom of the pores compared to the walls. One of the ways to create different conductivity is selective

crystallisation. Fortunately, during the pores preparation process, current passes mostly through the bottom of the tubes [45]. It makes possible a selective electrochemical modification of pore bottom without strong effect on the walls.

Influence of the anodisation parameters on crystallinity of the titania was demonstrated by Shibata, Zhu [41] and Xing *et al.* [48]. The authors showed that dense anodic titania films prepared at higher anodisation voltage [41] and at longer anodisation time [48] had better crystallinity. Additionally, it was shown in our recent paper [40] that zinc electrodeposition rate raises with increasing the titania barrier layer thickness. At the same time, the thickness of the anodic barrier layer depends on the oxidation voltage and becomes bigger at higher potential. Therefore, an additional anodisation step was applied to the as-prepared template. The treatment of the prepared template was done in a 1M sulphuric acid in two steps. The solution and procedure of anodisation were the same as those used in our previous work where the compact anodic titania films were studied [40]. The first step was performed in galvanostatic mode at 10 mA/cm^2. The second step took place in potentiostatic mode at 80 V during 2.5 hours. Galvanostatic mode was changed to potentiostatic one when the potential reached 80 V. The anodisation voltage at this process is two times higher than template formation voltage (40 V) that, together with long oxidation time, results in thicker and better crystallized barrier layer in comparison with that in the as-prepared template.

Effect of such an additional anodisation on the template structure was analysed by TEM. Regular porous structure with relatively thick barrier layer on the bottom (compared to the as-prepared template, Figure VI. 2) is seen in Figure VI. 8a. Moreover, the selected area electron diffraction shows significant difference in crystallinity of the anodic titania at walls and barrier parts. The diffraction pattern of walls does not represent separate reflections indicating that the material is amorphous (Figure VI. 8b). Nevertheless, at the diffraction pattern from the barrier layer shows rings, which confirm the polycrystalline structure of this area (Figure VI. 8c). The reflections are not sharp due to very small size of the crystallites.

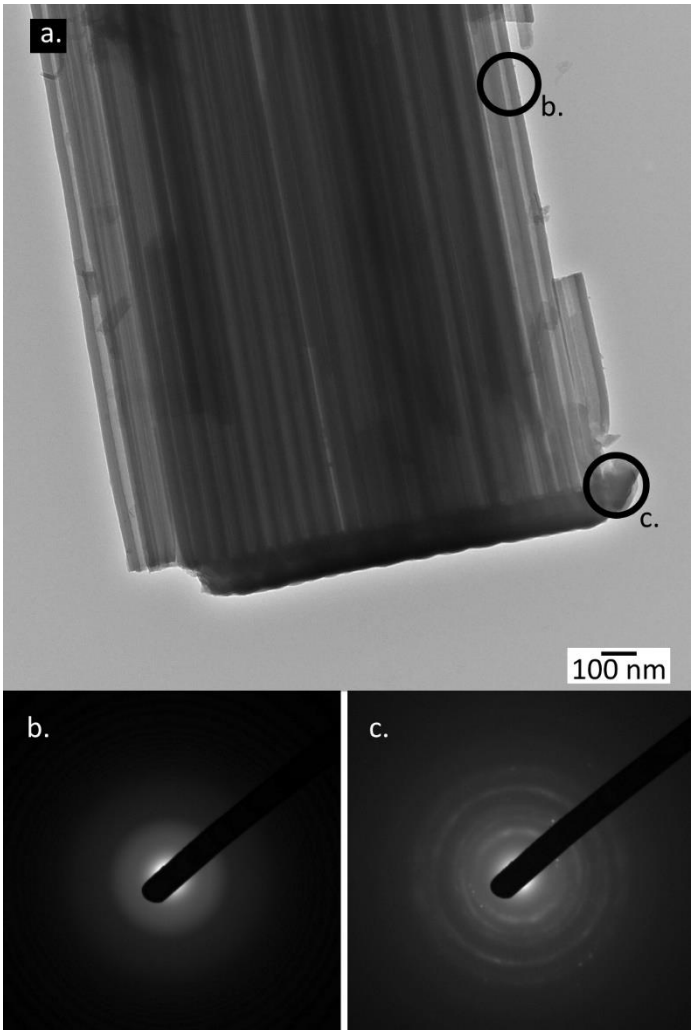

Figure VI. 8 TEM image of titanium dioxide tube after bottom crystallization (a), selected area electron diffraction pattern of the walls (b) and bottom part (c).

Zinc deposition in the template after crystallisation of the barrier layer was performed at the same condition as in two cases described above. The GDOES results obtained on this specimen are presented in Figure VI. 9. Zinc signal after 1 hour of deposition has a high intensity in the beginning of sputtering, afterward the intensity slowly decreases until the template bottom is reached. The amount of zinc is comparatively high along the whole length of titania pores, and in this way the filling of the pores had to start from the bottom. A gradual decrease of the zinc signal happens because the template is imperfect. Although reduction occurs mainly on the bottom part there is also some deposition simultaneously on the walls (although in a far less degree than in the case of the as-prepared template).

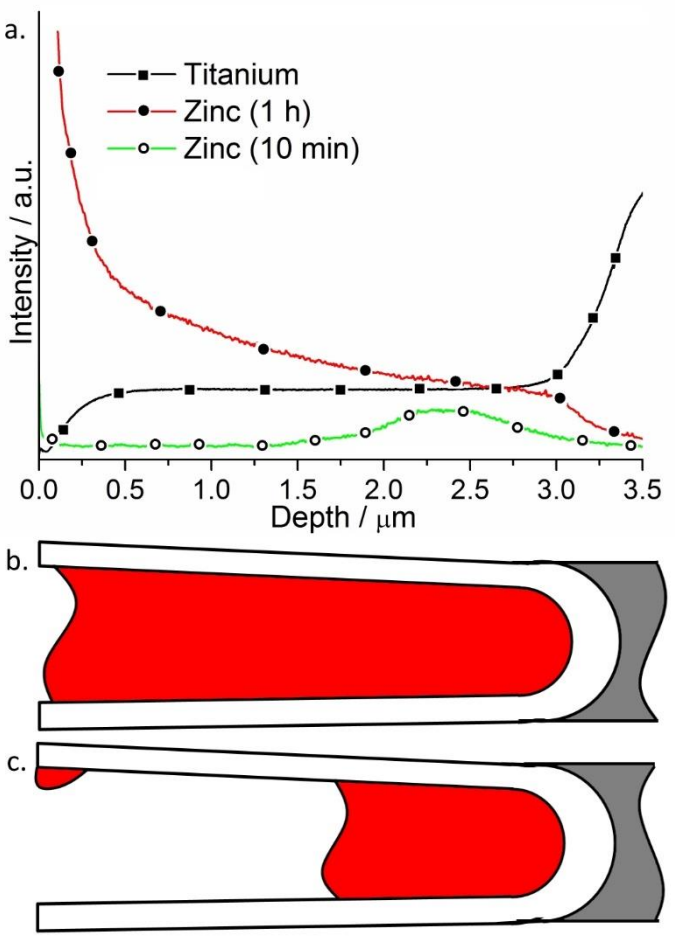

Figure VI. 9 Qualitative depth profile of a porous titanium oxide measured by GDOES after zinc deposition during 10 min and 1 h (a) and schematic representation of the pores filling after 1 h (b) and 10 min (c) of deposition.

An additional proof of the suggested mechanism of pore filling can be obtained after analysis of the electrode prepared after 10 minutes of deposition (Figure VI. 9a, green line). Zinc signal has a peak close to the bottom and almost background signal in the beginning of sputtering. This difference of the zinc signal is explained by a small amount of zinc which was deposited at different parts of the tubes. Filling of the tubes after 1 hour and after 10 minutes of deposition are presented schematically in Figure VI. 9b and c correspondingly.

It is evident from SEM image and agrees with GDOES results that most of the pores are filled by secondary material (Figure VI. 10a). Besides, the fill-factor is about 90% that is much higher than that in the case of the as-prepared template. The STEM image presented in Figure VI. 10b demonstrates homogeneous pores filling. EDX spectrum shows four elements (Figure VI. 10c): titanium, oxygen, zinc and copper

indicating that porous anodic titania (Ti, O) was successfully filled by zinc as a secondary material. The copper signal comes from a TEM grid.

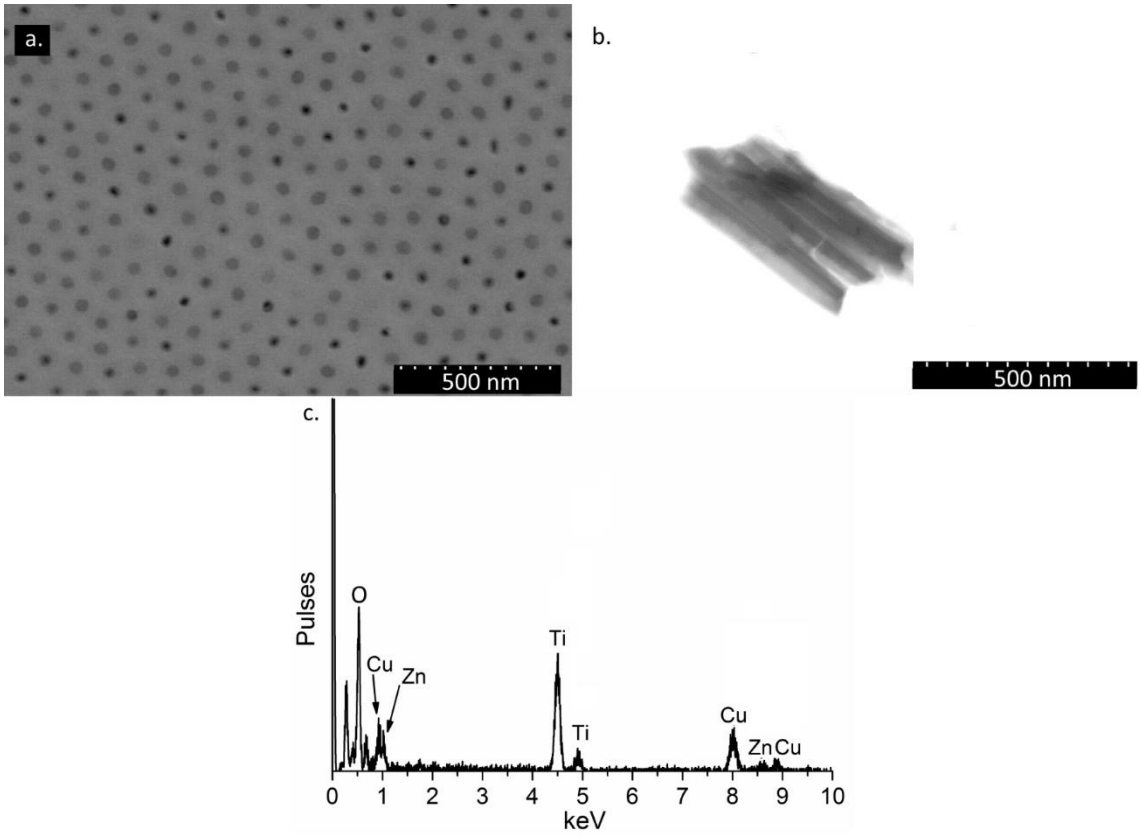

Figure VI. 10 SEM (after plasma polishing) (a) and STEM (b) micrographs obtained after electrodeposition in template after bottom crystallization for 1 h. The EDS spectrum recorded after zinc deposition (c).

Conclusions

Electrodeposition of zinc from a 0.5M $ZnCl_2$ solution in choline chloride/ethylene glycol eutectic solvent in porous anodic titania templates was successfully performed using pulse technique. It was demonstrated that electrodeposition in the as-prepared template occurs in random places without regular pore filling. Annealing of the template at 450^{o}C converts amorphous titania of the as-prepared template to anatase. It improves conductivity of the template along the full length of the pores and allows regular deposition over the whole pore surface. Successful bottom up filling was performed in the template with additional electrocrystallization of the barrier layer.

Acknowledgements

The financial support of the European Commission and Portuguese Foundation for Science and Technology (FCT) in frame of the projects PIRSES-GA-2011-295273 – NANEL and PTDC/CTM-NAN/113570/2009, respectively, is gratefully acknowledged. M. Starykevich also thanks prof. Patrik Schmuki and Nhat Truong Nguyen (University of Erlangen-Nuremberg) for advising on TEM samples preparation.

References

[1] R.C. Furneaux, W.R. Rigby, A.P. Davidson, The formation of controlled-porosity membranes from anodically oxidized aluminium, *Nature*, 337 (1989) 147-149.
[2] S. Berger, F. Jakubka, P. Schmuki, Formation of hexagonally ordered nanoporous anodic zirconia, *Electrochemistry Communications*, 10 (2008) 1916-1919.
[3] H. Tsuchiya, J.M. Macak, A. Ghicov, L. Taveira, P. Schmuki, Self-organized porous TiO_2 and ZrO_2 produced by anodization, *Corrosion Science*, 47 (2005) 3324-3335.
[4] E.P. Haripriya, K.V. Oomman, P. Maggie, K.M. Gopal, A.G. Craig, Synthesis and photoelectrochemical properties of nanoporous iron (III) oxide by potentiostatic anodization, *Nanotechnology*, 17 (2006) 4285.
[5] J.M. Macak, P. Schmuki, Anodic growth of self-organized anodic TiO_2 nanotubes in viscous electrolytes, *Electrochimica Acta*, 52 (2006) 1258-1264.
[6] M. Starykevich, A.D. Lisenkov, A.N. Salak, M.G.S. Ferreira, M.L. Zheludkevich, Electrodeposition of Zinc Nanorods from Ionic Liquid into Porous Anodic Alumina, *ChemElectroChem*, 1 (2014) 1484-1487.
[7] D. Kim, F. Schmidt-Stein, R. Hahn, P. Schmuki, Gravity assisted growth of self-organized anodic oxide nanotubes on titanium, *Electrochemistry Communications*, 10 (2008) 1082-1086.
[8] L. Zaraska, G.D. Sulka, M. Jaskuła, Anodic alumina membranes with defined pore diameters and thicknesses obtained by adjusting the anodizing duration and pore opening/widening time, *Journal of Solid State Electrochemistry*, 15 (2011) 2427-2436.
[9] A. Elsanousi, J. Zhang, H.M.H. Fadlalla, F. Zhang, H. Wang, X. Ding, Z. Huang, C. Tang, Self-organized TiO_2 nanotubes with controlled dimensions by anodic oxidation, *Journal of Materials Science*, 43 (2008) 7219-7224.
[10] A. Ghicov, H. Tsuchiya, J.M. Macak, P. Schmuki, Titanium oxide nanotubes prepared in phosphate electrolytes, *Electrochemistry Communications*, 7 (2005) 505-509.
[11] S.Z. Chu, K. Wada, S. Inoue, M. Isogai, Y. Katsuta, A. Yasumori, Large-Scale Fabrication of Ordered Nanoporous Alumina Films with Arbitrary Pore Intervals by Critical-Potential Anodization, *Journal of The Electrochemical Society*, 153 (2006) B384-B391.
[12] T. Aerts, T. Dimogerontakis, I. De Graeve, J. Fransaer, H. Terryn, Influence of the anodizing temperature on the porosity and the mechanical properties of the porous anodic oxide film, *Surface and Coatings Technology*, 201 (2007) 7310-7317.
[13] T. Ruff, R. Hahn, P. Schmuki, From anodic TiO_2 nanotubes to hexagonally ordered TiO_2 nanocolumns, *Applied Surface Science*, 257 (2011) 8177-8181.
[14] Y. Ji, K.-C. Lin, H. Zheng, J.-j. Zhu, A.C.S. Samia, Fabrication of double-walled TiO_2 nanotubes with bamboo morphology via one-step alternating voltage anodization, *Electrochemistry Communications*, 13 (2011) 1013-1015.
[15] J.M. Macak, H. Hildebrand, U. Marten-Jahns, P. Schmuki, Mechanistic aspects and growth of large diameter self-organized TiO_2 nanotubes, *Journal of Electroanalytical Chemistry*, 621 (2008) 254-266.
[16] D. Fang, K. Huang, S. Liu, D. Qin, High density copper nanowire arrays deposition inside ordered titania pores by electrodeposition, *Electrochemistry Communications*, 11 (2009) 901-904.
[17] R. Chen, D. Xu, G. Guo, L. Gui Silver Selenide Nanowires by Electrodeposition, *Journal of The Electrochemical Society*, 150 (2003) G183-G186.
[18] R. Inguanta, M. Butera, C. Sunseri, S. Piazza, Fabrication of metal nano-structures using anodic alumina membranes grown in phosphoric acid solution: Tailoring template morphology, *Applied Surface Science*, 253 (2007) 5447-5456.

[19] J. Xu, X. Huang, G. Xie, Y. Fang, D. Liu, Study on the structures and magnetic properties of Ni, Co-Al2O3 electrodeposited nanowire arrays, *Materials Research Bulletin*, 39 (2004) 811-818.
[20] J.M. Macak, B.G. Gong, M. Hueppe, P. Schmuki, Filling of TiO_2 Nanotubes by Self-Doping and Electrodeposition, *Advanced Materials*, 19 (2007) 3027-3031.
[21] J.M. Macak, K. Sirotna, P. Schmuki, Self-organized porous titanium oxide prepared in Na_2SO_4/NaF electrolytes, *Electrochimica Acta*, 50 (2005) 3679-3684.
[22] S. Bauer, S. Kleber, P. Schmuki, TiO_2 nanotubes: Tailoring the geometry in H_3PO_4/HF electrolytes, *Electrochemistry Communications*, 8 (2006) 1321-1325.
[23] H. Tsuchiya, J.M. Macak, L. Taveira, E. Balaur, A. Ghicov, K. Sirotna, P. Schmuki, Self-organized TiO2 nanotubes prepared in ammonium fluoride containing acetic acid electrolytes, *Electrochemistry Communications*, 7 (2005) 576-580.
[24] D.M. F. Endres, A. Abbott, *Electrodeposition from Ionic Liquids*, WILEY-VCH Verlag GmbH & Co. KGaA, Weinheim, 2008.
[25] E.L. Smith, A.P. Abbott, K.S. Ryder, Deep Eutectic Solvents (DESs) and Their Applications, *Chemical Reviews*, 114 (2014) 11060-11082.
[26] A.P. Abbott, R.C. Harris, K.S. Ryder, Application of Hole Theory to Define Ionic Liquids by their Transport Properties†, *The Journal of Physical Chemistry B*, 111 (2007) 4910-4913.
[27] A.P. Abbott, Model for the Conductivity of Ionic Liquids Based on an Infinite Dilution of Holes, *ChemPhysChem*, 6 (2005) 2502-2505.
[28] A.P. Abbott, G. Capper, D.L. Davies, R.K. Rasheed, V. Tambyrajah, Novel solvent properties of choline chloride/urea mixtures, *Chemical Communications*, (2003) 70-71.
[29] A.P. Abbott, D. Boothby, G. Capper, D.L. Davies, R.K. Rasheed, Deep Eutectic Solvents Formed between Choline Chloride and Carboxylic Acids: Versatile Alternatives to Ionic Liquids, *Journal of the American Chemical Society*, 126 (2004) 9142-9147.
[30] A. Bakkar, V. Neubert, Electrodeposition onto magnesium in air and water stable ionic liquids: From corrosion to successful plating, *Electrochemistry Communications*, 9 (2007) 2428-2435.
[31] A.H. Whitehead, M. Pölzler, B. Gollas, Zinc Electrodeposition from a Deep Eutectic System Containing Choline Chloride and Ethylene Glycol, *Journal of The Electrochemical Society*, 157 (2010) D328-D334.
[32] A.P. Abbott, J.C. Barron, G. Frisch, S. Gurman, K.S. Ryder, A. Fernando Silva, Double layer effects on metal nucleation in deep eutectic solvents, *Physical Chemistry Chemical Physics*, 13 (2011) 10224-10231.
[33] A.P. Abbott, J.C. Barron, G. Frisch, K.S. Ryder, A.F. Silva, The effect of additives on zinc electrodeposition from deep eutectic solvents, *Electrochimica Acta*, 56 (2011) 5272-5279.
[34] N.M. Pereira, P.M.V. Fernandes, C.M. Pereira, A. Fernando Silva, Electrodeposition of Zinc from Choline Chloride-Ethylene Glycol Deep Eutectic Solvent: Effect of the Tartrate Ion, *Journal of The Electrochemical Society*, 159 (2012) D501-D506.
[35] L. Vieira, R. Schennach, B. Gollas, The effect of the electrode material on the electrodeposition of zinc from deep eutectic solvents, *Electrochimica Acta*, 197 (2016) 344-352.
[36] L. Vieira, A.H. Whitehead, B. Gollas, Mechanistic Studies of Zinc Electrodeposition from Deep Eutectic Electrolytes, *Journal of The Electrochemical Society*, 161 (2014) D7-D13.
[37] S. Salomé, N.M. Pereira, E.S. Ferreira, C.M. Pereira, A.F. Silva, Tin electrodeposition from choline chloride based solvent: Influence of the hydrogen bond donors, *Journal of Electroanalytical Chemistry*, 703 (2013) 80-87.
[38] A.P. Abbott, K.E. Ttaib, G. Frisch, K.S. Ryder, D. Weston, The electrodeposition of silver composites using deep eutectic solvents, *Physical Chemistry Chemical Physics*, 14 (2012) 2443-2449.
[39] A.P. Abbott, G. Capper, K.J. McKenzie, K.S. Ryder, Electrodeposition of zinc–tin alloys from deep eutectic solvents based on choline chloride, *Journal of Electroanalytical Chemistry*, 599 (2007) 288-294.
[40] M. Starykevich, A.N. Salak, D.K. Ivanou, K.A. Yasakau, P.S. André, R.A.S. Ferreira, M.L. Zheludkevich, M.G.S. Ferreira, Effect of the Anodic Titania Layer Thickness on Electrodeposition of Zinc on Ti/TiO2 from Deep Eutectic Solvent, *Journal of The Electrochemical Society*, 164 (2017) D88-D94.
[41] T. Shibata, Y.C. Zhu, The effect of film formation conditions on the structure and composition of anodic oxide films on titanium, *Corrosion Science*, 37 (1995) 253-270.
[42] J. Kapusta-Kołodziej, L. Zaraska, G.D. Sulka, Nanoporous anodic titania observed at the bottom side of the oxide layer, *Applied Surface Science*, 315 (2014) 268-273.
[43] J.M. Macak, S.P. Albu, P. Schmuki, Towards ideal hexagonal self-ordering of TiO_2 nanotubes, *physica status solidi (RRL) – Rapid Research Letters*, 1 (2007) 181-183.

[44] S.P. Albu, A. Ghicov, S. Aldabergenova, P. Drechsel, D. LeClere, G.E. Thompson, J.M. Macak, P. Schmuki, Formation of Double-Walled TiO_2 Nanotubes and Robust Anatase Membranes, *Advanced Materials*, 20 (2008) 4135-4139.
[45] S. Berger, J. Kunze, P. Schmuki, A.T. Valota, D.J. LeClere, P. Skeldon, G.E. Thompson, Influence of Water Content on the Growth of Anodic TiO_2 Nanotubes in Fluoride-Containing Ethylene Glycol Electrolytes, *Journal of The Electrochemical Society*, 157 (2010) C18-C23.
[46] J.M. Macak, H. Tsuchiya, L. Taveira, S. Aldabergerova, P. Schmuki, Smooth Anodic TiO_2 Nanotubes, *Angewandte Chemie International Edition*, 44 (2005) 7463-7465.
[47] A. Michaelis, *Valve Metal, Si and Ceramic Oxides as Dielectric Films for Passive and Active Electronic Devices*, in: Electrochemical Surface Modification, Wiley-VCH Verlag GmbH & Co. KGaA, 2008, pp. 1-106.
[48] J. Xing, Z. Xia, J. Hu, Y. Zhang, L. Zhong, Time dependence of growth and crystallization of anodic titanium oxide films in potentiostatic mode, *Corrosion Science*, 75 (2013) 212-219.

Chapter VII

General conclusions and final remarks

The aim of this work was the electrodeposition of 1-D metallic nanoparticles from deep eutectic solvent using porous anodic templates. This subject has been fully investigated using a step-by-step approach for two most common metallic substrates. The studies were started from the modelling of reduction processes on the dense barrier layer, which mimics the pore bottom and then, the obtained results were applied to the porous templates. One more important feature, namely the adsorbed layer of DES on the anodic oxide/DES interface which formed in the considered systems was thoroughly studied.

Templates preparation and characterization

There were two different metal substrates used for preparation of dense and porous anodic layers in the work. Series of the samples with different thickness of the oxide films on both titanium and aluminium substrates were successfully prepared in solutions of sulfuric acid and ammonium pentaborate, correspondingly. The thickness of the barrier films was estimated using the complementary techniques such as GDOES, EIS and ellipsometry.

Porous anodic templates on aluminium and titanium were formed in an oxalic acid aqueous solution and in fluoride containing ethylene glycol based electrolyte, correspondingly. Both types of the prepared templates were well-ordered and had similar morphology: the pore diameter of 60-70 nm and the wall thickness of 20-30 nm.

Studies of the dense barrier layer influence

The electrodeposition studies were initially performed on flat electrodes covered by dense anodic films. These studies showed a strong impact of structure and thickness of the barrier layer on the electrodeposition process, but the influence is very different in aluminium oxide and in titanium oxide. As alumina film is an insulator, it was found that the zinc electroreduction rate is lower when the barrier film is thicker. Moreover, the formation of a dense organic layer by specific adsorption of the electrolyte components, such as choline cation and ethylene glycol on the alumina surface was revealed. The organic layer was shown to have an adverse impact due to additional limitation on migration of zinc species to the electrode surface. The way to avoid or at least to minimize the effect of the organic layer formation was suggested. It was shown that relatively small AC perturbation overlapped on the potential results in destabilization of the layer and

enhances the zinc reduction. Furthermore, the temperature increase causes growing of the kinetics energy that hinders the layer stabilization.

The dense anodic titania was revealed to show the opposite thickness related behaviour in comparison to that of alumina. Reduction of zinc species occurs much faster on thicker anodic films than on thinner ones. It was explained by crystallization of the titania layer at higher potentials that leads to higher conductivity of the layer and higher rate of zinc reduction. Moreover, neither adsorption of the organic components on the electrode surface nor formation of a dense organic layer have been detected in contrast to alumina. It suggests again that each type of templates should be studied separately in spite of their apparent similarity. Additionally, based on the chronoamperometric measurements confirmed by SEM and AFM observations, the nucleation mechanism has been determined for different film thicknesses and overvoltages.

Porous anodic templates filling

The porous anodic alumina has been successfully used as the template for electrodeposition of zinc nanowires. The main advantage of this method is the use of porous films directly on the substrate without any intermediate stages. The electrofilling of this type of templates by electrodeposition from DES was reported for the first time. A two-step process was developed and used for the electrosynthesis. The first step is AC pre-nucleation of zinc on the pore bottom. The second step is the galvanostatic pores filling. The optimal conditions, including current density, frequency, relaxation time have been found. As a result, highly uniform, well-ordered zinc nanorods have been obtained.

The porous anodic titania has been chosen as the another template for the zinc nanorods formation due to conductive behavior of the oxide. Electrodeposition of zinc was performed in the titania-based templates modified in three different ways. The first one was used as-prepared. It is found that electrodeposition occurs randomly along the full length of the pores that leads to sealing of the pores and thus to a non-uniform filling. Amorphous titania in the second template was converted to the anatase phase by annealing. It improved conductivity of the template and allowed regular zinc electroreduction over the whole pore surface. This modification is suitable for production of coaxial structures. The last modification, selective bottom crystallization, allowed a bottom up filling of the pores and formation of the zinc nanorods. The electrochemical

parameters, such as pulse length, current density, relaxation time, and their influence on the fill-factor have been also studied.

My contribution to the work presented (published papers)

The main part of the work and data reported in chapters III-VI were obtained and analysed by myself. The papers were also written by myself although the final corrections were performed together with my supervisors. Since almost all the works required additional characterization techniques such as ellipsometry, AFM, XRD *etc*., other researchers from our group and other groups assisted me with that. In general, my work was more focused on the electrochemical experiments: templates preparation, zinc electrodeposition, pores filling *etc*.

More specifically:

Chapter III: I have prepared all templates, suggested two-step technique for deposition and performed pores electrofilling. The characterizations were mostly performed by myself except some SEM observations.

Chapter IV: The template synthesis, zinc electrodeposition and characterization were fully performed by myself, but some advices concerning the electrochemical measurements were received from my colleagues.

Chapter V: The core work such as template synthesis, zinc electrodeposition and electrochemical studies has been done by myself. I also performed nearly all characterization of the samples, except for the ellipsometry and AFM.

Chapter VI: I have performed all the work.

The full list of publications is presented below:

Core publications of the thesis:

1. **M. Starykevich**, A.D. Lisenkov, A.N. Salak, M.G.S. Ferreira, M.L. Zheludkevich, Electrodeposition of Zinc Nanorods from Ionic Liquid into Porous Anodic Alumina, *ChemElectroChem*, 1 (2014) 1484-1487.
2. **M. Starykevich**, A.N. Salak, D.K. Ivanou, A.D. Lisenkov, M.L. Zheludkevich, M.G.S. Ferreira, Electrochemical deposition of zinc from deep eutectic solvent on barrier alumina layers, *Electrochimica Acta*, 170 (2015) 284-291.

3. **M. Starykevich**, A.N. Salak, D.K. Ivanou, K.A. Yasakau, P.S. André, R.A.S. Ferreira, M.L. Zheludkevich, M.G.S. Ferreira, Effect of the Anodic Titania Layer Thickness on Electrodeposition of Zinc on Ti/TiO_2 from Deep Eutectic Solvent, *Journal of The Electrochemical Society*, 164 (2017) D88-D94.
4. **M. Starykevich**, A.N. Salak, M.L. Zheludkevich, M.G.S. Ferreira, Modification of Porous Titania Templates for Uniform Metal Electrodeposition from Deep Eutectic Solvent, *Journal of The Electrochemical Society*, 164 (2017) D335-D341.

Other publications:

1. D.K. Ivanou, **M. Starykevich**, A.D. Lisenkov, M.L. Zheludkevich, H.B. Xue, S.V. Lamaka, M.G.S. Ferreira, Plasma anodized ZE41 magnesium alloy sealed with hybrid epoxy-silane coating, *Corrosion Science*, 73 (2013) 300-308.
2. X. Lu, S.P. Sah, N. Scharnagl, M. Störmer, **M. Starykevich**, M. Mohedano, C. Blawert, M.L. Zheludkevich, K.U. Kainer, Degradation behavior of PEO coating on AM50 magnesium alloy produced from electrolytes with clay particle addition, *Surface and Coatings Technology*, 269 (2015) 155-169.
3. A.N. Salak, O.V. Ignatenko, A.L. Zhaludkevich, A.D. Lisenkov, **M. Starykevich**, M.L. Zheludkevich, M.G.S. Ferreira, High-pressure zinc oxysulphide phases in the ZnO–ZnS system, *physica status solidi (a)*, 212 (2015) 791-795.
4. D.K. Ivanou, K.A. Yasakau, S. Kallip, A.D. Lisenkov, **M. Starykevich**, S.V. Lamaka, M.G.S. Ferreira, M.L. Zheludkevich, Active corrosion protection coating for a ZE41 magnesium alloy created by combining PEO and sol-gel techniques, *RSC Advances*, 6 (2016) 12553-12560.
5. B. Kuznetsov, M. Serdechnova, J. Tedim, **M. Starykevich**, S. Kallip, M.P. Oliveira, T. Hack, S. Nixon, M.G.S. Ferreira, M.L. Zheludkevich, Sealing of tartaric sulfuric (TSA) anodized AA2024 with nanostructured LDH layers, *RSC Advances*, 6 (2016) 13942-13952.
6. H. Maltanava, S. Poznyak, **M. Starykevich**, M. Ivanovskaya, Electrocatalytic activity of Au nanoparticles onto TiO2 nanotubular layers in oxygen electroreduction reaction: size and support effects, *Electrochimica Acta*, 222 (2016) 1013-1020.

7. S.A. Ulasevich, S.K. Poznyak, A.I. Kulak, A.D. Lisenkov, **M. Starykevich**, E.V. Skorb, Photocatalytic Deposition of Hydroxyapatite onto a Titanium Dioxide Nanotubular Layer with Fine Tuning of Layer Nanoarchitecture, *Langmuir,* 32 (2016) 4016-4021.
8. M. Serdechnova, M. Mohedano, B. Kuznetsov, C.L. Mendis, **M. Starykevich**, S. Karpushenkov, J. Tedim, M.G.S. Ferreira, C. Blawert, M.L. Zheludkevich, PEO Coatings with Active Protection Based on In-Situ Formed LDH-Nanocontainers, *Journal of The Electrochemical Society,* 164 (2017) C36-C45.
9. M. Mohedano, M. Serdechnova, **M. Starykevich**, S. Karpushenkov, A.C. Bouali, M.G.S. Ferreira, M.L. Zheludkevich, Active protective PEO coatings on AA2024: Role of voltage on in-situ LDH growth, *Materials & Design,* 120 (2017) 36-46.
10. A.N. Salak, D.D. Khalyavin, I. Zamaraite, A. Stanulis, A. Kareiva, A.D. Shilin, V.V. Rubanik, Y.V. Radyush, A.V. Pushkarev, N.M. Olekhnovich, **M. Starykevich**, R. Grigalaitis, M. Ivanov, J. Banys, Metastable perovskite Bi1-xLaxFe0.5Sc0.5O3 phases in the range of the compositional crossover, *Phase Transitions,* (2017) 1-9.

Future activities

I would like to continue the detailed research of the current subject in order to enhance the cross disciplinary knowledge about two new and forward-looking areas, namely, exploration of porous anodic films and ionic liquids.

The future activities are to be divided in two groups. The first one is electrodeposition of different secondary materials for specific applications. For instance, the elecrodeposition methods developed for zinc can be can be applied to magnetic, semiconducting materials or to materials with high catalytic activity. I have already started investigation on conversion of zinc nanorods to zinc oxide and zinc sulphide.

The second group of my research activities I would like to link with anodic processes in DES. Although this area is rarely studied, it has a great potential in electropolishing and anodization of metals, doping of the anodic films by different species with the view to improve corrosion protection, conductivity, stability *etc*. Both areas are interesting and attractive for me.